UNIVERSITÀ DEGLI STUDI DI NAPOLI FEDERICO II

DEPARTMENT OF CHEMICAL, MATERIALS AND PRODUCTION ENGINEERING
(DICMAPI)
PHD IN INDUSTRIAL PRODUCTS AND PROCESSES ENGINEERING
XXIX CYCLE

"DEVELOPMENT AND SCALE-UP OF 3D ENDOGENOUS HUMAN SKIN EQUIVALENT MODELS AS PLATFORM FOR COSMETICS TESTING"

Supervisor

Prof. Paolo Netti

Advisors

Giorgia Imparato, PhD

Francesco Urciuolo, PhD

Costantino Casale, PhD

Coordinator

Prof. Giuseppe Mensitieri

PhD Student

Francesca Rescigno

2014/2017

Table of Contents

Chapter 1. Skin models for cosmetics testing: an overview

Chapter 2. A novel approach for skin tissue engineering: endogenous human skin equivalent models

Chapter 3. Endogenous 3D human skin equivalent as a novel testing platform

Chapter 4. Scale-up strategy for skin models production

Abstract

The current necessity of development new biological *in vitro* models that mimic the characteristics and the complexity of human tissue arises from the need to find a valid alternative to animal models to test and validate new products, and to screen substances and procedures for tissue repair and regeneration. In particular, in the cosmetics field, big multinational companies have developed and devised methods for the realization of testing platforms in large scale, since the European Regulations (Decree 76/768/EEC and the EU Cosmetic Regulation 1223/2009) ban the putting on the market cosmetic products whose ingredients, or parts thereof, have been tested on animal models. in this scenario, researchers have been spent many efforts to develop innovative tissue engineering strategies to create 3D skin equivalent models that faithfully recapitulate the characteristics of human skin in terms of organization, complexity, architecture and responsivity to specific exogenous stimuli.

The optimization of the process to produce these skin equivalent represents a crucial step to obtain i) tissue in large scale in order to allow the screening of a large number of molecules/exogenous factor ii) a high-fidelity replica of the native counterpart in order to evaluate the effect of molecules/exogenous factor on the mechanical properties and ECM composition organization and hydration. For this purpose, in my PhD work, after a deep study of the literature, it was developed a method of production of 3D skin equivalent models in large scale with great reproducibility.

In the first part of the thesis, there is a description of the principal systems that composed the human skin and a summary about the main arguments of European Regulation related to cosmetics testing, the development of alternatives animal

tests and its principal applications. In the second chapter, we exploited a bottom-up tissue engineering approach to build up the skin tissues. Such approach allowed to obtain skin tissues composed of endogenous extracellular matrix (ECM), produced by human dermal fibroblasts and by stratified epithelial cells that constitute a fully differentiated *epithelium* resembling the human epidermis. In the third chapter, we performed a morphological characterization of our 3D skin tissue by histological, biochemical and mechanical analysis in order to better describe the main features of this human skin equivalent models. Furthermore, to validate the skin produced as testing platform, we induced different kinds of damages (UVA, H_2O_2) and after evaluating the effect on the tissue, with the aim to study the effectiveness of molecules having antioxidant and photo-protective action.

Finally, in the last part of thesis, we described firstly, a comparison between 3D skin models designed by us with the commercially available gold standard models produced by best international companies, and then a scale-up strategy in order to improve the production process of 3D-skin equivalent models with the prospective of realization of a start-up. In this last part, we described phases and all critical steps of human skin equivalent production passing from the realization of skin tissue in small scale to the large scale and the development of a working plan of all activities to better control step by step the quality and the effectiveness of final product.

All results reported in my thesis strongly suggested a possible use of the developed skin tissues as a valid alternative to the use of animal models for the testing of new cosmetic compounds.

Chapter 1.
Skin models for cosmetics testing: an overview

1.1 INTRODUCTION

Over the last years, Tissue Engineering (TE) has become established in biomedical and scientific scenario as a new emerging field consisting of several interdisciplinary applications that combine the principles and methods of life science with those of engineering, aiming at repairing or regenerating portions or of whole biological tissue and organs (bone, cartilage, bladder, skin, cornea, blood cells, muscle, liver, pancreas, intestine, etc.) [1]–[4]. The purpose of TE research is very clear: establishing a new clinical technology that makes possible medical applications for diseases that have been too difficult to be cured by existing methods. Initially, it was thought that the principles of TE could be applied only virtually, but today it is known that many applications are widely used not only in tissue regeneration, but also in the industrial field [5], [6]. The classical approach of TE is based on the paradigm according to which, by three elements, which cells, scaffold and soluble factors, it is possible to induce the regeneration of damaged tissue, in attempting to replace traditional medical treatments that in some cases It cannot be applied [4].

The biological materials are made up of cells, cellular signaling and extracellular matrix (ECM). The cells are the core of the tissue that need an adequate systems of signal transduction and/or ECM to exert its functions. The ECM is a of collagen and elastin fiber network synthetized by the cells themselves and secreted in the extracellular space. This complex structure supports biological processes and cell proliferation as well as guarantees resistance and support to the tissue. Single

cells, without a three-dimensional guide, are indeed not able to organize a 3D tissue with its complex architecture, since the only cell proliferation is not sufficient. Single cells need a 3D support, defined “scaffold” whose main function is to support and control cellular processes, as well as the proliferation, differentiation and the synthesis of organic molecules and mediators, known as growth factors, which act in an autocrine and paracrine pathways on cellular processes [7].

As it is known from the literature, the first 3D tissue models made through the application of TE principles were skin equivalent, bone, cornea and cartilage, all tissues more frequently damaged [8]. In parallel with the new methods of regenerative medicine, several companies and industries, from the ‘90s, started off methods suitable for the implementation of tissue equivalent models as *in vitro* test systems in order to verify the safety of substances, active ingredients and cosmetic products [9]. The *in vitro* models became important tools in the pharmaceutical and cosmetics industries for research and development. The best model useful for these studies is the human skin, but the difficulties linked to samples availability, legal and bioethical issues related to the use of cadaver skin, biopsy material or cosmetic surgery, they have increased the need to develop innovative methods aimed to the realization of *in vitro* tissue equivalent models. Furthermore, the availability of tissues is limited not only by the sources, but also by the current regulations. Until the early 2000s in fact, all the tests performed by cosmetic companies before putting a finished product on the market, were carried out on animal models [10].

1.2 STRUCTURE AND FUNCTIONS OF HUMAN SKIN

The skin is named also integumentary system and it is the continuous largest organ of the body and it performs many vital functions, including protection

against external physical, chemical, and biologic assailants, as well as prevention of excess water loss from the body and a role in thermoregulation [11]. The integumentary system is formed by the skin and its derivative structures (Figure 1). The skin is composed of three layers: the epidermis, on the upper part, the dermis, and subcutaneous tissue [11]. The outermost level, the epidermis, consists of a specific population of cells known as keratinocytes, which synthesize keratin, a long, threadlike protein with a protective role. The middle layer, the dermis, is fundamentally made up of collagen, while the subcutaneous tissue contains small lobes of fat cells known as lipocytes. The thickness of these layers varies considerably, depending on the geographic location on the anatomy of the body. The palms and soles of the feet for example, have the thickest epidermal layer, measuring approximately 1.5 mm. The dermis is thickest on the back, where it is 30–40 times as thick as the overlying epidermis (Figure 1) [12].

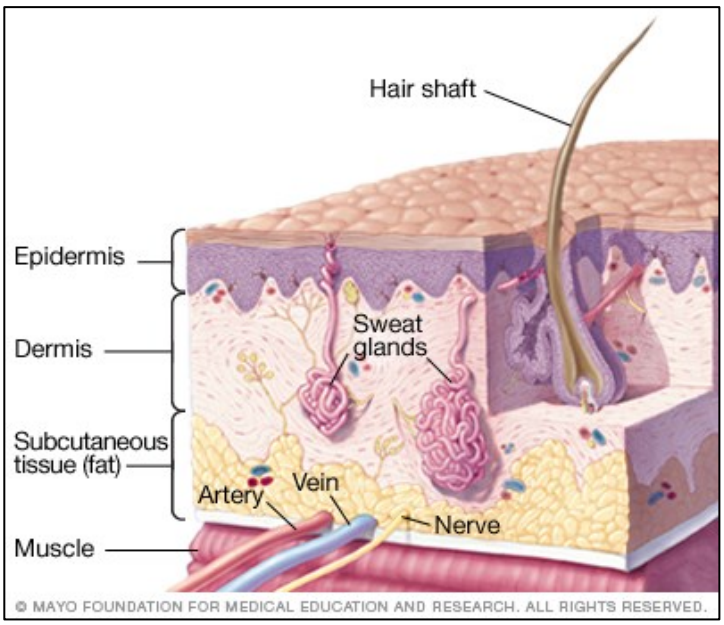

Figure 1. The structure of integumentary apparatus (Mayo's Foundation).

1.2.1 Epidermis

The epidermis is a stratified, squamous *epithelium* layer that is composed primarily of two types of cells: keratinocytes and dendritic cells. [13]. The epidermis includes also a number of other cell populations, such as melanocytes, Langerhans cells, and Merkel cells, but the keratinocyte cell type comprises the majority of the cells. The epidermis commonly is divided into four layers according to keratinocyte morphology and position as they differentiate into horny cells, including the basal cell layer (stratum germinativum), the squamous cell layer (stratum spinosum), the granular cell layer (stratum granulosum), and the cornified or horny cell layer (*stratum corneum*) [12], [13]. The lower three layers that constitute the living, nucleated cells of the epidermis (Figure 2) [13].

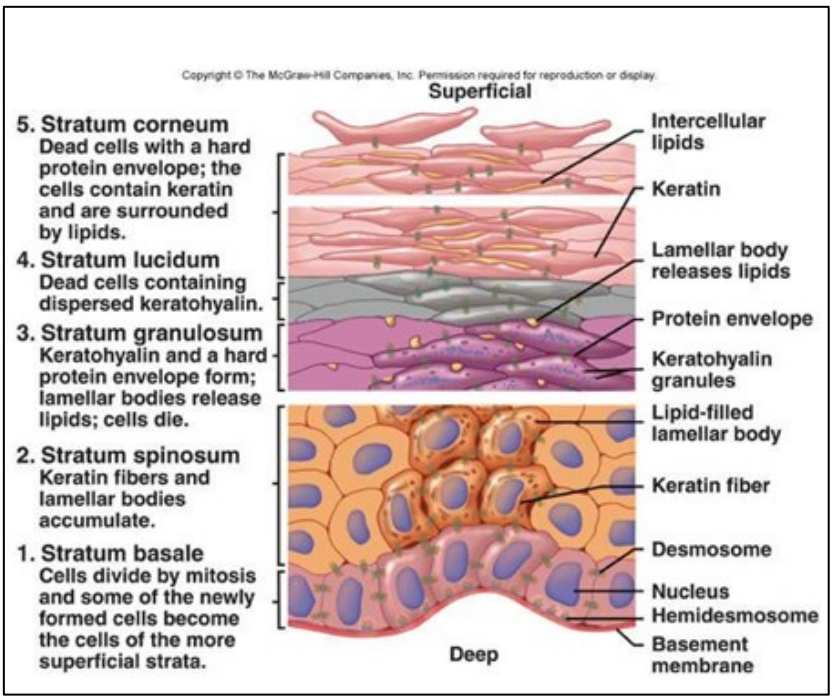

Figure 2. Epidermal layers of human skin (McGrow and Hill Companies).

The epidermis is a dynamic tissue in which cells are constantly in unsynchronized motion, as differing individual cell populations pass not only one another but also melanocytes and Langerhans cells move toward the surface of the skin. [14]. The basal epidermal cells guarantee a continually renewing of all layers of epidermis and gives rise to derivative structures, such as pilosebaceous apparatuses, nails, and sweat glands [13].

Keratinocytes

Keratinocytes derived from ectodermal compartment and the differentiation process that occurs as the cells migrate from the basal layer to the surface of the skin results in “keratinization”, a process in which the keratinocyte first passes through a synthetic and then a degradative phase [14]. During the keratinization phase, the cell builds up a cytoplasmic supply of keratin, a fibrous intermediate filament that serves as part of the cell’s cytoskeleton. Bundles of these keratin filaments converge on and terminate at the plasma membrane forming the intercellular attachment plates known as desmosomes. During the degradative phase of keratinization, cellular organelles are lost, and the cell finally is known as a horny cell or corneocyte. The process of maturation resulting in cell death is known as “terminal differentiation” [15].

Basal layer

The basal layer, or stratum germinativum, represents the deepest layer of epidermis and it contains column-shaped keratinocytes that attach to the basement membrane with their long axis perpendicular to the dermis [13]. Epidermal stem cells in the basal layer are clonogenic cells with a long lifespan that progress through the cell cycle very slowly under normal conditions. Migration of a basal cell from the basal layer to the cornified layer in humans

takes at least 14 days, and the transit through the cornified layer to the outermost epidermis requires another 14 days [14].

Spinous cell layer

The spinous layer is 5–10 cells thick and is composed of a variety of cells that differ in shape, structure, and subcellular properties depending on their location. Parabasal spinous cells, for example, are polyhedral in shape and have a rounded nucleus, whereas cells of the upper spinous layers are generally larger in size, become flatter as they are pushed toward the surface of the skin, and contain lamellar granules that containing glycoproteins, glycolipids, phospholipids, free sterols, and a number of acid hydrolases, including lipases, proteases, acid phosphatases, and glycosidases [14]. Desmosomes are located in the intercellular spaces between spinous cells and they promote mechanical coupling between cells of the epidermis and provide resistance to physical stresses [13]. The desmosomal plaques are composed of six polypeptides found on the cytoplasmic side of the cell membrane that are important in the regulation of the calcium required for desmosomal assembly and maintenance [16]–[18]. Gap junctions, another type of connection between epidermal cells, forming an intercellular pore, in order to allow physiologic communication via chemical signals for cell metabolism, growth, and differentiation [19].

Granular layer

The granular layer is the most superficial layer of the epidermis containing living cells holding abundant keratohyaline granules in their cytoplasm. These cells are responsible of keratinization *phenomenon* by synthesis and modification of specific proteins [14]. The keratohyaline has an enzymatic action in the production

of “soft” keratin in the epidermis by providing periodic cutting of keratin filaments [20]. Lysosomal enzymes are found at high levels in the stratum granulosum because the granular layer is a keratogenous zone of the epidermis and here, the dissolution of cellular organelles is prepared as the cells of the granular layer undergo the abrupt terminal differentiation process to a horny cell of the cornified layer [14].

Cornified layer

Horny cells (corneocytes) are anucleated cells that provide mechanical protection to the underlying epidermis and a barrier to prevent water loss and invasion by foreign substances [21]. The corneocytes, rich in protein and low in lipid content, are surrounded by a continuous extracellular lipid matrix have lost their nuclei during terminal differentiation [13], [14]. In The physical accordance to the position inner the cornified layer, biochemical properties of cells are vary: cells in the middle can bind water molecules than the deeper layers because of the high concentration of free aminoacids found in the cytoplasm of middle layer cells. Desmosomes undergo proteolytic degradation as the cells progress outward, contributing to the shedding of corneocytes during desquamation [15].

1.2.2 Dermis

The dermis is an integrated system composed of three elements: fibroblasts, macrophages and adipocytes. Cells are embedded in a fibrous, filamentous and amorphous connective tissue that accommodates stimulus-induced entry by nerve and vascular networks. The dermis comprises the bulk of the skin and provides its pliability, elasticity and tensile strength and interacts with the epidermis in maintaining the properties of both tissues. The dermis does not undergo a series of differentiation events similar to epidermal differentiation, but

the structure and organization of the connective tissue components are predictable in a depth-dependent manner. The matrix of dermis is composed of collagen, glycosaminoglycans and elastic fibers, that vary in a depth-dependent manner and undergo turnover and remodeling *phenomena* in normal skin, in pathologic processes, and in response to external stimuli [14]. The main components of dermis developed from mesodermal compartment except for nerves, which, like melanocytes, that derive from the neural crest. Only by the 12th week, fibroblasts are actively synthesizing reticulum fibers, elastic fibers, and collagen, while, a vascular network develops and fat cells have appeared beneath the dermis by the 24th week. Small collagen bundles composed the infant dermis whereas the adult dermis contains thicker bundles of collagen [15]. The dermal compartment can be divided in two specific regions: papillary region and reticular region, whereas the deepest layer is the hypodermis, which is primarily made up of adipose tissue. The papillary region is composed of loose areolar connective tissue; the reticular region lies under the papillary region and is usually thicker. Blood vessels that supply the capillaries of the papillary region run through the reticular layer [22].

Fibroblasts

Fibroblasts represent the main cellular component of dermal compartment, and encompass any stromal cell that does not express markers for a more specific mesenchymal lineage [23]. Despite this imprecise definition, fibroblasts are an impressively heterogeneous and dynamic cell lineage. Depending on their resident depth of dermis, fibroblasts express different quantities of collagen and ratios of collagen type I and III [24]. Thanks to their plastic origin in nature, cells that share fibroblasts' mesenchymal origin, including adipocytes and pericytes, are able to de-differentiate into fibroblasts with an appropriate stimulus [25]–[29]. Likewise,

fibroblasts themselves are capable of altering their cellular profile, with the most common transition being that into contractile myofibroblasts [23], [30]–[32]. For all these reasons, fibroblast is a malleable cell, capable of altering its function and physiology or even transforming into a new cell type, based on its location within the body [23]. The molecular mechanisms driving these alterations are probably due both to soluble signaling molecules and the resident molecular framework of the fibroblasts extracellular microenvironment [23], [33].

Collagen

Collagen is the main component of dermis; it is a fibrous structural protein for the entire body (tendons, ligaments, the lining of bones, and the dermis). Collagen bundles and elastic fibers play a role in maintaining the elastic and resistance to physical stresses and deformation of the skin. Collagen fibers undergo a continuous turnover where proteolytic enzymes, called collagenases, degrade bundles replaced quickly by new fibers [15]. Collagen synthesis and deposition in the ECM started from fibroblasts, that integrate the precursor molecule, named procollagen, a helical polypeptide chain, in order to assembly procollagen precursors into collagen fibrils. Collagen fibers are rich in glycine, hydroxyproline, and hydroxylysine alternating with typical sequences. The major constituent of the dermis is type I collagen that, with collagen III, co-polymerize to form extended mechanically stiff fibrils [34], [35]. Collagen fibers have a differential deposition in the papillary and deep reticular dermis [36], in fact, the architecture of these fibrils appears disorganized, composed into bundles which in turn are often oriented parallel to the dermal-epidermal junction (DEJ) or organized into basket-weave arrangements [37]. Type IV collagen is localized to perpendicularly oriented, found in the basement membrane zone anchoring fibrils which play a

key role in securing the dermis to the DEJ [38]; it represents the major structural component of anchoring fibrils with collagen type VII, which is produced primarily by keratinocytes [13], [15], [22] [39].

Elastin

Elastic fibers are responsible for skin elasticity and they are synthesized mainly during development and growth by fibroblasts in skin. The elastic fiber consists of two distinct components: elastin and fibrillin-rich microfibrils. Elastin is synthesized as a 70 kDa monomer precursor and secreted as soluble tropoelastin monomers which are then cross-linked in the presence of extracellular microfibrils to form insoluble elastic fibers [40]. Elastogenesis is controlled by elastin binding chaperone and may bring the tropoelastin molecule to the microfibrillar scaffold that regulates the deposition and/or the orientation of tropoelastin monomers [41], [42]. Interaction between tropoelastin and microfibrils is mediated by ionic bonding involving non-oxidized lysine side chains of tropoelastin [43]. Microfibrils can assemble independent of elastin to form functional structure within the ECM, while, insoluble elastin has not been observed in the absence of microfibrils [42]. Size, orientation and function of elastic fibers may change over a lifetime [44].

Glycosaminoglycans

The dermal ECM is not wholly composed of fibrous proteins but it contains also other components that plays an important role in skin biology as glycosaminoglycans (GAGs) [39]. GAGs are long, linear polysaccharide composed of repeats of specific disaccharide units [45]. Among GAGs, chondroitin-sulfate, dermatan-sulfate, keratan-sulfate, heparin-sulfate, heparin and hyaluronic acid, are involved in various structural and space-filling functions and many

physiological regulations [46]. The main role of GAGs is the capability to bind water molecules and to contribute to maintenance skin water content and skin hydration [46]–[48]. The glycosylation of core proteins contribute to various physiological functions, including collagen and elastic fibers formation, cell adhesion and migration [47]. Hyaluronic acid (HA) is a minor component of the normal dermis and it represents the key molecule in skin hydration by means of interactions with other skin components modulating skin moisture [46]. HA is composed of repeating alternating units of glucuronic acid and N-acetylglucosamine, all connected by β-linkages, GlcAβ (1→ 3) GlcNAcβ (1→4). In particular HA regulates water balance and osmotic pressure and it acts as an organizer of the ECM, stabilizing molecular structures by electrostatic interactions [46].

1.2.3 Dermal-epidermal junction

The dermal-epidermal junction (DEJ) is a high specialized component located at the interface between the epidermis and the dermis. The DEJ separates these two compartments and regulates the overall structural integrity of the skin system. This complex structure permits the transit of migrating cells as melanocytes and Langerhans cells but restricts the diffusion of molecules between two compartments supporting the polarity, proliferation, migration, and differentiation of epidermal keratinocytes [49]. In particular, DEJ is composed of four descriptive zones: the cell membranes of the basal keratinocyte which contain hemidesmosomes, the lamina lucida, an electron-lucent region seen by electron which anchoring filaments traverse; third, the lamina densa and finally the sub-basal lamina, which contains anchoring fibrils [49]–[51]. Each zones contains ubiquitous components, as laminin in the upper region, collagen type IV and heparan-sulphate proteoglycan predominantly in the lamina densa and type

VII collagen within the anchoring fibrils in the sub-basal lamina densa [50]. The regulation of the adhesive interactions of hemidesmosomes with the underlying basement membrane is essential in various biologic processes, such as wound healing, tissue morphogenesis and cancer development and progression [49], [50].

1.3 TISSUE ENGINEERING OF THE SKIN

In the vast scenario of *in vitro* tissue development by the application of TE approaches, the realization of skin models represents the most interesting innovation: *in vitro* generated skin models find growing interest as promising tools in basic research and clinical application in regenerative medicine and in the field of cosmetic testing. Skin equivalents, in fact, are employed from a side, in order to study tissue regeneration processes and mechanisms of pathogenesis (skin regeneration, wound healing *phenomenon*, genetic and structural alteration of epidermis) and from another side, as a useful screening platforms for the characterization and identification of compounds and active ingredients of cosmetic products, since abolishing the use of animal models. Although the demand for human tissue is growing, the lack of availability by the sources and the respective regulations have made the *in vitro* models important tools for research and development in the pharmaceutical and cosmetics industries. The clinical demand for tissue-engineered dermal and composite skin replacements continues to be high, despite there being a number of such products (Dermagraft, Apligraf) available today [52]. Limitations of these products include poor mechanical properties, high costs and limitation of size [53] (Figure 3).

Figure 3. Apligraf skin model.

Although these *in vitro* models may serve as alternatives, they cannot completely satisfy the physiological or anatomical requirements found in *in vivo* models. Pharmaceutical and cosmetics industries developed strategies and innovative protocol for the realization of noncommercial *in vitro* human skin equivalents (HSE). The need for alternative models to assess dermal toxicity is great in biomedical research to test or evaluate the toxicity of numerous compounds. In order to reduce or replace animals in scientific research, ‘‘animal alternatives’’ are being pursued. For this purpose, HSE are employed to replace animal models with alternative test methods as three dimensional models of human skin. The 3D model has important advantages compared to monolayer cell culture and to simple epidermis model in efficacy testing: the possibility of long-term cultivation with repeated application of active principles and cosmetic formulations, the similarity to human skin allows to study dermis-epidermis interaction, characterization of keratinocytes differentiation and keratinization [54], [55]. In general, these *in vitro* models of skin consist of keratinocytes cultured over fibroblast-populated dermal matrices: briefly dermal fibroblasts are encapsulated within ECM components like collagen, fibrin, kitosan-glycosamminoglycan

matrices or seeded onto decellularized dermis and cultured from a few days to a week. After this time, keratinocytes are seeded on top of the dermal equivalents, cultured under submerged conditions for few days and then the culture is exposed to the air (commonly defined air–liquid interface culture condition) in order to obtain epidermal differentiation, stratification and development of a cornified layer [56]–[58]. The various dermal substitutes used to mimic full-thickness human skin include decellularized/de-epidermized dermis [56], [58] collagen type I [30], collagen-glycosaminoglycans [59], fibrin [60]–[62], fibroblast-derived matrix [63] and synthetic polymers [60].

1.3.1. Alternative non-animal testing and european regulations

The 7th amendment to the EU Cosmetics Directive prohibits to put animal-tested cosmetics on the market in Europe after 2013. Before the European regulation 1238/2016, the Directive 76/768/CEE, established prohibitions about animal testing for cosmetics products:

- the prohibition of testing of finished cosmetic products and ingredients on animal models (Experimental Prohibition);
- the prohibition of finished cosmetic products containing ingredients or part of that they have been tested on animals (prohibition of placing on the market).

The prohibition of placing on the market cosmetics products tested in animals became effective on 11 March 2013. In that context, the European Commission invited stakeholder bodies (industry, non-governmental organizations, EU Member States, and the Commission's Scientific Committee on Consumer Safety) to identify scientific experts in five toxicological areas, i.e. toxicokinetic, repeated dose toxicity, carcinogenicity, skin sensitization, and reproductive toxicity for

which the Directive foresees that the 2013 deadline could be further extended in case alternative and validated methods would not be available in time. The selected experts were asked to analyze the status and prospects of alternative methods and to provide a scientifically sound estimate of the time necessary to achieve full replacement of animal testing. However, the experts were also of the opinion that alternative methods may be able to give hazard information, i.e. to differentiate between sensitizers and non-sensitizers ahead of 2017. For toxicokinetic, the timeframe was 5–7 years to develop the models still lacking to predict lung absorption and renal/biliary excretion, and even longer to integrate the methods to fully replace the animal toxicokinetic models. For the systemic toxicological endpoints of repeated dose toxicity, carcinogenicity and reproductive toxicity, the time horizon for full replacement could not be estimated. In early 2003, the 7th amendment the European Union's Cosmetics Directive (76/768/EEC) was adopted stipulating an immediate end to animal testing in the EU for cosmetic products and a complete ban of animal testing for ingredients by 11 March 2009, irrespective of the availability of alternative methods. The European Centre for the Validation of Alternative Methods (ECVAM), hosted by the Institute for Health and Consumer Protection of the European Commission's Joint Research Centre, was asked to coordinate this activity. ECVAM, existing since 1991, has invested considerable time and resources in coordinating and promoting the development, validation and use of alternative methods. The most favorable outlook in terms of the time estimated for full animal replacement (5 years or less) was in the area of skin irritation. Test methods for skin corrosion, skin absorption/penetration and phototoxicity were already adopted into legislation at that time. Prospects for the mid to long-term (over 5 and up to 15 years) included the areas of eye irritation, acute toxicity, skin sensitization, genotoxicity and mutagenicity, and toxicokinetic and metabolism.

- Toxicokinetic

  Toxicokinetic is the endpoint that informs about the penetration into and fate within the body of a toxic substance, including the possible emergence of metabolites and their absorption, distribution, metabolism and excretion (ADME). While toxicokinetic is an intrinsic part of an *in vivo* animal study, when developing an alternative approach based on *in vitro* studies, toxicokinetic becomes an absolutely crucial and indispensable first step in translating the observations *in vitro* to the human *in vivo* situation. Toxicokinetic studies are important for safety assessment of a cosmetic ingredient, testing for systemic toxicity is only necessary if the ingredient penetrates into the body following dermal, oral, or inhalation exposure and if internal exposure potentially exceeds critical levels, i.e. the internal Threshold of Toxicological Concern (TTC). Toxicokinetic studies are also necessary to evaluate the possible range of target doses at the cell or tissue level that can be expected from realistic external human exposure scenarios to cosmetics. This information is crucial for determining the dose range that should be used for *in vitro* testing. Kinetics in the *in vitro* system and dose–response information is also crucial to translate *in vitro* results to the (human) *in vivo* situation.

- Skin sensitization

  Skin sensitization represents the toxicological endpoint associated with chemicals that have the intrinsic ability to cause skin allergy, termed allergic contact dermatitis (ACD) in humans. The mechanisms at the basis of the induction of skin sensitization are rather complex but relatively well understood and involve the following key steps: skin bioavailability, haptenation (binding to proteins), epidermal inflammation, dendritic cell

activation, dendritic cell migration and T-cell proliferation. Skin sensitization (and ACD) appears only after repeated exposure. All predictive tests conducted to identify substance causing sensitization historically has been based on animal testing. In recent years, non-animal alternative methods have been developed and evaluated to identify skin sensitization hazard potential. a range of non-animal test methods that address the above-mentioned key mechanisms involved in skin sensitization would be necessary to yield an alternative measure of skin sensitizer potency.

- Repeated dose toxicity

  The term “repeated dose toxicity” comprises the general toxicological effects occurring as a result of repeated daily dosing with, or exposure to, a substance for a part of the expected lifespan (sub-chronic exposure) or, in case of chronic exposure, for the major part of the lifespan of the experimental animal. The onset and progression of this toxicity is influenced by the interplay between different cell types, tissues and organs, including the concomitant contribution of toxicokinetic, hormonal effects, autonomic nervous system, immunosystem and other complex systems. Current repeated dose toxicity studies provide information on a wide range of endpoints because changes in many organs and tissues are taken into account. They allow evaluation of an integrated response and its quantitative (dose–response) aspects, making its replacement very challenging. For this purpose, alternative methods have been developed in order to evaluate quantitative risks based on the perturbation of a biological systems, or molecular pathways leading to toxicity. The aim of evaluation of repeated dose toxicity is defining quantitative safety

assessment related to repeated dose toxicity of cosmetic ingredients. The best approach is based on combining and interpreting data on multiple targets obtained from a variety of alternative methods and on the extrapolation between exposure routes. In conclusion, in the last years, the progress of (basic) research and development paved the way to transfer basic research results into practical and robust alternative test methods that allow adequate safety assessment and risk management.

- Carcinogenicity

  Carcinogenesis is a long-term process characterize by a complex sequence of events, biological interactions and aberrant molecular pathways that could be triggered by chemical substances depending to mode of action and target organs. The 2-year cancer assay in rodents is widely regarded as the "gold standard" to evaluate the cancer hazard and potency of a chemical substance. It is clear that the animal testing ban under the 7th amendment of the Cosmetics Directive will have a strong impact on the ability to evaluate and conduct a quantitative risk assessment for potential carcinogenicity of new cosmetic ingredients. This impact is not only due to the ban on the cancer assay itself, but mainly to the ban on *in vivo* genotoxicity testing, any repeated dose toxicity testing, and other tests such as *in vivo* toxicokinetic studies and *in vivo* mechanistic assays.

- Reproductive toxicity

  Reproductive toxicity is probably the most difficult endpoint to be replaced, since it has not only to provide an understanding of the many mechanisms and their interactions which are essential for male and female fertility but also an understanding of the development of the entire human

being during its prenatal life and for this reason only animal models are hitherto accepted as adequately representing the complexity and providing an assessment of the complex interaction of chemicals on the reproductive system. Despite this, in the last decades, some non-animal *in vitro* tests have been developed and validated that address specific aspects, such as embryotoxic or endocrine disrupting effects, of the overall reproductive system; in fact, only selected mechanisms, which lead to reproductive toxicity, can be mimicked *in vitro*. The available tests are used as screening tools or for providing additional or supporting mechanistic information, but no single alternative method or set of methods is yet available that could replace the current animal tests used for assessing reproductive toxicity of chemical substances and support safety assessments.

- Conclusions

Thanks to recent advances in cell-based research including use of stem cells, and the development of two-dimensional and three-dimensional cell (co)-cultures, are facilitating the production of much more sophisticated structures more similar to tissues in the body which can be used as complex system to study molecular pathways, cellular behavior, short and long term effects of chemicals and active compound. These 3D tissue model promise the development of a more predictive risk assessment, based on a better understanding biological events triggered by a chemical. It is important to say that, each alternative method may not be able to generate all required information, but their combination that might provide a sufficient basis for a complete safety assessment for active principles and chemical compound. [10].

1.3.2. Insights from *in vitro* skin models for clinical applications

The first attempts to create *in vitro* artificial skin models date back to the 70's, when Rheinwald and his research group, managed to grow human primary epidermal cells in serial culture on a layer of lethally irradiated 3T3 murine fibroblasts. This first attempt was unsuccessful, and Rheinwald understood the importance of cellular crosstalk between keratinocytes and fibroblasts [64]. Subsequently, cultured epidermal autografts (CEAs) were tested but they showed several limitations depending on the wound site and status, age of the patient, and knowledge and experience of the operator [65]–[69]. Only in 1981 Bell et al. [70] developed a dermo-epidermal *in vitro* system that was tested on animals, and after this first experiments, the technique of realization was perfected, in order to obtain the commercial model named Apligraf, which was fabricated using human allogeneic fibroblasts and keratinocytes. Thanks to advances in TE regeneration protocols, several dermo-epidermal skin substitutes, consisting of human autologous keratinocytes and fibroblasts in bovine collagen, were applied in severe burn patients to induce skin regeneration, demonstrating the importance of epithelial–mesenchymal interactions and the relevance of cross-talk between fibroblasts and keratinocytes for the establishment of a functional basement membrane [71], [72]. In the 1980s there were developed acellular matrices based on collagen and GAGs, giving birth to the actual model commercially available as Integra Artificial Skin (Figure 4) (commonly referred to as Integra) that represented the major step in tissue engineering of skin and it paved the way to new and more complex dermo-epidermal skin model, in order to optimize clinical skin substitution with superior functional and cosmetic results [65].

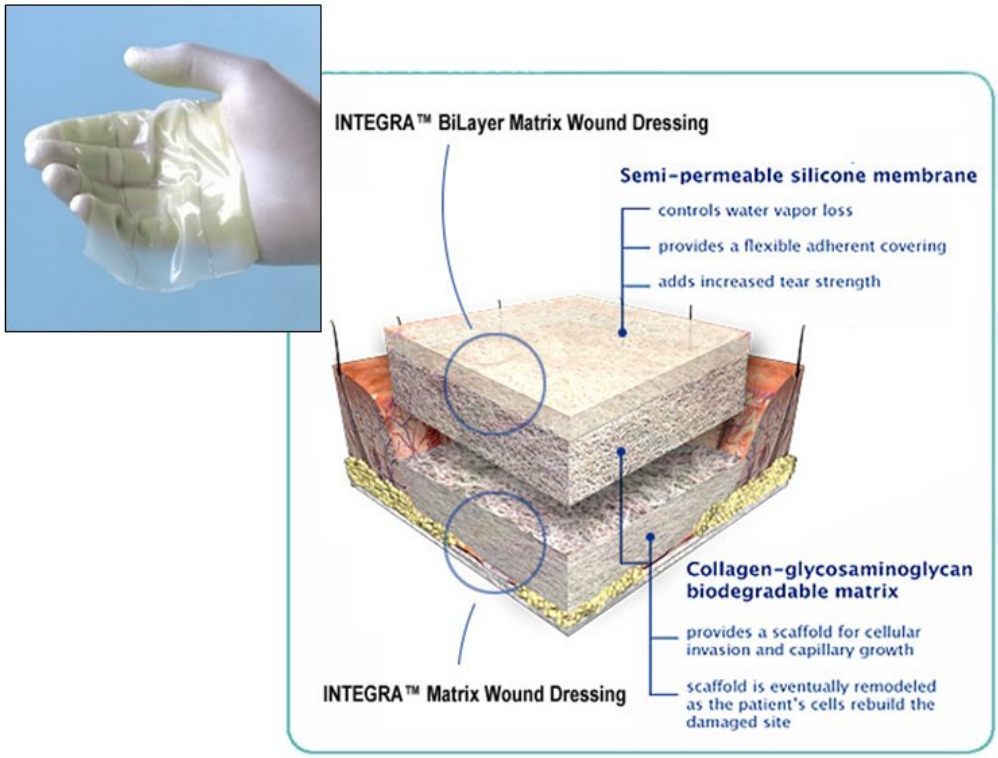

Figure 4. Schematic representation of Integra Skin model.

Based on these studies, various companies and start-ups have developed *in vitro* skin tissue equivalent models for pharmaceutical, cosmetic and chemical compound screening and testing. These commercially available skin tissue equivalents for *in vitro* testing offer significant advantages over the traditional monolayer co-cultures but also differ in important ways from natural skin tissue: organotypic cultures predominantly utilize mitotically-active early passage fibroblasts derived from human foreskins, abdomen, forearm or breast tissues which proliferate within the dermal matrix resulting in 3–4 fold increase over a 3 week culture period [60], [73]. Further, studies also reveal the importance of fibroblast-keratinocyte crosstalk for the generation of a well-organized basement membrane, and for the optimal keratinocytes differentiation [56]. Studies on

organotypic cultures on type I collagen and de-epidermized dermis have demonstrated the role of keratinocyte-fibroblast interactions that influence the formation of basement membrane and which in turn can influence the keratinocyte phenotype [58], [74]–[76]. In fact, in organotypic cultures, a functional basal membrane was observed by the presence of specific markers as collagen type IV and VII, laminin-5, laminin-10/11, expressed only in the presence of fibroblasts that release soluble factors like EGF, KGF and GM-CSF [55], [56]. Several attempts are tested to optimize such variables as timing of keratinocyte addition to the co-culture, and fibroblast seeding densities inner collagen matrices [58]. As explained already, organotypic culture of full-thickness skin equivalents principally involves the following steps: seeding and culture of fibroblasts onto/within dermal matrices followed by keratinocyte seeding on the surface of matrices and culture at air–liquid interface. Similarly, we observed contraction *phenomenon* of collagen-based dermal matrix with and without the presence of fibroblasts, while contraction of the fibrin-based dermal matrix was minimal irrespective of the presence or absence of fibroblasts. Experiments with scaffold-reinforced fibrin-based dermal matrices and extended culture periods of up to 12 weeks have previously been reported [60], [61], highlighting the inherent properties of different dermal matrices and the potential enhancements that may be made to culture models under the right conditions. Several studies and investigations on HSEs suggest the presence of a complex 3D system whit all molecular and cellular pathway typical of native skin compartment: investigations suggest the existence of receptors in epidermal and/or dermal regions, they have been primarily focused on skin keratinocytes and information on their role and expression among the heterogeneous dermal fibroblasts is limited. Other studies have demonstrated the presence of neurohormone receptors and neurotransmitter systems in non-neuronal skin cells which are involved in skin

homeostasis and inflammation like acetylcholine (nicotinic and muscarinergic), adrenergic, histamine, opioid, cannabinoid, kinin, prostanoid, vasoactive intestinal peptide, somatostatin and neuropeptide receptors. Experiments accomplished on *in vitro* HSEs demonstrated that the exposure of dermal fibroblasts to nicotine produces an increase in cell cycle and apoptosis related regulators and an upregulation of MMP-1 and collagen type-I suggesting an alteration in ECM turnover [77]. In summary, with the advent of organotypic models our knowledge of skin biology and of the roles of fibroblasts/fibroblast-keratinocyte crosstalk has grown significantly. However, all *in vitro* models of native skin developed during this years, lack of all aspects of the complexity of the *in vivo* counterpart, for instance, barrier functions, innervation, a continuous blood supply, presence of skin appendages, and interactions with immune cells [56]. A several group of organotypic 3D system are employed as skin substitutes for clinical applications. It is possible to dived engineered skin substitutes in two large groups of application: large and deep burn wounds, or chronic situations, as disabling scars, and chronic ulcers, that can be ideally replaced by an adequate skin graft [78].

Skin autografts are harvested from uninjured areas and then applied to the excised or debrided areas of the wounded skin of the same individual previous an adequate tissue preparation in order to agree the merge between the capillary network of the wound with that of the skin graft. However, many problems arise from skin autografts: if a dermal substitute reaches a threshold thickness [79], vascularization is too slow to assure nutrition of the overlying epidermis resulting in epidermal necrosis or graft loss. For this reason, most dermal substitutes thicker than 1 mm are applied using a two-step approach in order to avoids epidermal necrosis, as the dermal substitute is given sufficient time to vascularize [65]. Other problems liked to skin transplant may be the lack of pigmentation and

elasticity, contraction and low mechanical proprieties of tissue, the lack of protection against UV ray exposition. Therefore, bioengineered HSEs could be used to provide a more permanent solution. Several commercial products were developed during the last 30 years. Most of them were designed for permanent use, some of them as temporary substitutes. All skin substitutes are fabricated using a similar approach, using cells of different origins (autologous, allogenic or xenogeneic) and polymers as biodegradable scaffold for cell attachment and proliferation. In the vast scenario of HSEs for clinical application, it is possible to classified them into epidermal, dermal and dermo-epidermal substitutes. Epidermal substitutes contain autologous keratinocytes often grown in the presence of murine fibroblasts [65] and can be classified into several types: acellular skin substituted and cellular autologous skin substitutes [80]. Examples are Biobrane, employed in the late 1970, is now used as temporary substitute, composed of nylon mesh, which acts as a “dermis” and a silicon membrane which acts as an “epidermis” and it is used as a temporary coverage for superficial or mid dermal partial thickness wounds, burns, donor sites and congenital diseases such as epidermolysis bullosa; Integra Skin Substitute developed by Yannas and Burke [80], [81] is a bi-layered skin substitute made of a silicone membrane water resistant; the dermal part is made of bovine collagen and shark chondroitin-6-sulphate glycosaminoglycan that allows the whole vascularization within 2-3 weeks from the application; Alloderm, is essentially formed from acellular matrix derived from a cadaveric dermis adequately processed without epidermal layer. However, this acellular matrix represents a good natural niche for fibroblast and endothelial cells to generate neodermis [82]. After application to prepared dermis, these substitutes are colonized and vascularized by underlying cells [65]. Cellular allogenic substitutes include Transcyte, Dermagraft, Apligraf**.**

Trancyte is a tissue substitute made from a nylon mesh and allogenic fibroblasts from neonatal foreskin embedded into the mesh and allowed to grow for 3-6 weeks to obtain a cellular matrix which enhances tissue regeneration.; Dermagraft is similar to Trancytes but lacks the silicon layer and also contains a fibroblasts mixed in a polyglycolic acid matrix in a bag of circulating nutrients [83]**,** while, Apligraf is an example of an organotypical skin substitute composed of both dermis and epidermis fabricated by mixing living fibroblasts from neonatal foreskin with bovine collagen type I and neonatal foreskin keratinocytes seeded on the surface of dermal compartment for 4 days in order to allow cell proliferation. High calcium concentration and the air-liquid interface culture system allowed cellular differentiation and keratinization of *epithelium* [84]. In the 1998, FDA (Food and Drug Administration) approved the clinical use of Apligaf for treatment of venous and diabetic ulcers [81], [85] and for the conventional treatment of non-infected partial or full thickness venous ulcers which have not responded to conventional treatment. Cellular autologous skin substitutes include tissue systems employed as a temporary coverage of skin surface for the treatment of large wound regeneration by autologous keratinocytes for the permanent skin coverage [65], [80].

Among cellular autologous substitutes, most tissue systems belong to the category of cultured epidermal autograft, also called CEA (Epicel, Epidex) for which keratinocytes obtained from skin biopsy of patient, are grown to stratified cell sheets in order to obtain the final product in 3 weeks [65], [86], [87]. Once applied to the pre-treated dermal wound bed, CEAs can be employed directly or in combination of other methods [65]. Cultured skin substitutes (CSS), are tissue systems based on both epidermal and dermal components, with a minimal risk of infection transmission, and they act as a permanent coverage. The most

commonly used type is a hyaluronic acid derived substitute. Hyaluronic acid facilitates the growth and movement of dermal cells and controls matrix hydration [80]. Actually, skin substitutes commercially available are classified on the basis of tissue composition: epidermal, dermal, and full-thickness models.

Epidermal models

Several companies offer epidermal HSEs including Genzyme's Epicel based on the use of a cultured keratinocytes obtained from a small biopsy. Keratinocytes are cultured aseptically for a period of several weeks to expand the cell population into many skin grafts. The resulting grafts are sheets of skin approximately 50 cm^2 and two to eight cell layers thick [64].

Dermal models

Dermal skin replacements add greater mechanical stability and prevent the wound from contracting. The most commonly used are Transcyte, Dermagraft, Alloderm and Strattice and finally Integra Dermal Regeneration Template [56].

Full thickness models

Full-thickness models of HSEs are composed of both epidermal and dermal layers; keratinocytes and fibroblasts, either autologous or allogeneic, are utilized to prepare the bilayer structures. These full-thickness skin substitutes are more complete skin systems and they are very close to native skin mimicking the principal features and proprieties. In fact, primary keratinocytes cultured for few weeks on fibroblasts, epidermal cells can proliferate and differentiate recapitulating histological structure of the epidermis *in vivo.* Fibroblasts provide an ample support for keratinocytes [56] Apligraf is an example of bilayered skin

model, while a new product called PermaDerm is a can act as a permanent cover of large burns and injuries. It uses keratinocytes and fibroblasts seeded into a collagen sponge.

1.3.3. Commercially available human skin equivalents for *in vitro* applications

Among HSE commercially available, various skin models have been developed as platform for chemical and pharmacological applications in order to substitute animal models. Also in this case, HS for cosmetics testing belong to different groups: epidermal or dermal models and full-thickness model [78]. These 3D skin model are employed to study safety of different substances and chemicals, in terms of corrosiveness, phototoxicity, irritation. Actually, the implementation of 3D *in vitro* HSE is required by international companies to:

- test the efficacy of newly developed formulations and products and thus to use them for claim support;
- differentiate compounds that cause reversible and irreversible toxicity without resorting to *in vivo* animal testing;
- provide accurate and measurable mechanistic information that can be utilized to determine whether a molecule or compound can be altered to reduce irritation or toxicity, without loss of efficacy;
- objectively compare the toxicity and efficacy of newly-developed compounds with those already in use in the market place for the same purpose;
- evaluate the long-term stability or shelf-life of finished products or raw materials;
- determine the potential health risks of employees exposed to chemicals (worker safety)

HSE can be utilized to test drug permeation of cosmetics and personal care products applied topically on skin surface. The SC (corneous layer) is a major barrier to the uptake of drug molecules into and through the human skin, and the mechanistic principles for drug transport in the skin models are rather similar, so for this purpose it is important for cosmetic and pharmaceutical companies to have a reliable *in vitro* screening system to test the number of drugs/active ingredients that permeate into the epidermis, dermis, and across the membrane. In recent years, companies such as L'Oréal and SkinEthic have invested heavily in the development of skin models for pharmaceutical, cosmetic and chemical compounds testing, but from several studies revealed that actual available skin models have a less efficient barrier function than the native human skin. Drug permeability in cultured skin models is higher than in intact human skin *in vitro*, sometimes the difference is even 2–3 orders of magnitude [78]. The permeation barrier of skin models is generally less developed and more permeable to molecules than native counterpart. One of most highly developed applications of commercial reconstructed epidermis models is *in vitro* prediction of the cutaneous irritancy of topically applied products and active compounds. The cutaneous uptake of chemicals applied topically, is the first step in the induction of skin damage since keratinocytes are known to play a crucial role in the initiation and regulation of epidermal inflammation [88]. The use of three-dimensional human keratinocyte cultures is the logical choice for the skin irritation tests because of the test material will be applied topically on the surface of the corneous layer in order to mimic exposure conditions and concentrations of the *in vivo* application. Typically, skin models are pre-treated with tested chemical by incubation, then treated with drug by a topical application during the whole experiment. Irritation markers are either released into the culture medium under the viable epidermis or they can be detected from keratinocyte cells with different

techniques (MTT, Alamar Blue as viability tests or LDH enzyme activity to evaluate cell membrane integrity). The process of alternative methods validation is regulated by ECVAM (European Centre for the Validation of Alternative Methods) and it involved in three principal phases: pre-validation (protocol refinement; phase I), protocol transfer between laboratories (phase II), and protocol performance (i.e. the reproducibility and predictive ability of the tests; phase III) and formal validation study (to meet the criteria of test sensitivity and specificity >60% for correct classification, based on statistical data analysis) [78].

Some 3D *in vitro* reconstructed human skin models were already developed in the 1990' including the EpiSkin model (L'Oréal) and EpiDerm model (MatTek Corporation), and subsequently, additional *in vitro* skin models were included to the commercial market, as EST1000 skin model (Cell System), Phenion full-thickness skin model (Henkel), Straticell model (Straticell), StrataTest model (Stratatek), and more recently introduced Labcyte model.

Episkin and SkinEthic RHE skin models

The EpiSkin model (Figure 5a) was developed in 1991 and it is composed of a collagen lattice mixed with human fibroblasts, surfaced with a film of type IV collagen, with a fully differentiated *epithelium*. In 1997 this model was acquired by L'Oréal [89]. The SkinEthic model (Figure 5b) was fabricated in 1990, by seeding human keratinocytes on inert filters, which are exposed to the air-liquid interface in order to allow differentiation of epidermis [90]. Actually, both models have been scientifically validated for skin corrosion and irritation assessment by ECVAM. In fact, in 2007, ECVAM announced the validation of EpiSkin as a full replacement method for assessing the skin irritancy potential of chemicals. In addition, both models are used for screening acute and chronic irritation of

topically applied formulation and testing phototoxicity [91], genotoxicity, barrier function and metabolism of cosmetic compounds [92].

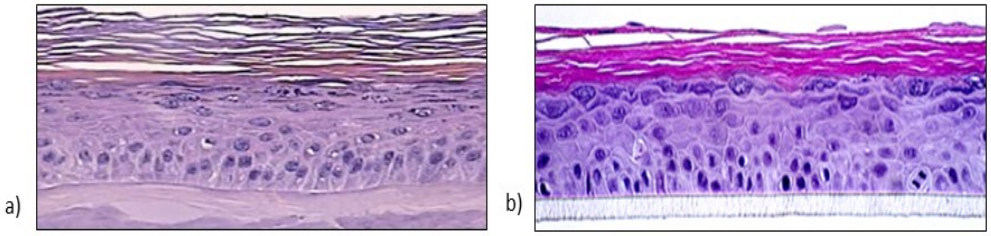

Figure 5. Histological images of Episkin and SkinEthic RHE skin models; (a and b respectively).

EpiDerm and EpiDermFT skin models

The EpiDerm *in vitro* reconstructed skin model, fabricated by MatTek Corporation, is composed of human epidermal keratinocytes that develop a fully-differentiated *epithelium* with a basement membrane and *stratum corneum*, after air-liquid interface culture system on a polycarbonate filters. This 3D model was introduced to the commercial market in 1993 and later, the company, introduced also a full-thickness model called EpiDermFT composed of an epidermis completely differentiated ion a dermis compartment, obtained mixing human dermal fibroblasts and exogenous bovine collagen (Figure 6a). Later, MatTek introduced a melanocyte containing epidermal model called MelanoDerm. EpiDerm models are employed by several industries in product development, safety assessment and drug discovery. The most important supplication are skin irritation, skin corrosion, and in particular, *in vitro* skin irritation data collected using this model, correlate well with human dermal irritation effects caused by compounds and chemicals, with pre-validation studies performed on phototoxicity and dermal penetration. Several additional applications using EpiDerm models include cosmetic products

testing, skin metabolism, genotoxicity, nanotoxicity and pharmacology. Also MelanoDerm is one of innovative model fabricated by MatTek Corporation employed for several applications; MelanoDerm System consists of normal, human-derived epidermal keratinocytes (NHEK) and melanocytes (NHM) cultured to form a multilayered, highly differentiated model of the human epidermis. The NHM within co-cultures undergo melanogenesis leading to tissue pigmentation. The cultures are grown on tissue culture inserts at the air-liquid interface, allowing for topical application of skin lighteners or self-tanning agents. MelanoDerm provides a useful *in vitro* means to evaluate cosmetic and pharmaceutical agents designed to modulate skin pigmentation. Actually, the same company realized a new pathological model, named Psoriasis, a diseased 3D model of psoriasis produced from normal human epidermal keratinocytes and psoriatic fibroblasts harvested from psoriatic lesions (https://www.mattek.com/products/psoriasis/).

The EST1000 skin model

The EST1000 skin model is an *in vitro* 3D RHE produced by Cell System (Troisdorf), became epiCS in 2012. This skin system is fabricated stating from normal human keratinocytes that form a multilayered, highly differentiated model of the human epidermis (Figure 6b). Due to the skin barrier function of the epidermis, liquid, creamy and solid substances can be applied topically-onto the *stratum corneum* to closely mimic the *in vivo* situation. Substances can also be applied systemically by adding to the cell culture medium (http://reconstructed-human-epidermis.com/overview/epics/). The model is used in a wide range of regulatory toxicology tests as irritation, corrosion and phototoxicity analysis and actually, was validated and approved for skin corrosion testing according to the OECD guideline 431 [93]. In 2013 the company launched the pigmented RHE "epiCS-M"

available with melanocytes from donors of three different photo-types: Caucasian, Afro-American and Asian-Caucasian.

The Phenion Full-thickness skin model

This model produced by Henkel (Germany), was introduced commercially in 2006. It consists in human fibroblasts isolated by biopsy are grown in an artificial matrix equivalent (Figure 6c). After the development of this dermal equivalent, keratinocytes obtained from the same donor are seeded on the top of the first compartment. Within several days an epidermal tissue featuring all typical epidermal layers, including a multilayered *stratum corneum*, develops. This model was employed for skin irritation, photoxicity, dermal adsorption , and genotoxicity studies [94]–[96]

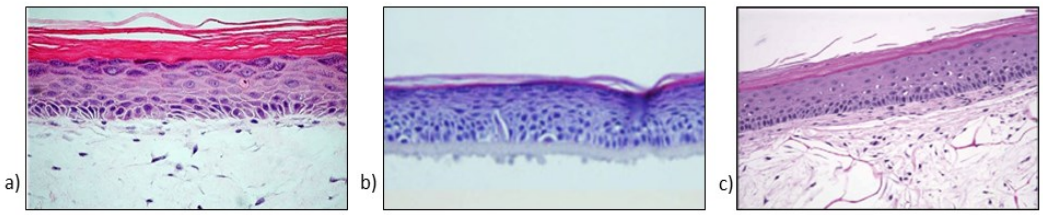

Figure 6. Histological images of most important commercially available human skin models. a) EpiDermFT; b) EST1000; c) Phenion FT.

Other skin models

The StratiCELL skin model was fabricated by the company Straticell (Les Isnes) and is a reconstituted human epidermis with and without pigmentation, composed of normal human keratinocytes and melanocytes cultured on a polycarbonate membrane in a well-defined serum-free medium at the air-liquid interface in order to allow keratinocytes differentiation. Actually, this 3D skin system is preparing for catch-up skin irritation validation and the models were also

evaluated for usefulness in nanotoxicology testing. Additional specific safety applications of the StratiCELL skin model are currently being evaluated (genotoxicity and phototoxicity). This model represents a relevant tool for safety and dermato-cosmetic activity testing, for penetration and absorption studies and for providing insights into mechanisms of action of an active or product. Recently, it was fabricated a new skin model (MEL/001) using melanocytes from african or caucasian donors in order to reproduce the reconstitution of dark tanned and light tanned pigmented tissues, respectively. This model represents a relevant tool to investigate and characterize molecular pathways involved in skin melanogenesis, de/pro-pigmentation as well as to study new active ingredients and to evaluate photo-protection (http://www.straticell.com/en/In-Vitro-Skin-Models/in-vitro-reconstituted-epidermis.php).

The LabCyte skin model (EPI-model) is produced by Japan Tissue Engineering Corporation and it consists of human epidermal cells seeded on inserts. After human epidermal cells proliferation, the exposure to the air-liquid interface solicits keratinization, creating a cultured epidermis model similar to the human epidermis. The EPI-model has undergone validation for skin corrosion and skin irritation in accordance with the OECD test guideline 431 and 439 [97]. The Vitrolife-SKIN skin model is produced by Gunze Corporation (Kyoto) and is commercially available as a kit containing 24 collagen sponges without cells and culture medium. The models are not ready to use and it need to be prepared in the laboratory, cultivating cells in sponges for several days in order to obtain a 3D skin model composed of a dermis and an epidermis with cornified layers as described in the literature. Recently, this model was validated for corrosion and obtained the JACVAM (Japanese Centre for the Validation of Alternative Methods)

validity statement that the Vitrolife-SKIN corrosion assay complies with the OECD guideline (http.//jacvam.jp/files/effort/01001/01_001_05_en.pdf.2008), [98].

The StrataTest skin model is developed by the company StrataTech (Madison), and it consists of a fully-stratified human skin tissue enriched of dermal and epidermal components. The epidermal compartment is generated by the terminal differentiation of a spontaneously immortalized keratinocytes cell line (NIKS) [99]. The dermal counterpart contains normal human fibroblasts embedded in a fibrous collagen matrix [100]. Unlike other skin models, StrataTest requires keratinocytes from the same source, in order to obtain a consistent**,** reproducible test platform. Several tests described the biological response to chemical compound treatments [100] antibiotics formulations [102]. In particular NIKS cells are able to be genetically modified by non-viral methods to generate stably-transfected clones [103]. Data collected with skin irritation tests are comparable to native skin *in vivo*, and for these reasons the model is preparing for catch-up skin irritation validation.

In addition to the skin model described above, which can be considered the most used models in industry today, several other *in vitro* 3D skin systems are fabricated. The company BIOalternatives, has developed an in-house reconstructed epidermis model, called EPI-Ba, mostly used for pre-clinical efficacy studies [104]. The company commercializes a “3D epidermal kit” which contains all necessary materials and reagents, including epidermal cells, to reconstitute a 3D epidermal model in the laboratory [105], provides 3D tissue models ‘on demand’, including both epidermal and dermal-epidermal models using its proprietary chemically defined medium (http://www.sterlab.com/ingenierie_tissulaire/laboratoire_ingenierie_tissulaire.html). Finally, the UK-based biotech company Evocutis (Innovenn) has developed a

full-thickness skin equivalent called LabSkin, consisting of a fully differentiated epidermis on top of a dermal compartment composed of fibroblasts embedded in a fibrin matrix. The model also allows microorganisms to be grown on its surface, mimicking infection or the skin natural microflora. This configuration ensures available assays include assessments for antimicrobial and pre-biotic activity, penetration, anti-ageing and anti-inflammatory properties. Actually, the applications of LabSkin have extended to wound healing studies researching active compound and ingredients efficacy (http://www.innovenn.co.uk/labskin/).

Conclusions

Commercially available 3D skin systems have become reliable tools in toxicity and efficacy testing for both pre-clinical and regulatory purpose. This overview of the most used skin models focused the attention on different testing applications including skin corrosion, skin irritation, phototoxicity, dermal adsorption, skin sensitization and genotoxicity tests [98]. All these 3D skin models were resumed in the Table 1 [106].

Brand	Company	FDA Approval	Product Description
1. Clinical skin replacements and grafts			
Integra® DRT (Dermal Regeneration Template)	Integra Lifesciences	1996	Thin silicone film covering a porous matrix of cow collagen and glycosaminoglycan
Apligraf®	Organogenisis	1998	Fibroblasts and collagen combined in dermal matrix onto which keratinocytes are seeded to form an epidermal layer
Epicel®	Genzyme	2007	Autologous keratinocytes grown *ex vivo* in the presence of proliferation-arrested mouse fibroblasts
Transcyte®/Dermagraft®	Advanced Tissue Sciences/Advanced Biohealing	1997/2001	Cryopreserved dermal substitute: human fibroblast seeded onto polymer mesh and cultured *ex vivo*
Orcel®	FortiCell Bioscience	2001/2008	Human epidermal keratinocytes and dermal fibroblasts are cultured in separate layers into a Type I bovine collagen sponge
Alloderm®/Strattice®	LifeCell Co.	None	Acellular cadaver skin matrix
StrataGraft®	StrataTech	None	Full thickness skin substitute where a near-diploid human keratinocytes cell line, NIKS, was utilized.
2. *In Vitro* Permeation and Toxicity Screening Models			
SkinEthic Rhe (Reconstructed Human Epidermis)	SkinEthic		Human keratinocytes cultured on an inert polycarbonate filter at the air-liquid interface in chemically defined medium
Episkin	SkinEthic		Human keratinocytes cultured on a collagen base which permit terminal differentiation and reconstruction of the epidermis with a functional stratum corneum
Epiderm	MatTek		Neonatal human-derived epidermal keratinocytes (NHEK) cultured to form a multi-layered, highly differentiated model of the human epidermis
EpidermFT	MatTek		Neonatal human-derived dermal fibroblasts (NHFB) and NHEK co-cultured to form a multi-layered, highly differentiated model of the human dermis and epidermis
StrataTest	StrataTech		Full thickness skin model where a near-diploid human keratinocytes cell line, NIKS, was utilized.
Epidermal Skin Test 1000 (EST1000)	CellSystems Biotechnologie GmbH		Reconstructed epidermal model made from primary human keratinocytes; it comprises a fully differentiated epidermis with viable and cornifiedcell layers
Advanced Skin Test 2000 (AST2000)	CellSystems Biotechnologie GmbH		It comprises a dermal equivalent with embedded fibroblasts as a basis and epidermal layer of keratinocytes on top; it is a full thickness model.

Table 1. Most important 3D human skin model commercially available today.

1.4 REFERENCES

[1] R. Langer, J. P. Vacanti, C. A. Vacanti, A. Atala, L. E. Freed, and G. Vunjak-Novakovic, “Tissue Engineering: Biomedical Applications,” *Tissue Eng.*, vol. 1, no. 2, pp. 151–161, Jun. 1995.

[2] F. Rosso, G. Marino, A. Giordano, M. Barbarisi, D. Parmeggiani, and A. Barbarisi, “Smart materials as scaffolds for tissue engineering,” *J. Cell. Physiol.*, vol. 203, no. 3, pp. 465–470, Jun. 2005.

[3] J. A. Hubbell, “Biomaterials in tissue engineering,” *Biotechnol. Nat. Publ. Co.*, vol. 13, no. 6, pp. 565–576, Jun. 1995.

[4] R. M. Nerem and A. Sambanis, “Tissue Engineering: From Biology to Biological Substitutes,” *Tissue Eng.*, vol. 1, no. 1, pp. 3–13, Mar. 1995.

[5] F. Pampaloni, E. G. Reynaud, and E. H. K. Stelzer, “The third dimension bridges the gap between cell culture and live tissue,” *Nat. Rev. Mol. Cell Biol.*, vol. 8, no. 10, pp. 839–845, Oct. 2007.

[6] M. J. Lysaght and A. L. Hazlehurst, “Tissue engineering: the end of the beginning,” *Tissue Eng.*, vol. 10, no. 1–2, pp. 309–320, Feb. 2004.

[7] S. Yang, K. F. Leong, Z. Du, and C. K. Chua, “The design of scaffolds for use in tissue engineering. Part I. Traditional factors,” *Tissue Eng.*, vol. 7, no. 6, pp. 679–689, Dec. 2001.

[8] H. C. Ott *et al.*, “Regeneration and orthotopic transplantation of a bioartificial lung,” *Nat. Med.*, vol. 16, no. 8, pp. 927–933, Aug. 2010.

[9] H. Fernandes, L. Moroni, C. van Blitterswijk, and J. de Boer, “Extracellular matrix and tissue engineering applications,” *J. Mater. Chem.*, vol. 19, no. 31, p. 5474, 2009.

[10] S. Adler *et al.*, “Alternative (non-animal) methods for cosmetics testing: current status and future prospects-2010,” *Arch. Toxicol.*, vol. 85, no. 5, pp. 367–485, May 2011.

[11] J. Kanitakis, “Anatomy, histology and immunohistochemistry of normal human skin,” *Eur. J. Dermatol. EJD*, vol. 12, no. 4, pp. 390-399; quiz 400-401, Aug. 2002.

[12] S. H. Pincus, “Andrews’ Diseases of the Skin: Clinical Dermatology,” *JAMA J. Am. Med. Assoc.*, vol. 247, no. 23, p. 3268, Jun. 1982.

[13] D. J. Tobin, “Biochemistry of human skin—our brain on the outside,” *Chem Soc Rev*, vol. 35, no. 1, pp. 52–67, 2006.

[14] J. A. McGrath and J. Uitto, “Anatomy and Organization of Human Skin,” in *Rook’s Textbook of Dermatology*, T. Burns, S. Breathnach, N. Cox, and C. Griffiths, Eds. Oxford, UK: Wiley-Blackwell, 2010, pp. 1–53.

[15] E. McLafferty, “The integumentary system: anatomy, physiology and function of skin,” *Nurs. Stand. R. Coll. Nurs. G. B. 1987*, vol. 27, no. 3, pp. 35–42, Sep. 2012.

[16] J. A. Fairley, G. A. Scott, K. D. Jensen, L. A. Goldsmith, and L. A. Diaz, “Characterization of keratocalmin, a calmodulin-binding protein from human epidermis,” *J. Clin. Invest.*, vol. 88, no. 1, pp. 315–322, Jul. 1991.

[17] H. Hennings and K. A. Holbrook, “Calcium regulation of cell-cell contact and differentiation of epidermal cells in culture. An ultrastructural study,” *Exp. Cell Res.*, vol. 143, no. 1, pp. 127–142, Jan. 1983.

[18] M. S. Lin, J. M. Mascaró, Z. Liu, A. España, and L. A. Diaz, “The desmosome and hemidesmosome in cutaneous autoimmunity,” *Clin. Exp. Immunol.*, vol. 107 Suppl 1, pp. 9–15, Jan. 1997.

[19] R. Caputo and D. Peluchetti, “The junctions of normal human epidermis. A freeze-fracture study,” *J. Ultrastruct. Res.*, vol. 61, no. 1, pp. 44–61, Oct. 1977.

[20] A. G. Matoltsy, “Keratinization,” *J. Invest. Dermatol.*, vol. 67, no. 1, pp. 20–25, Jul. 1976.

[21] S. M. Jackson, M. L. Williams, K. R. Feingold, and P. M. Elias, “Pathobiology of the *stratum corneum*,” *West. J. Med.*, vol. 158, no. 3, pp. 279–285, Mar. 1993.

[22] Boundless, *Boundless Anatomy and Physiology*. 2016.

[23] L. E. Tracy, R. A. Minasian, and E. J. Caterson, “Extracellular Matrix and Dermal Fibroblast Function in the Healing Wound,” *Adv. Wound Care*, vol. 5, no. 3, pp. 119–136, Mar. 2016.

[24] M. Ali-Bahar, B. Bauer, E. E. Tredget, and A. Ghahary, “Dermal fibroblasts from different layers of human skin are heterogeneous in expression of collagenase and types I and III procollagen mRNA,” *Wound Repair Regen. Off. Publ. Wound Heal. Soc. Eur. Tissue Repair Soc.*, vol. 12, no. 2, pp. 175–182, Apr. 2004.

[25] Z. A. Andrade, J. de-Oliveira-Filho, and A. L. Fernandes, “Interrelationship between adipocytes and fibroblasts during acute damage to the subcutaneous adipose tissue of rats: an ultrastructural study,” *Braz. J. Med. Biol. Res. Rev. Bras. Pesqui. Medicas E Biol.*, vol. 31, no. 5, pp. 659–664, May 1998.

[26] T. Matsumoto *et al.*, “Mature adipocyte-derived dedifferentiated fat cells exhibit multilineage potential,” *J. Cell. Physiol.*, vol. 215, no. 1, pp. 210–222, Apr. 2008.

[27] S. S. Tholpady *et al.*, “The cellular plasticity of human adipocytes,” *Ann. Plast. Surg.*, vol. 54, no. 6, pp. 651–656, Jun. 2005.

[28] C. Schrimpf and J. S. Duffield, “Mechanisms of fibrosis: the role of the pericyte,” *Curr. Opin. Nephrol. Hypertens.*, vol. 20, no. 3, pp. 297–305, May 2011.

[29] J. Karén, A. Rodriguez, T. Friman, L. Dencker, C. Sundberg, and B. Scholz, “Effects of the histone deacetylase inhibitor valproic acid on human pericytes *in vitro*,” *PloS One*, vol. 6, no. 9, p. e24954, 2011.

[30] V. Moulin, D. Garrel, F. A. Auger, M. O’Connor-McCourt, G. Castilloux, and L. Germain, “What’s new in human wound-healing myofibroblasts?,” *Curr. Top. Pathol. Ergeb. Pathol.*, vol. 93, pp. 123–133, 1999.

[31] G. Gabbiani, “The myofibroblast in wound healing and fibrocontractive diseases: The myofibroblast,” *J. Pathol.*, vol. 200, no. 4, pp. 500–503, Jul. 2003.

[32] B. Hinz, “Formation and Function of the Myofibroblast during Tissue Repair,” *J. Invest. Dermatol.*, vol. 127, no. 3, pp. 526–537, Mar. 2007.

[33] S. L. K. Bowers, I. Banerjee, and T. A. Baudino, “The extracellular matrix: At the center of it all,” *J. Mol. Cell. Cardiol.*, vol. 48, no. 3, pp. 474–482, Mar. 2010.

[34] A. J. Bailey, “Molecular mechanisms of ageing in connective tissues,” *Mech. Ageing Dev.*, vol. 122, no. 7, pp. 735–755, May 2001.

[35] J. Gosline, M. Lillie, E. Carrington, P. Guerette, C. Ortlepp, and K. Savage, “Elastic proteins: biological roles and mechanical properties,” *Philos. Trans. R. Soc. B Biol. Sci.*, vol. 357, no. 1418, pp. 121–132, Feb. 2002.

[36] M. El-Domyati *et al.*, “Intrinsic aging vs. photoaging: a comparative histopathological, immunohistochemical, and ultrastructural study of skin,” *Exp. Dermatol.*, vol. 11, no. 5, pp. 398–405, Oct. 2002.

[37] H. K. Graham *et al.*, “Tissue section AFM: In situ ultrastructural imaging of native biomolecules,” *Matrix Biol. J. Int. Soc. Matrix Biol.*, vol. 29, no. 4, pp. 254–260, May 2010.

[38] D. R. Keene, L. Y. Sakai, G. P. Lunstrum, N. P. Morris, and R. E. Burgeson, “Type VII collagen forms an extended network of anchoring fibrils,” *J. Cell Biol.*, vol. 104, no. 3, pp. 611–621, Mar. 1987.

[39] E. C. Naylor, R. E. B. Watson, and M. J. Sherratt, “Molecular aspects of skin ageing,” *Maturitas*, vol. 69, no. 3, pp. 249–256, Jul. 2011.

[40] E. C. Davis and R. P. Mecham, “Intracellular trafficking of tropoelastin,” *Matrix Biol. J. Int. Soc. Matrix Biol.*, vol. 17, no. 4, pp. 245–254, Aug. 1998.

[41] A. Hinek and M. Rabinovitch, “67-kD elastin-binding protein is a protective ‘companion’ of extracellular insoluble elastin and intracellular tropoelastin,” *J. Cell Biol.*, vol. 126, no. 2, pp. 563–574, Jul. 1994.

[42] B. W. Robb, H. Wachi, T. Schaub, R. P. Mecham, and E. C. Davis, “Characterization of an *In vitro* Model of Elastic Fiber Assembly,” *Mol. Biol. Cell*, vol. 10, no. 11, pp. 3595–3605, Nov. 1999.

[43] E. Noblesse *et al.*, “Lysyl oxidase-like and lysyl oxidase are present in the dermis and epidermis of a skin equivalent and in human skin and are associated to elastic fibers,” *J. Invest. Dermatol.*, vol. 122, no. 3, pp. 621–630, Mar. 2004.

[44] F. Duplan-Perrat *et al.*, “Keratinocytes influence the maturation and organization of the elastin network in a skin equivalent,” *J. Invest. Dermatol.*, vol. 114, no. 2, pp. 365–370, 2000.

[45] K. R. Taylor and R. L. Gallo, “Glycosaminoglycans and their proteoglycans: host-associated molecular patterns for initiation and modulation of inflammation,” *FASEB J. Off. Publ. Fed. Am. Soc. Exp. Biol.*, vol. 20, no. 1, pp. 9–22, Jan. 2006.

[46] R. Stern and H. I. Maibach, “Hyaluronan in skin: aspects of aging and its pharmacologic modulation,” *Clin. Dermatol.*, vol. 26, no. 2, pp. 106–122, Apr. 2008.

[47] J.-H. Oh *et al.*, “Intrinsic aging- and photoaging-dependent level changes of glycosaminoglycans and their correlation with water content in human skin,” *J. Dermatol. Sci.*, vol. 62, no. 3, pp. 192–201, Jun. 2011.

[48] J. M. Waller and H. I. Maibach, “Age and skin structure and function, a quantitative approach (II): protein, glycosaminoglycan, water, and lipid content and structure,” *Skin Res. Technol. Off. J. Int. Soc. Bioeng. Skin ISBS Int. Soc. Digit. Imaging Skin ISDIS Int. Soc. Skin Imaging ISSI*, vol. 12, no. 3, pp. 145–154, Aug. 2006.

[49] R. E. Burgeson and A. M. Christiano, “The dermal—epidermal junction,” *Curr. Opin. Cell Biol.*, vol. 9, no. 5, pp. 651–658, Oct. 1997.

[50] R. Timpl, “Macromolecular organization of basement membranes,” *Curr. Opin. Cell Biol.*, vol. 8, no. 5, pp. 618–624, Oct. 1996.

[51] L. Borradori and A. Sonnenberg, “Hemidesmosomes: roles in adhesion, signaling and human diseases,” *Curr. Opin. Cell Biol.*, vol. 8, no. 5, pp. 647–656, Oct. 1996.

[52] K. W. Ng, W. Tham, T. C. Lim, and D. Werner Hutmacher, “Assimilating cell sheets and hybrid scaffolds for dermal tissue engineering,” *J. Biomed. Mater. Res. A*, vol. 75, no. 2, pp. 425–438, Nov. 2005.

[53] K. W. Ng and D. W. Hutmacher, “Reduced contraction of skin equivalent engineered using cell sheets cultured in 3D matrices,” *Biomaterials*, vol. 27, no. 26, pp. 4591–4598, Sep. 2006.

[54] K. Schlotmann, M. Kaeten, A. F. Black, O. Damour, M. Waldmann-Laue, and T. Förster, “Cosmetic efficacy claims *in vitro* using a three-dimensional human skin model,” *Int. J. Cosmet. Sci.*, vol. 23, no. 5, pp. 309–318, Oct. 2001.

[55] A. El Ghalbzouri, M. F. Jonkman, R. Dijkman, and M. Ponec, “Basement membrane reconstruction in human skin equivalents is regulated by

fibroblasts and/or exogenously activated keratinocytes," *J. Invest. Dermatol.*, vol. 124, no. 1, pp. 79–86, Jan. 2005.

[56] G. Sriram, P. L. Bigliardi, and M. Bigliardi-Qi, "Fibroblast heterogeneity and its implications for engineering organotypic skin models *in vitro*," *Eur. J. Cell Biol.*, vol. 94, no. 11, pp. 483–512, Nov. 2015.

[57] M. Rosdy and L. C. Clauss, "Terminal epidermal differentiation of human keratinocytes grown in chemically defined medium on inert filter substrates at the air-liquid interface," *J. Invest. Dermatol.*, vol. 95, no. 4, pp. 409–414, Oct. 1990.

[58] A. El Ghalbzouri, P. Hensbergen, S. Gibbs, J. Kempenaar, R. van der Schors, and M. Ponec, "Fibroblasts facilitate re-epithelialization in wounded human skin equivalents," *Lab. Investig. J. Tech. Methods Pathol.*, vol. 84, no. 1, pp. 102–112, Jan. 2004.

[59] M. Varkey, J. Ding, and E. E. Tredget, "Differential collagen-glycosaminoglycan matrix remodeling by superficial and deep dermal fibroblasts: potential therapeutic targets for hypertrophic scar," *Biomaterials*, vol. 32, no. 30, pp. 7581–7591, Oct. 2011.

[60] K. Boehnke, N. Mirancea, A. Pavesio, N. E. Fusenig, P. Boukamp, and H.-J. Stark, "Effects of fibroblasts and microenvironment on epidermal regeneration and tissue function in long-term skin equivalents," *Eur. J. Cell Biol.*, vol. 86, no. 11–12, pp. 731–746, Dec. 2007.

[61] S. Muffler *et al.*, "A stable niche supports long-term maintenance of human epidermal stem cells in organotypic cultures," *Stem Cells Dayt. Ohio*, vol. 26, no. 10, pp. 2506–2515, Oct. 2008.

[62] H.-J. Stark *et al.*, "Authentic fibroblast matrix in dermal equivalents normalises epidermal histogenesis and dermoepidermal junction in

organotypic co-culture," *Eur. J. Cell Biol.*, vol. 83, no. 11–12, pp. 631–645, Dec. 2004.

[63] D. Janson, G. Saintigny, C. Mahé, and A. El Ghalbzouri, "Papillary fibroblasts differentiate into reticular fibroblasts after prolonged *in vitro* culture," *Exp. Dermatol.*, vol. 22, no. 1, pp. 48–53, Jan. 2013.

[64] J. G. Rheinwald and H. Green, "Serial cultivation of strains of human epidermal keratinocytes: the formation of keratinizing colonies from single cells," *Cell*, vol. 6, no. 3, pp. 331–343, Nov. 1975.

[65] S. Böttcher-Haberzeth, T. Biedermann, and E. Reichmann, "Tissue engineering of skin," *Burns J. Int. Soc. Burn Inj.*, vol. 36, no. 4, pp. 450–460, Jun. 2010.

[66] G. G. Gallico, N. E. O'Connor, C. C. Compton, O. Kehinde, and H. Green, "Permanent coverage of large burn wounds with autologous cultured human *epithelium*," *N. Engl. J. Med.*, vol. 311, no. 7, pp. 448–451, Aug. 1984.

[67] B. S. Atiyeh and M. Costagliola, "Cultured epithelial autograft (CEA) in burn treatment: three decades later," *Burns J. Int. Soc. Burn Inj.*, vol. 33, no. 4, pp. 405–413, Jun. 2007.

[68] V. Ronfard, J. M. Rives, Y. Neveux, H. Carsin, and Y. Barrandon, "Long-term regeneration of human epidermis on third degree burns transplanted with autologous cultured *epithelium* grown on a fibrin matrix," *Transplantation*, vol. 70, no. 11, pp. 1588–1598, Dec. 2000.

[69] C. A. Hernon *et al.*, "Clinical experience using cultured epithelial autografts leads to an alternative methodology for transferring skin cells from the laboratory to the patient," *Regen. Med.*, vol. 1, no. 6, pp. 809–821, Nov. 2006.

[70] E. Bell, H. P. Ehrlich, D. J. Buttle, and T. Nakatsuji, “Living tissue formed *in vitro* and accepted as skin-equivalent tissue of full thickness,” *Science*, vol. 211, no. 4486, pp. 1052–1054, Mar. 1981.

[71] S. T. Boyce, M. J. Goretsky, D. G. Greenhalgh, R. J. Kagan, M. T. Rieman, and G. D. Warden, “Comparative assessment of cultured skin substitutes and native skin autograft for treatment of full-thickness burns,” *Ann. Surg.*, vol. 222, no. 6, pp. 743–752, Dec. 1995.

[72] H.-J. Stark, M. Baur, D. Breitkreutz, N. Mirancea, and N. E. Fusenig, “Organotypic Keratinocyte Cocultures in Defined Medium with Regular Epidermal Morphogenesis and Differentiation,” *J. Invest. Dermatol.*, vol. 112, no. 5, pp. 681–691, May 1999.

[73] N. Maas-Szabowski, H. J. Stark, and N. E. Fusenig, “Keratinocyte growth regulation in defined organotypic cultures through IL-1-induced keratinocyte growth factor expression in resting fibroblasts,” *J. Invest. Dermatol.*, vol. 114, no. 6, pp. 1075–1084, Jun. 2000.

[74] D.-Y. Lee and K.-H. Cho, “The effects of epidermal keratinocytes and dermal fibroblasts on the formation of cutaneous basement membrane in three-dimensional culture systems,” *Arch. Dermatol. Res.*, vol. 296, no. 7, pp. 296–302, Jan. 2005.

[75] R. Fleischmajer *et al.*, “Skin fibroblasts are the only source of nidogen during early basal lamina formation *in vitro*,” *J. Invest. Dermatol.*, vol. 105, no. 4, pp. 597–601, Oct. 1995.

[76] H. Smola, H. J. Stark, G. Thiekötter, N. Mirancea, T. Krieg, and N. E. Fusenig, “Dynamics of basement membrane formation by keratinocyte-fibroblast interactions in organotypic skin culture,” *Exp. Cell Res.*, vol. 239, no. 2, pp. 399–410, Mar. 1998.

[77] J. Arredondo *et al.*, “Central role of fibroblast alpha3 nicotinic acetylcholine receptor in mediating cutaneous effects of nicotine,” *Lab. Investig. J. Tech. Methods Pathol.*, vol. 83, no. 2, pp. 207–225, Feb. 2003.

[78] S. Pappinen, E. Pryazhnikov, L. Khiroug, M. B. Ericson, M. Yliperttula, and A. Urtti, “Organotypic cell cultures and two-photon imaging: tools for *in vitro* and *in vivo* assessment of percutaneous drug delivery and skin toxicity,” *J. Control. Release Off. J. Control. Release Soc.*, vol. 161, no. 2, pp. 656–667, Jul. 2012.

[79] S. MacNeil, “Progress and opportunities for tissue-engineered skin,” *Nature*, vol. 445, no. 7130, pp. 874–880, Feb. 2007.

[80] Alrubaiy, “Skin Substitutes: A Brief Review of Types and Clinical Applications,” *Oman Med. J.*, 2009.

[81] D. M. Supp and S. T. Boyce, “Engineered skin substitutes: practices and potentials,” *Clin. Dermatol.*, vol. 23, no. 4, pp. 403–412, Aug. 2005.

[82] Y. M. Bello, A. F. Falabella, and W. H. Eaglstein, “Tissue-engineered skin. Current status in wound healing,” *Am. J. Clin. Dermatol.*, vol. 2, no. 5, pp. 305–313, 2001.

[83] J. D. Raguse and H. J. Gath, “The buccal fad pad lined with a metabolic active dermal replacement (Dermagraft) for treatment of defects of the buccal plane,” *Br. J. Plast. Surg.*, vol. 57, no. 8, pp. 764–768, Dec. 2004.

[84] K. H. Lee, “Tissue-engineered human living skin substitutes: development and clinical application,” *Yonsei Med. J.*, vol. 41, no. 6, pp. 774–779, Dec. 2000.

[85] R. E. Horch, M. G. Jeschke, G. Spilker, D. N. Herndon, and J. Kopp, “Treatment of second degree facial burns with allografts--preliminary results,” *Burns J. Int. Soc. Burn Inj.*, vol. 31, no. 5, pp. 597–602, Aug. 2005.

[86] P. Shakespeare, “Burn wound healing and skin substitutes,” *Burns J. Int. Soc. Burn Inj.*, vol. 27, no. 5, pp. 517–522, Aug. 2001.

[87] F. M. Wood, M. L. Kolybaba, and P. Allen, “The use of cultured epithelial autograft in the treatment of major burn wounds: eleven years of clinical experience,” *Burns J. Int. Soc. Burn Inj.*, vol. 32, no. 5, pp. 538–544, Aug. 2006.

[88] A. Gröne, “Keratinocytes and cytokines,” *Vet. Immunol. Immunopathol.*, vol. 88, no. 1–2, pp. 1–12, Sep. 2002.

[89] E. Tinois, J. Tiollier, M. Gaucherand, H. Dumas, M. Tardy, and J. Thivolet, “*In vitro* and post-transplantation differentiation of human keratinocytes grown on the human type IV collagen film of a bilayered dermal substitute,” *Exp. Cell Res.*, vol. 193, no. 2, pp. 310–319, Apr. 1991.

[90] Y. Poumay, F. Dupont, S. Marcoux, M. Leclercq-Smekens, M. Hérin, and A. Coquette, “A simple reconstructed human epidermis: preparation of the culture model and utilization in *in vitro* studies,” *Arch. Dermatol. Res.*, vol. 296, no. 5, pp. 203–211, Oct. 2004.

[91] F. X. Bernard, C. Barrault, A. Deguercy, B. De Wever, and M. Rosdy, “Development of a highly sensitive *in vitro* phototoxicity assay using the SkinEthic reconstructed human epidermis,” *Cell Biol. Toxicol.*, vol. 16, no. 6, pp. 391–400, 2000.

[92] R. M. Walmsley and N. Billinton, “How accurate is *in vitro* prediction of carcinogenicity?: Genotoxicity testing,” *Br. J. Pharmacol.*, vol. 162, no. 6, pp. 1250–1258, Mar. 2011.

[93] L.-M. Koeper, A. Schulz, H. J. Ahr, and H.-W. Vohr, “*In vitro* differentiation of skin sensitizers by cell signaling pathways,” *Toxicology*, vol. 242, no. 1–3, pp. 144–152, Dec. 2007.

[94] B. De Wever, S. Kurdykowski, and P. Descargues, “Human Skin Models for Research Applications in Pharmacology and Toxicology: Introducing NativeSkin ® , the ‘Missing Link’ Bridging Cell Culture and/or Reconstructed Skin Models and Human Clinical Testing,” *Appl. Vitro Toxicol.*, vol. 1, no. 1, pp. 26–32, Mar. 2015.

[95] M. Meloni, A. Farina, and B. de Servi, “Molecular modifications of dermal and epidermal biomarkers following UVA exposures on reconstructed full-thickness human skin,” *Photochem. Photobiol. Sci. Off. J. Eur. Photochem. Assoc. Eur. Soc. Photobiol.*, vol. 9, no. 4, pp. 439–447, Apr. 2010.

[96] K. Ackermann, S. L. Borgia, H. C. Korting, K. R. Mewes, and M. Schäfer-Korting, “The Phenion full-thickness skin model for percutaneous absorption testing,” *Skin Pharmacol. Physiol.*, vol. 23, no. 2, pp. 105–112, 2010.

[97] M. Katoh, F. Hamajima, T. Ogasawara, and K.-I. Hata, “Assessment of human epidermal model LabCyte EPI-MODEL for *in vitro* skin irritation testing according to European Centre for the Validation of Alternative Methods (ECVAM)-validated protocol,” *J. Toxicol. Sci.*, vol. 34, no. 3, pp. 327–334, Jun. 2009.

[98] B. DE WEVER, D. PETERSOHN, and K. R. MEWES, “Overview of human three-dimensional (3D) skin models used for dermal toxicity assessment,” *HPC Today*, vol. 8, no. 1, pp. 18–22, 2013.

[99] B. L. Allen-Hoffmann, S. J. Schlosser, C. A. Ivarie, C. A. Sattler, L. F. Meisner, and S. L. O’Connor, “Normal growth and differentiation in a spontaneously immortalized near-diploid human keratinocyte cell line, NIKS,” *J. Invest. Dermatol.*, vol. 114, no. 3, pp. 444–455, Mar. 2000.

[100] C. A. Rasmussen, A. L. Gibson, S. J. Schlosser, M. J. Schurr, and B. L. Allen-Hoffmann, “Chimeric composite skin substitutes for delivery of autologous

keratinocytes to promote tissue regeneration," *Ann. Surg.*, vol. 251, no. 2, pp. 368–376, Feb. 2010.

[101] J. A. Loertscher, C. A. Sattler, and B. L. Allen-Hoffmann, "2,3,7,8-Tetrachlorodibenzo-p-dioxin alters the differentiation pattern of human keratinocytes in organotypic culture," *Toxicol. Appl. Pharmacol.*, vol. 175, no. 2, pp. 121–129, Sep. 2001.

[102] A. L. Gibson, M. J. Schurr, S. J. Schlosser, A. R. Comer, and B. L. Allen-Hoffmann, "Comparison of therapeutic antibiotic treatments on tissue-engineered human skin substitutes," *Tissue Eng. Part A*, vol. 14, no. 5, pp. 629–638, May 2008.

[103] C. L. Thomas-Virnig *et al.*, "Inhibition of Multidrug-resistant Acinetobacter baumannii by Nonviral Expression of hCAP-18 in a Bioengineered Human Skin Tissue," *Mol. Ther.*, vol. 17, no. 3, pp. 562–569, Mar. 2009.

[104] K. Guilloteau *et al.*, "Skin Inflammation Induced by the Synergistic Action of IL-17A, IL-22, Oncostatin M, IL-1{alpha}, and TNF-{alpha} Recapitulates Some Features of Psoriasis," *J. Immunol. Baltim. Md 1950*, Mar. 2010.

[105] J. Nousbeck *et al.*, "Insulin-like growth factor-binding protein 7 regulates keratinocyte proliferation, differentiation and apoptosis," *J. Invest. Dermatol.*, vol. 130, no. 2, pp. 378–387, Feb. 2010.

[106] Z. Zhang and B. B. Michniak-Kohn, "Tissue Engineered Human Skin Equivalents," *Pharmaceutics*, vol. 4, no. 4, pp. 26–41, Jan. 2012.

Chapter 2.
A novel approach for skin tissue engineering: endogenous human skin equivalent models

2.1 INTRODUCTION

Actually, the existing *in vitro* skin models reported in literature and widely described in the previous chapter, are employed in large scale for several applications and are currently the most used by cosmetic and pharmaceutical industries [1]–[3]. Due to the success and the efficacy, a number of research groups have developed the skills and new methods to characterize these 3D skin system in order to compare all features to the native skin [4], [5]. From these studies, however, it showed that, although these 3D skin models represent a valid system mimicking the most basic characteristics of human skin, and they respond effectively to chemical compounds and active substances to which they are exposed, they have non-negligible limitations. According to the authors, in fact, the models commercially available are essentially based on cellularized fibrillar exogenous collagen matrices, often enriched in fibrin and glycosaminoglycans (GAGs), totally lack of structural complexity without an adequate evaluation of dermal compartment, since an endogenous ECM is completely absent [1]. Another limitation verified of these models is the absence of desquamation events of the *stratum corneum*; in fact, the native skin undergoes to a continuous cellular recycling of epithelial tissues thanks to stem cells pull, but in this case the outermost layer does not exfoliate, but, on the contrary, it seems tend to thicken over the time. Finally, all these 3D skin models have an ineffective barrier function of epithelial layer due to an inadequate lipids content that does not confer the impermeability, a fundamental characteristic to exert protection against specific substances which cannot penetrate in the underlying dermis [1]. In conclusion,

even if this models are widely used as *in vitro* dermal substitutes, they represent too simplified models to mimic the complex structure of dermis made up on cells embedded in a structured extracellular matrix (ECM) composed by collagen, elastin and GAGs. For these reasons, an exogenous bovine collagen cannot mimic correctly such a complex network as ECM, and it is not able to allow the recapitulation of pathways that *in vivo* play a fundamental role in *phenomena* such as aging, photoaging or other events in which the structural proteins of ECM are involved. In the light of these considerations, my work fits in this scenario and tries to make available an equivalent skin model able to reproduce the complexity and characteristics of native counterpart, and in the same time, a 3D innovative skin platform with an endogenous ECM that mimics the structure of dermal compartment.

ECM, in fact, is the non-cellular component present within all tissues and organs provides the principal means by which mechanical information is communicated between tissue and cellular levels of function. The ECM allows not only the physical support for the cellular constituents but also a substrate for crucial biochemical and biomechanical cues that are required for tissue morphogenesis, differentiation and homeostasis. These mechanical signals play a central role in controlling cell fate and establishing tissue structure and function. The ECM is a highly dynamic system that is constantly enzymatically or non-enzymatically remodeled; thanks to its physical and biochemical characteristics it lends the biochemical and mechanical properties of each organ, such as tensile and compressive strength and elasticity, mediating protection by a buffering action that maintains extracellular homeostasis and water retention. In fact, ECM microstructure and mechanical properties are considered among the major signaling sources regulating cellular behavior, in particular, differentiation by

signaling pathways involved in the *phenomenon* known as mechanotransduction process [6]. In this scenario, the aim of my work was the development of a human skin equivalent *in vitro* model that is able to reproduce the mean features of native counterpart exceeding all limitations of others commercially available models, in order to employ this organotypic tissue system as a complex and reliable testing platform that best replace the animal models. In particular, the innovation of our human skin equivalents (HSE), resides in an innovative approach that replaces all the exogenous matrices with a totally endogenous ECM produced by human dermal fibroblasts in a dynamic culture system. The endogenous ECM takes part to the dermal compartment that mimics the native human dermis. On the top of dermis, there is the epithelial compartment, completely differentiated consisting of human keratinocytes adequately stratified at air-liquid interface culture condition. The production of our HSE is trigged by a complex multistep process according to an innovative bottom-up approach: starting from small pre-assembled modules, we fabricated a 3D tissue model perfectly organized and architecturally defined. The current traditional tissue engineering strategies employ the classical top-down approach, which cells are seeded on a biodegradable polymer scaffold, in an attempt to recreate the tissue microarchitecture through the synthesis of the ECM and often, by means of the perfusion of molecular mediators, such as growth factors and mechanical stimulation substances, which must be added to the system. However, the top-down approaches fail to effectively recreate the intricate microstructural characteristics of biological tissues [7]. To overcome the top-down approach limitations, in order to re-create biomimetic structures, through the bottom-up approach, we designed modular units that can be used as "building blocks" to obtain more complex engineered tissues for more dimensions with microscale structural features that perfectly reproduce the natural organization of the tissue

[8]–[10] (Figure 1). These building blocks, named HD-µTP, are modular units that we assembled in a specific device in order to develop endogenous human dermis equivalents (HDE), that subsequently, are enriched in human keratinocytes seeded on the surface of dermis, obtaining a complete human skin model, composed of dermis and epidermis reproducing with high fidelity all features of native human skin.

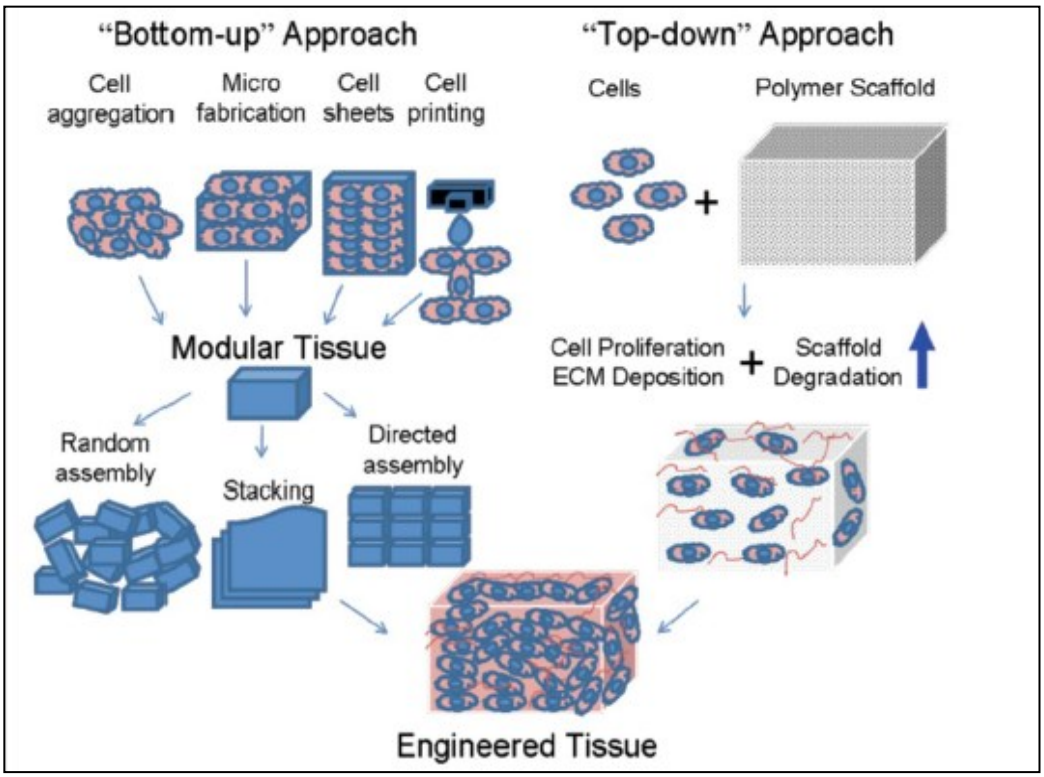

Figure 1. Bottom-up & top-down approaches. In the bottom-up approach there are multiple methods for creating modular tissues, which are then assembled into engineered tissues with specific micro-architectural features. In the top-down approach, cells and biomaterial scaffolds are combined and cultured until the cells fill the support structure to create an engineered tissue (by courtesy of Costantino Casale, from "3D complex endogenous tissue equivalent *in vitro*: processing and biotechnological application").

2.2 MATERIALS AND METHODS

2.2.1 Porous scaffold preparation

Gelatin Porous Microbeads (GPMs) were prepared according to a modified double emulsion technique (O/W/O) [10]. Gelatin type B (Sigma Aldrich) was dissolved into 10 ml of water containing TWEEN 85 (6% w/v) (Sigma Aldrich). The solution was kept at 60°C. Toluene containing SPAN 85 (3% w/v) (Sigma Aldrich) was continuously added to the aqueous gelatin solution (8 % w/v) to obtain primary oil in water emulsion. The added toluene formed droplets in the gelatin solution until saturation. Beads of gelatin containing droplets of toluene were produced through the addition of excess toluene (30 ml). The overload of toluene allowed the obtaining of a double emulsion (O/W/O). After cooling below 5°C, 20 ml of ethanol was added to extract toluene and stabilize GPMs. The resulting microspheres had a diameter of 50-200 µm and they were washed and filtered with acetone and then dried at RT. Microspheres were separated selectively by using commercial sieves (Sieves IG/3EXP). GPMs with 75-150 µm size range were recovered and further processed. Microbeads morphology were examined by means of Scanning Electron Microscopy (SEM).

2.2.2 Crosslinking of GPMs

GPMs were stabilized by means of chemical treatment with D-(+)-Glyceraldehyde (GAL) (Sigma Aldrich) in order to make them stable in aqueous environment at body temperature (37°C). In particular, GPMs were dispersed into acetone/water solution containing 4% of GAL and mixed at 4°C for 24 h. The crosslinked microspheres were washed and filtered with acetone and then dried at RT. GPM were sterilized by absolute ethanol sub-immersion for 24 h before use.

2.2.3 Cell source

Primary cells were extracted from human tissue biopsies surplus obtained by "Azienda Ospedaliera di Rilievo Nazionale e di Alta Specializzazione (AORN) A. Cardarelli/Santobono/Pausillipon at Urology and Biotechnology Centre AORN" according to the project "Realization of human skin equivalent *in vitro* after approval of ethical committee".

2.2.4 Fibroblasts and keratinocytes isolation and culture

Fibroblasts. Primary human fibroblasts were isolated from human breast biopsy (25 years old) using a standardized procedure. Briefly, the tissue was scraped in order to remove subcutaneous fat, incubated for 1 h with penicillin/streptomycin solution (Microgem) 2% in PBS and 50 µg/ml of gentamycin solution (Lonza) in PBS at 4°C alternatively. Finally, biopsy was divided into pieces incubated overnight in 1.8 U/ml of dispase solution (Life Technologies) prepared in PBS at 4˚C. After dispase digestion, dermal sheets were separated from epidermis with forceps. For isolation of human dermal fibroblasts (HDF), dermal pieces were scraped and put in 30 ml collagenase A solution (Roche) at concentration of 2,5 mg/ml for 40 minutes at 37°C. Pieces were suspended in a little volume of Minimum Essential Medium with Earle's salts (Microgem) supplemented with 10% fetal bovine serum (FBS), 100 mg/ml L-glutamine, 100 U/ml penicillin/streptomycin (P/S), and 0, 1 mM non-essential amino acids. In this way, HDF will migrate on the surface of the Petri Dishes. HDF were maintained at 37°C in humidified atmosphere containing 5% CO_2 and propagated in monolayer culture onto 150 cm^2 tissue culture flasks in culture medium (Minimum Essential Medium with Earle's salts) containing 20% FBS, 100 mg/ml L-glutamine, 100 U/ml P/S, and 0,1 mM non-essential amino acids with a cell density of $8x10^3/cm^2$. HDF were maintained at same conditions and used from 5 to 9 passages.

Keratinocytes. Human keratinocytes were isolated from human foreskins after routine phimosis surgery with the informed consent of the patient**,** following the procedure:

Day 1: separation of dermis from epidermis. Foreskin samples derived from phimosis surgery were transported in saline solution in sterility condition and store at 4°C. The biopsy was rinsed 3 times with PBS, and incubated at 4°C for 1 h in different antibiotics solution, as P/S solution (Microgem) 2% and 50 µg/ml of gentamycin solution (Lonza), prepared in PBS, alternatively. Between an incubation and the other, the tissue was scraped in order to remove subcutaneous fat from the dermis side leaving intact the *epithelium*. Finally, after the last incubations, the sample was cut into strips of about 3 mm width. Strips were transferred into new small Petri Dish, wash with PBS and incubated at 4˚C with about 20-30 ml of dispase solution 1.8 U/ml prepared in PBS (Life Technologies) over night (for max 16 h).

Day 2: keratinocyte extraction. Once digestion completed, dispase enzymatic activity was inactivated by washing with cold PBS for 3 times. Skin strips were transferred in a Petri dishes in order to separate epidermis from dermis with tweezers. For keratinocytes extraction, epidermis strips were cut in small pieces and transferred into 10 ml of pre-heated Trypsin/EDTA solution at 0,05% (Lonza) for 5 minutes at 37°C in water bath. The enzyme reaction was stopped after 5 minutes by using FBS and KGM_2 with 5% FBS. In order to allow the mechanical separation of cells from epithelial keratins, pieces were resuspended by vigorous pipetting for 5 minutes. The cell suspension was filtered by a nylon cell strainer with a filter pore size of 100 µm (Falcon) in order to separate cells from residual tissue fragments. Cells were counted and centrifuged at 1200 rpm for 5 minutes. Primary keratinocytes were maintained in culture in tissue flasks with a cellular

density of $2x10^4/cm^2$. After 4 h from seeding, medium was changed and again changed every 2 days. Let cell culture up 70% of confluence before trypsinization. Primary keratinocytes were grown in KGM_2 (Promocell) culture medium. The growth medium contains the base medium, separate vial of calcium chloride and other supplement mix that are: BPE (bovine pitutary extract), hEGF, insulin (recombinant human), hydrocortisone, epinephrine and transferrin. The formulation is optimized for initial seeding of 5000 cells/cm² up to sub-confluence. During this time, basal medium was supplemented with 0.1% transferrin, 0.1% epinephrine, 0.1% hydrocortisone,0.1% insulin, 0.1% H-EGF, 0.4% BPE, 5% FBS, 1%P/S and calcium chloride at 0.06 µM. All cells were grown at 37° C in 5% CO_2 atmosphere.

2.2.5 HD-µTP precursors fabrication

HDF of passages 5-9 and GPMs crosslinked at 4% were used to start human dermis µ-tissue precursor fabrication (HD-µTP). Before using dry GPM were sterilized by absolute ethanol sub-immersion for 24 h. Successively, in order to remove completely the ethanol several washings in PBS were performed. Before cell seeding PBS was removed and replaced with the culture medium. HD-µTP cultivation was initiated by inoculating HDF with scaffold at initial concentration of 10 cells/bead. The culture suspension ($9.5x10^6$ HDF and 172 mg of microbeads) was loaded dynamically in spinner flasks (Integra Bioscience) and stirred intermittently at 30 rpm (5 minutes stirring and 30 minutes static incubation) for 6 h post-inoculation, and then continuously agitated at 30 rpm. The rate of disappearance of free cells from inoculated cultures was determined as an indication of cell attachment to microcarriers. During the intermittent stirring phase culture sample (500 µl) was taken each hour and allowed to settle for 1 minute in an eppendorf tube. The microcarrier-free supernatant was introduced

into a hemocytometer for cell counting. After counting the free cells in the medium with a hemocytometer, the number of cells adhering to microbeads (cell/microbead ratio) was evaluated. The growth medium was replenished on the first day and every 2 days until the end of experiments (9 days in total). From the 2nd day 50µg/ml of ascorbic acid (TCI) was added. HD-µTP samples were taken for assay at day 1, 3, 6 and 9. About 1 ml aliquots were collected at day 1, 3, 6 and 9 from spinner culture for the cell adhesion assay on the microcarriers. Briefly, 300 µl of the same aliquots was transferred to a cell culture dish (w/2 mm grid Nunc) for microcarrier counting, the experiment was performed in triplicate. After that the microcarriers suspension was placed in the 1.5 ml eppendorf tube, gently washed twice with PBS, and then treated with trypsin solution (Lonza) to allow cell harvesting. Finally, the detached cells were counted using a hemocytometer. After 9 days, microtissues precursor were transferred into maturation chamber in order to provide the assembly of microtissues and the fabrication of macrotissue by using a bottom up approach as previously described [9].

2.2.6 3D Human dermis equivalent model: HD-µTP molding

In order to obtain a compact 3D human dermis equivalent system, the HD-µTP suspension was withdrawn from the spinner flask and transferred and cultured in an assembling chamber. First of all, HD-µTP suspension was transferred from the spinner flask to a 50 ml centrifuge tube and, after settling, loaded by pipetting into the maturation chamber to allow their molding in disc-shaped construct (1 mm in thickness, 5 mm in diameter). During the filling procedure, the maturation chamber was accommodated on a device connected with a vacuum pump to make the process faster and to assure that weren't any bubble in the maturation space. The maturation chamber had a "sandwich-like" structure: in the middle, there was a silicon mold with blank spaces, where HD-µTP were loaded and

assembled. The silicon mold was delimited on both the top and bottom sides by two stainless steel rigid grids characterized by a porous mesh (18 lm) that was able to retain the µTPs but to allow the flow of nutrients present in culture medium. Two polytetrafluoroethylene (PTFE) rings were placed on the grids on both sides of the system that was sealed by stainless steel screws and bolts. The system was autoclavabled in each part. Furthermore, four assembling chamber was placed on the bottom of a bioreactor (Bellco) and completely surrounded by culture medium. The spinner was operated at 60 rpm and the medium was changed every 2 days and supplemented with ascorbic acid 50 µg/ml (TCI). After 6 weeks of culture the HD-µTP were assembled thanks to collagen deposition and ECM assessment and gelatin microscaffold carrier were degraded by the action of specific enzyme as metalloproteinases and gelatinase that take part to ECM remodeling during the maturation phase. Maturation of 3D-HDE was carried out in dynamic conditions by placing the chamber on the bottom of a bioreactor operated at 60 rpm at 37°C, 5% CO_2 and humidity 90%.

2.2.7 3D Human skin equivalent model fabrication

In order to obtain 3D full thickness human skin model, primary human keratinocytes obtained from biopsy were seeded on human dermis equivalent surface and subsequently it was induced cell proliferation and differentiation in specific culture condition. In this phase the culture medium was composed of KGM_2 0.1% transferrin, 0.1% epinephrine, 0.1% hydrocortisone,0.1% insulin, 0.1% h-EGF, 0.4% BPE, 5% FBS, 1%P/S and calcium chloride at 0.06 µM. For healthy epidermal reconstruction, surfaces of 3D human dermis equivalent model obtained during the maturation phase, were coated with human fibronectin solution (Sigma Aldrich) at concentration of 50 µg/ml prepared in sterile PBS with a minimal volume (about 10 µl/sample). It is important to allow to dry samples

under hood flow for at least 45 minutes at RT. During this time, keratinocytes were washed 3 or 4 times with PBS/EDTA 0,01M for 5 minutes and cellular colonies were detached using trypsin/EDTA (Lonza) for 5 minutes at 37°C. Cells were gently resuspended in culture medium enriched of 5% of FBS in order to stop trypsin enzymatic reaction, and subsequently counted and centrifuged at the appropriate numbers (150,000 cells/samples of 5 mm diameter) at 1200 rpm for 5 minutes. Cellular pellet was resuspended in a small volume needed for plating onto dermis surface (150,000 cell in a minimal volume of 10-15 µl). It is important do not touch the drops on dermis surfaces for about 10 minutes in order to allow cell attachment. Dermis samples were incubated at 37°C for 2,5/3 h adding a culture medium drops each 10 minutes to allow keratinocytes survival and adhesion. We prepared a control in Petri dishes in order to check cell adhesion. When cells on control Petri dishes were attached, 3 h after seeding, the medium was added first on the bottom of the well and after the rest of volume gently into the insert submerging whole samples. During the submerged phase, keratinocytes proliferate on dermis surface. The day after the seeding, culture media enriched of FBS 5% was substituted with KGM_2 3% FBS, and after 2 days, with KGM_2 0% FBS. Human skin equivalent samples remained in submerged conditions for about 6 days from seeding. After 6 days of submerged conditions, the cultures were raised to the air/liquid interface for 14 days. In this phase, the culture medium contains the base medium with 0.1% transferrin, 0.1% epinephrine, 0.1% hydrocortisone, 0.1% insulin, 1% P/S, without EGF and BPE and with calcium chloride at 1.88 µM.

2.2.8 Characterization of HD-µTP

Histological analysis

Morphological analysis of HD-µTP were performed on histological section of samples at 9th days of dynamic culture in spinner flask. In order to evaluate collagen deposition and 3D organization of HD-µTP, samples were fixed with 10% neutral-buffered formalin fixative for 2–4 h at RT and rinsed twice with PBS buffer solution. After the fixation and dehydration procedure, samples were embedded in paraffin to be sectioned and stained. 5 µm transverse sections of samples were stained using hematoxylin-eosin solutions (Bio-Optica), Masson's Trichrome (Sigma Aldrich) following standard procedure and analyzed by an optical microscope (BX53; Olympus).

Collagen structure by Second Harmonic Generation (SHG) imaging

Second harmonic generation (SHG) imaging has recently emerged as a noninvasive tool for high-resolution imaging of fibrillar type I collagen in tissues. Simultaneous interaction of two near-infrared (NIR) photons with non-centrosymmetric structures can result in emission of a single photon at exactly half the wavelength of the excitation light. In particular, collagen type I produces a very robust SHG signal with a nonlinear excitation wavelength between 700 and 1064 nm, allowing a window of detection from 350 to 532 nm. Because individual collagen fibrils are the source of the SHG signal, this method has the potential to spatially resolve collagen organization at the submicrometer level and provide information regarding physiological changes in collagen structure that correlate with tissue function.

The samples for SHG imaging were fixed with were fixed in 4% paraformaldehyde solution and rinsed in twice in PBS and observed in their 3D structure. SHG

imaging in our samples were performed using a Confocal Leica TCS SP5 II femtosecond laser scanning system (Leica), coupled to a tunable compact mode-locked Ti:sapphire laser (Chamaleon Compact OPO-Vis, Coherent). The samples were observed by using λ_{ex} = 840nm (two photons) and λ_{em} = 415-425nm. The SHG images, having a size of 200µmx200µm, were acquired with a resolution of 12 bit, 1024x1024 pixel by using a HCX IRAPO L 25X N.A. 0.95 water immersion objective.

2.2.9 Characterization of 3D human dermis equivalent models

Histological analysis

For characterization of dermis structures, morphological analysis of 3D human dermis equivalent models was performed on histological section of samples at 6^{th} weeks of maturation phase in bioreactor culture system. Samples were fixed with 10% neutral-buffered formalin fixative for 2–4 h at RT and rinsed twice with PBS buffer solution. After the fixation and dehydration procedure, samples were embedded in paraffin to be sectioned and stained. 5 µm transverse sections of samples were stained using hematoxylin-eosin (Bio Optica) solutions, analyzed by an optical microscope (BX53; Olympus).

Collagen structure by Second Harmonic Generation imaging

In order to evaluate collagen assembly and composition, second harmonic generation (SHG) imaging was performed ad described previously for the characterization of HD-µTPs. The samples were prepared in the same manner and visualized using Confocal Leica TCS SP5 II femtosecond laser scanning system (Leica), coupled to a tunable compact mode-locked Ti:sapphire laser (Chamaleon Compact OPO-Vis, Coherent). The samples were observed by using λ_{ex} = 840nm (two photons) and λ_{em} = 415-425nm. The SHG images, having a size of

200µmx200µm, were acquired with a resolution of 12 bit, 1024x1024 pixel by using a HCX IRAPO L 25X N.A. 0.95 water immersion objective.

2.2.10 Characterization of 3D human skin equivalent models

Histological analysis

For visualization of dermis and epithelial structures, morphological analysis of 3D human skin equivalent models was performed on histological section of samples at 14th days air-liquid interface culture conditions. Samples were fixed with 10% neutral-buffered formalin fixative for 2–4 h at RT and rinsed twice with PBS buffer solution. After the fixation and dehydration procedure, samples were embedded in paraffin to be sectioned and stained. 5 µm transverse sections of samples were stained using hematoxylin-eosin (Bio Optica) solutions, analyzed by an optical microscope (BX53; Olympus).

Immunofluorescences and immunohistochemistry

3D skin tissues at 14th days of air-liquid interface culture conditions were rinsed gently in PBS and fixed with 10% neutral-buffered formalin fixative for 2–4 h at RT and rinsed twice with PBS buffer solution. After the fixation and dehydration procedure, samples were embedded in paraffin. Immunofluorescences were performed on 7 µm paraffin-embedded tissue sections in order to observe organization of 3D skin system and epithelial differentiation. Histological sections were deparaffinized and permeabilized with 0.2% Triton X-100 (Sigma Aldrich) in PBS and incubated with PBS/BSA (Bovine Serum Albumin, Sigma Aldrich) 6% as blocking solution for 2 h in wet conditions. Subsequently, the slices were incubated overnight with primary antibody for Versican (1:50, policlonal, Abcam), Keratin 10 (1:500, polyclonal, Covance), P63 (1:50, monoclonal, Abcam) Loricrin (1:1000, polyclonal, Covance), Involucrin (1:400, polyclonal, Covance), Laminin 5

(1:100, monoclonal, Abcam), Keratin 14 (1:500, polyclonal, Covance) after citrate antigen retrieval, to detect epithelial markers, at 4°C in wet conditions. Tissue sections were rinsed with PBS and incubated with secondary antibodies for 1 h at RT. The secondary antibodies used were: Alexa Fluor 546 donkey anti-rabbit (Life Techologies) and Alexa Fluor 488 goat anti-mouse IgG H&L (Abcam). Nuclei were stained with DAPI (4',6-diamidino-2-phenylindole, 1:10000) diluted in PBS for 15 minutes at RT. Immunohistochemical analysis were performed for Keratin 19 (1:50, Abcam) in accordance with protocol of Mouse and Rabbit Specific (ABC) Detection IHC kit (Abcam, UK).

2.3 RESULTS

2.3.1 HD-µTP assembly assessment

The spinner flasks were loaded with $9{,}5x10^6$ cells and 172 mg of microbeads, corresponding to 10 cells per bead with an initial cellular density of 70,000 cells/ml and in a minimal volume of 135 ml The first 6 h of the seeding phase were characterized by intermittent stirring to improve the cell-to-bead distribution and to obtain a lower proportion of unoccupied beads [11]. The disappearance of free cells from the inoculated spinner cultures was considered to indicate the attachment of cells to the microcarriers. Before proceeding with the loading of HD-µTP in the blank spaces of maturation chamber it was necessary to evaluate the aggregation of HD-µTP and deposition of an initial collagen matrix around and inside microcarriers. At 9^{th} day of dynamic culture in spinner flask, HD-µTP appeared as 3D small compact aggregates composed of cells, evenly distributed around and inside the microbeads (Figure 2a). Masson Trichrome staining revealed the histological composition of HD-µTP, which aggregates of porous microbeads were surrounded by collagen (blue) and cells (violet) that proliferated

exploiting the maximal available surface given by the interconnected porosity of GMPs (Figure 2b and c). Collagen deposition was confirmed by SHG signal (grey) (Figure 2c).

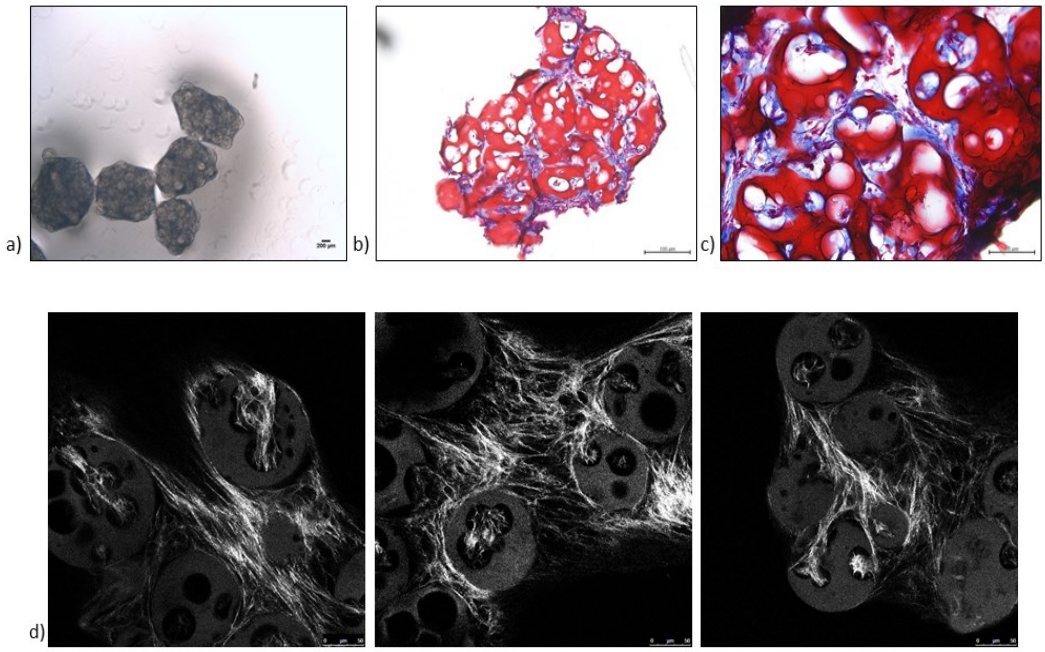

Figure 2. HD-µTP analysis. a) HD-µTP at optical microscope (Mag 4X); Masson Trichrome staining which showed cells around and inside microbeads (violet) and the ECM assembled (blue) surrounding 3D cell aggregates (b and c, Mag. 20X and 40X respectively); d) SHG signal: collagen fibers were assembled around cells and held together microscaffolds and cells in a 3D µTP construct. Bars in a-c) are 100 µm; bar in d) is 50 µm.

2.3.2 3D human dermis equivalent characterization

After HD-µTP assembly in the maturation chamber (Figure 3a and b), at the end of about 6 weeks of culture in the bioreactor (Figure 3c), we obtained an homogeneous and compact 3D human dermis equivalent model that preserved the shape and size after the removal from the chamber. The 3D dermis model was compact and intact with a smooth surface showing a significant elasticity and

firmness, furthermore, it appeared ductile, flexible, strong and resistant to torsion stress and at the pull (Figure 3d).

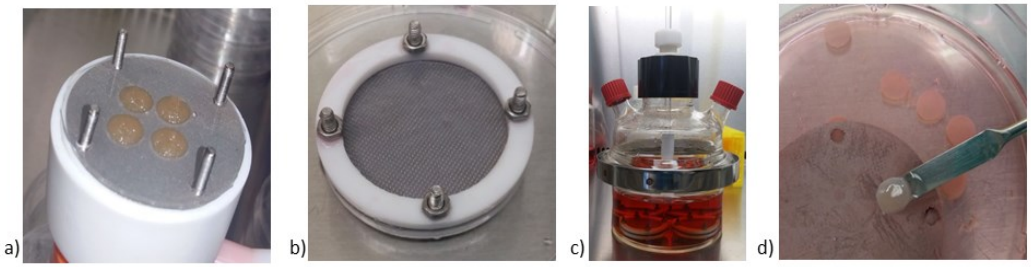

Figure 3. a) HD-µTP of 9th day of culture loaded in the maturation chamber; b) maturation chamber sealed with grids, PTFE rings, screws and bolts; c) bioreactor loaded with 4 maturation chambers sealed; d) 3D human dermis equivalents obtained after 6 weeks of maturation in bioreactor.

It was interesting to highlight that after 6 weeks of culture the tissue is completely made-up of endogenous ECM which composition and morphology were assessed by performing histological analysis and evaluation of SHG signal by Two-Photon technology microscope. The Figure 4 showed histological images of hematoxylin-eosin staining concerning 3D-HDE at 6 weeks of maturation. In Figure 4a and 4b it was possible to observe the ECM as a continuous network in its composition along the thickness of the samples with fibroblasts completely embedded in collagen matrix and the elongated nuclear morphology underlines the good condition of the cells in their own ECM. The collagen fibrils structure was observed by using MPM that allow to visualize unstained collagen structure by exploiting SHG (Figure 4c in grey).

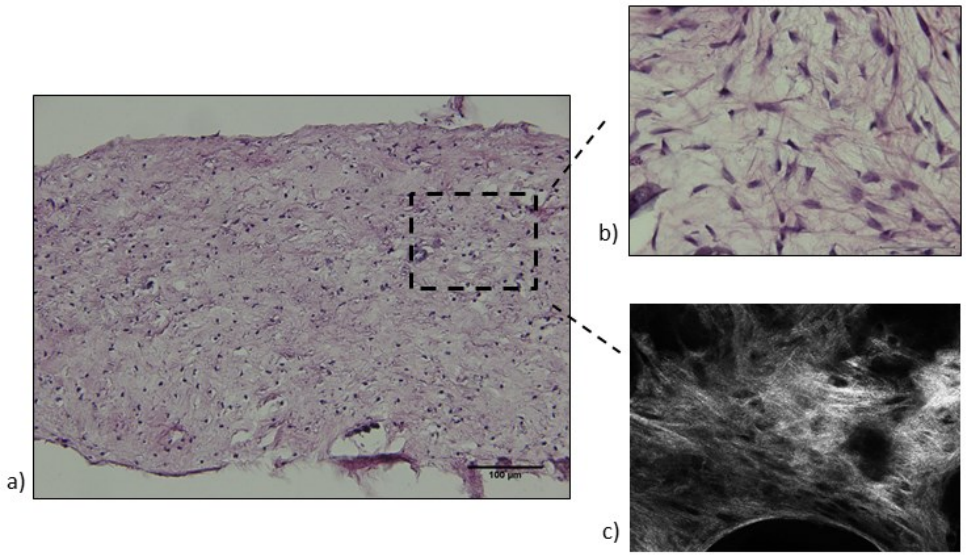

Figure 4. 3D human dermis model histological analysis. a) H&E staining on tissue section which showed dermal fibroblasts (violet) with their elongated nuclei perfectly embedded in and endogenous ECM (pink) with no trace of scaffold microbeads; b) H&E staining observation with a major magnification; c) SHG signal: stretched collagen fibers assembled to form compact and complex supporting network. Bars in a) is 100 µm; bar in b-c) are 50 µm.

2.3.3 3D human skin equivalent characterization

In order to develop a 3D full thickness human skin models, 3D dermis tissues were extracted from chambers and prepared for keratinocytes seeding (Figure 5a). 3D full proliferation and differentiation of primary keratinocytes were triggered modulating calcium concentration during the culture time and employing typical culture condition. During the submerged phase, 3D-HSE were fully covered by medium in a low calcium concentration, in order to allow cellular proliferation. After 6 days, samples were places in air-liquid condition: 3D-HSE were wet by lower medium in the well at high calcium concentration and the exposition to the air allows epidermal differentiation of keratinocytes on dermis surface (Figure 5b) [12]–[14].

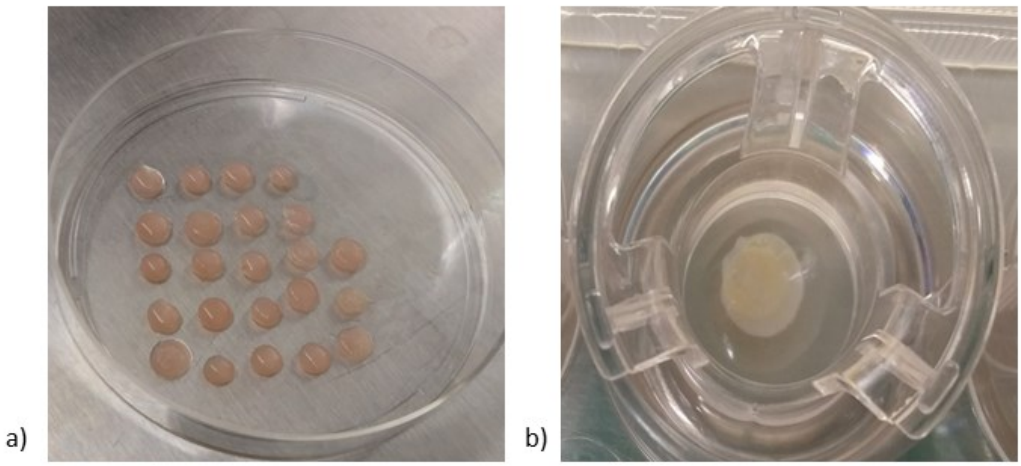

Figure 5. 3D-HSE fabrication. a) 3D human dermis equivalent coated with human plasma fibronectin under hood flow; b) 3D human dermis equivalent in a transweel insert after keratinocytes seedng.

In order to evaluate the epithelial differentiation at the end of human skin equivalent process, different epithelial markers were detected by histological staining, immunofluorescence and immunohistochemistry. The epidermal compartment at 14th day of air-liquid interface culture condition was assessed by H&E staining which showed a good differentiation of all epithelial layers, from basal stratum to corneous one. The epidermis was firmly anchored to dermis compartment through the basal membrane between both compartments. The epidermis was well integrated to the 3D dermal system which was compact, homogenous and rich of an endogenous matrix produced by cells and assembled during the maturation phase. The dermis compartment was devoid of gelatin microscaffold at the end of production process thanks to metalloproteinases remodeling (Figure 6a) [15]–[17]. As already described by Casale et al. [18] it was interesting to observe also the presence of appendage-like structures that originated in the basal layers of the epidermis and descended into the dermis

(Figure 6b). Similar structure *in vitro* were reported only by adding in the epidermal compartment hair buds or multipotent stem cells from neonatal mice able to grow into hair after mice grafting [19], [20]. We found "folliculoid" structures in our model, by using dermal and epidermal human adult cells, leading us to hypothesize that the produced 3D-HSE provide a physiological environment able to preserve the stem cells population obtained by extraction procedure, and to address the fate of such adult cells toward the genesis of appendage-like structures. We characterized these follicle-like structure by performing histology and immunofluorescence for the main epidermal and follicle markers and these results confirmed that our 3D human skin models well recapitulated the *in vivo* counterparts. Histological analysis showed a typical multilayered *epithelium* evenly distributed over the 3D human dermis equivalent surface. In particular, the basal and suprabasal layers displayed the presence of keratin 14 and keratin 10, respectively, while p63-positive staining of the cells in the germinative layer confirmed the maintaining of their staminal state [21]; laminin 5 appeared as a continuous thin line and it was used as a marker of the dermo-epidermal junction (DEJ). Finally, the terminal differentiation of epidermis was demonstrated by the expression of loricrin as typical signals was detected in the *stratum corneum*. The follicle-like structure appeared as finger-shaped projections associated with the basal layer of the epidermis that descended into the dermis and were positive for versican, a proteoglycan expressed *in vivo* in the dermal sheath surrounding bulge epithelial cells and in the core of the bulb region, indicating hair follicle development and cycling. It is known from literature that versican is a proteoglycan expressed in the epithelial tissue and in the dermis matrix, where it works as a modulator of cell proliferation and migration [22]. We found a spot signal of versican in the ECM, while in the epidermal compartment is visible as a homogenous signal that surround the follicle-like structure (Figure 6d, e, f, g).

Most importantly, keratin 19, a follicular stem cell marker, was found in the basal epidermal layers and in the follicle-like structures displaying a stronger signal the peripheral cells than in the inner cells (Figure 6c) [23].

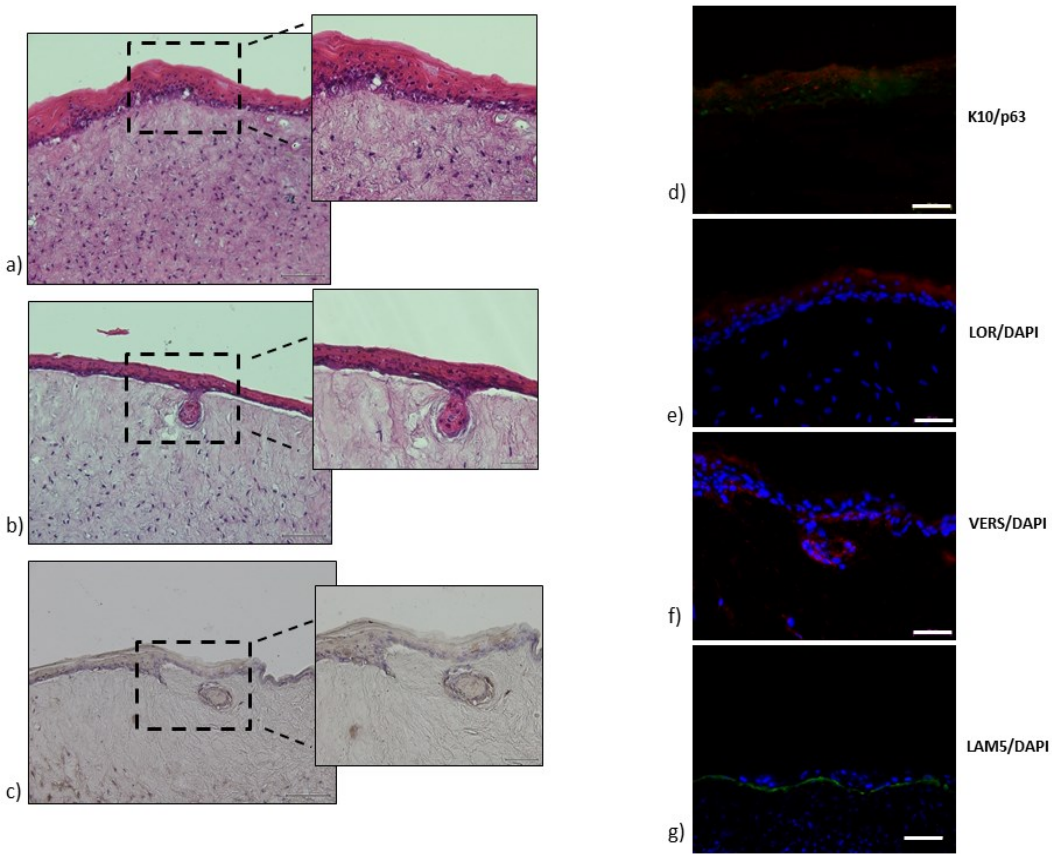

Figure 6. Histological analysis of 3D human skin equivalent model. a) H&E staining showed dermis and epidermis compartment separated by basal membrane. The dermis was highly cellularized, composed of dermal fibroblasts (violet) well distributed completely embedded in the endogenous ECM, assembled by cells themselves (pink); b) H&E staining of a follicle-like structure invagination inner the dermal compartment; it was clear the epidermal origin of follicle-like structure and the penetration of this structure inner the dermis; c) Immunohistochemistry for keratin19 (K19) (brown) with counter staining by using Mayer's hematoxylin; immunolabeling for epithelial markers as keratin 10 (K10) and p63, loricrin, versican, markers of stratified epithelial layers, and p63, typical marker used to evaluate the stemness of cell population , and Laminin 5, expressed by germinative layer at DEJ (d, e, f, g respectively). Cells was stained with DAPI. Bars in a-c) are 100 µm; bars in a-c) magnified images are 50 µm; bars in d-g) are 50 µm.

2.4 DISCUSSIONS

Actually, international cosmetic and pharmaceutical industries began to develop methods and skills for the realization of *in vitro* skin models in large scale for cosmetic testing and several applications [1], [2], [4].Therefore, studies conducted for the characterization of these 3D skin models commercially available, revealed that they although resembled native human skin, showed several limitations: indeed, these 3D skin models did not show a continuous cellular recycling of epithelial tissues, typical of native human epidermis, they exerted an ineffective barrier function for the inadequate lipids composition of the epidermal compartment and finally they lacked of a functional endogenous ECM as a stromal microenvironment able to support epidermal differentiation and stratification [1]. First of all, we realized a 3D human dermis equivalent model *in vitro* completely made up of endogenous extracellular matrix by HD-µTP aggregation in a maturation chamber after 5 weeks in dynamic culture conditions. Then, with the standardization of keratinocytes seeding procedure, we developed a full-thickness 3D human skin equivalent model *in vitro* having a thickness of 1 mm and a surface of 19,2 mm^2 completely made up of endogenous extracellular matrix. This model represents a real innovation in tissue engineering as an efficient 3D system that mimics all characteristics and features of native human skin. 3D-HSE allowed to overcome several problems and limitations associated with the 3D nature of the organotypic culture, such as difficulties in regulating distinct behavior of different cell types in the same construct [24]. Our 3D human skin system was obtained by setting the optimal conditions for keratinocyte extraction as well as their 2D expansion it is possible to preserve keratinocytes stemness and their capability to differentiate generating a full development epidermal layer, leading to the success of the epidermal compartment. By combining a dermal equivalent made up of completely endogenous ECM with keratinocytes cultured in serum-free conditions

and without feeder layer during the 2D expansion, 3D human skin models produced and assembles an endogenous ECM by primary fibroblasts that works as an optimal microenvironment with its mechanical features, providing support and anchorage for cells and chemical interactions, necessary for keratinocytes proliferation and differentiation. Finally, this human skin equivalent model can be employed as an effective alternative animal testing in order to substitute animals for drug and cosmetics screening.

2.5 REFERENCES

[1] F. Netzlaff, C.-M. Lehr, P. W. Wertz, and U. F. Schaefer, "The human epidermis models EpiSkin, SkinEthic and EpiDerm: an evaluation of morphology and their suitability for testing phototoxicity, irritancy, corrosivity, and substance transport," *Eur. J. Pharm. Biopharm. Off. J. Arbeitsgemeinschaft Pharm. Verfahrenstechnik EV*, vol. 60, no. 2, pp. 167–178, Jul. 2005.

[2] C. Faller, M. Bracher, N. Dami, and R. Roguet, "Predictive ability of reconstructed human epidermis equivalents for the assessment of skin irritation of cosmetics," *Toxicol. Vitro Int. J. Publ. Assoc. BIBRA*, vol. 16, no. 5, pp. 557–572, Oct. 2002.

[3] T. Hu, R. E. Bailey, S. W. Morrall, M. J. Aardema, L. A. Stanley, and J. A. Skare, "Dermal penetration and metabolism of p-aminophenol and p-phenylenediamine: application of the EpiDerm human reconstructed epidermis model," *Toxicol. Lett.*, vol. 188, no. 2, pp. 119–129, Jul. 2009.

[4] A. Coquette, N. Berna, A. Vandenbosch, M. Rosdy, and Y. Poumay, "Differential expression and release of cytokines by an *in vitro* reconstructed human epidermis following exposure to skin irritant and sensitizing chemicals," *Toxicol. Vitro Int. J. Publ. Assoc. BIBRA*, vol. 13, no. 6, pp. 867–877, Dec. 1999.

[5] A. El Ghalbzouri, P. Hensbergen, S. Gibbs, J. Kempenaar, R. van der Schors, and M. Ponec, "Fibroblasts facilitate re-epithelialization in wounded human skin equivalents," *Lab. Investig. J. Tech. Methods Pathol.*, vol. 84, no. 1, pp. 102–112, Jan. 2004.

[6] D. P. Bottaro, A. Liebmann-Vinson, and M. A. Heidaran, "Molecular signaling in bioengineered tissue microenvironments," *Ann. N. Y. Acad. Sci.*, vol. 961, pp. 143–153, Jun. 2002.

[7] J. W. Nichol and A. Khademhosseini, “Modular tissue engineering: engineering biological tissues from the bottom up,” *Soft Matter*, vol. 5, no. 7, p. 1312, 2009.

[8] F. Urciuolo, G. Imparato, C. Palmiero, A. Trilli, and P. A. Netti, “Effect of Process Conditions on the Growth of Three-Dimensional Dermal-Equivalent Tissue Obtained by Microtissue Precursor Assembly,” *Tissue Eng. Part C Methods*, vol. 17, no. 2, pp. 155–164, Feb. 2011.

[9] G. Imparato, F. Urciuolo, C. Casale, and P. A. Netti, “The role of microscaffold properties in controlling the collagen assembly in 3D dermis equivalent using modular tissue engineering,” *Biomaterials*, vol. 34, no. 32, pp. 7851–7861, Oct. 2013.

[10] C. Palmiero, G. Imparato, F. Urciuolo, and P. Netti, “Engineered dermal equivalent tissue *in vitro* by assembly of microtissue precursors,” *Acta Biomater.*, vol. 6, no. 7, pp. 2548–2553, Jul. 2010.

[11] Y. C. Ng, J. M. Berry, and M. Butler, “Optimization of physical parameters for cell attachment and growth on macroporous microcarriers,” *Biotechnol. Bioeng.*, vol. 50, no. 6, pp. 627–635, Jun. 1996.

[12] M. Rosdy and L. C. Clauss, “Terminal epidermal differentiation of human keratinocytes grown in chemically defined medium on inert filter substrates at the air-liquid interface,” *J. Invest. Dermatol.*, vol. 95, no. 4, pp. 409–414, Oct. 1990.

[13] M. Pruniéras, M. Régnier, and D. Woodley, “Methods for cultivation of keratinocytes with an air-liquid interface,” *J. Invest. Dermatol.*, vol. 81, no. 1 Suppl, p. 28s–33s, Jul. 1983.

[14] S. T. Boyce and R. G. Ham, “Calcium-regulated differentiation of normal human epidermal keratinocytes in chemically defined clonal culture and serum-free serial culture,” *J. Invest. Dermatol.*, vol. 81, no. 1 Suppl, p. 33s–40s, Jul. 1983.

[15] A. Page-McCaw, A. J. Ewald, and Z. Werb, “Matrix metalloproteinases and the regulation of tissue remodelling,” *Nat. Rev. Mol. Cell Biol.*, vol. 8, no. 3, pp. 221–233, Mar. 2007.

[16] I. Stamenkovic, “Extracellular matrix remodelling: the role of matrix metalloproteinases,” *J. Pathol.*, vol. 200, no. 4, pp. 448–464, Jul. 2003.

[17] V. M. Kähäri and U. Saarialho-Kere, “Matrix metalloproteinases in skin,” *Exp. Dermatol.*, vol. 6, no. 5, pp. 199–213, Oct. 1997.

[18] C. Casale, G. Imparato, F. Urciuolo, and P. A. Netti, “Endogenous human skin equivalent promotes *in vitro* morphogenesis of follicle-like structures,” *Biomaterials*, vol. 101, pp. 86–95, Sep. 2016.

[19] D. Larouche, K. Cuffley, C. Paquet, and L. Germain, “Tissue-engineered skin preserving the potential of epithelial cells to differentiate into hair after grafting,” *Tissue Eng. Part A*, vol. 17, no. 5–6, pp. 819–830, Mar. 2011.

[20] S. B. Mahjour, F. Ghaffarpasand, and H. Wang, “Hair follicle regeneration in skin grafts: current concepts and future perspectives,” *Tissue Eng. Part B Rev.*, vol. 18, no. 1, pp. 15–23, Feb. 2012.

[21] Y. Zheng, X. Du, W. Wang, M. Boucher, S. Parimoo, and K. S. Stenn, “Organogenesis From Dissociated Cells: Generation of Mature Cycling Hair Follicles From Skin-Derived Cells,” *J. Invest. Dermatol.*, vol. 124, no. 5, pp. 867–876, May 2005.

[22] D. R. Zimmermann, M. T. Dours-Zimmermann, M. Schubert, and L. Bruckner-Tuderman, “Versican is expressed in the proliferating zone in the epidermis and in association with the elastic network of the dermis,” *J. Cell Biol.*, vol. 124, no. 5, pp. 817–825, Mar. 1994.

[23] D. Larouche, C. Hayward, K. Cuffley, and L. Germain, “Keratin 19 as a stem cell marker *in vivo* and *in vitro*,” *Methods Mol. Biol. Clifton NJ*, vol. 289, pp. 103–110, 2005.

[24] B. Liu, Y. Liu, A. K. Lewis, and W. Shen, “Modularly assembled porous cell-laden hydrogels,” *Biomaterials*, vol. 31, no. 18, pp. 4918–4925, Jun. 2010.

Chapter 3.
Endogenous 3D human skin equivalent as a novel testing platform

3.1 INTRODUCTION

In this chapter, we deeply characterized our 3D endogenous human dermis and skin equivalent models demonstrating its effectiveness as responsive tissue system to external stimuli and to active compounds. We conducted a study on the Extracellular matrix (ECM) in order to evaluate its organization, composition and its dynamic changes during the assembling phase.

In fact, ECM, is not a merely "passive" matrix holding cells and tissues in place, but it has a functional importance as a dynamic repository for morphogens, cytokines and growth factors, which *in vivo* regulate several cellular processes recapitulating those found in the native tissues [1]–[4]. We observed cellular damage response as collagen and epithelial compartment re-arrangement and photo-protectants efficacy under simulated solar exposure. Our 3D human skin models best recapitulated a native 3D environment which the endogenous ECM explain a central role.

It is reasonable to argue that the 3D matrix commonly used as human skin equivalent (HSE) models include de-cellularized/de-epidermized dermis [5], [6], collagen type I [7], collagen-glycosaminoglycans [8], fibrin [9], fibroblast derived matrix [10], [11] , and synthetic polymers [12] do not mimic the complexity of native dermal compartment and its regulatory functions [5]. However, despite the success in generating 3D-HSE with a multilayered and differentiated epidermis, the complete recapitulation of the skin functionality, the rete ridge profile of the dermis-epidermis junction and the formation of a complete and functional skin

system have not been attained yet [13]. The functionality of our skin models is associated to the endogenous complex ECM network enriched of structural and elastic components. In fact, a functional and responsive ECM was composed of principal components as collagen, elastic fibers and glycosaminoglycans (GAGs) which, in turn, are synthesized, assembled and remodeled by cells.[1], [14], [15].

Dermal collagen and elastic fibers are ECM protein complexes produced by fibroblasts and involved in skin support and elasticity [16], while GAGs have various structural and physiological regulatory functions in the skin, including tissue water maintenance due to their water holding capacity [17]. Collagen comprises approximately 70-80% of the dry weight of the dermis is responsible for skin's tensile strength. The elastic fibers network occupies approximately 2-4 % of the dermis volume, provides resilience and suppleness. GAGs are composed of specific repeating disaccharide units attached to a core protein as proteoglycans, widely distributed throughout the skin; hyaluronic acid is the GAG most represented in the human skin [18]. GAGs bind up to 1000 times their volume and the skin hydration is highly related to their content and distribution [18], [19].

It is known that the ageing *phenomenon* altered texture and structure of skin by molecular alterations in protein, lipids and water. Changes in dermal structural proteins have been investigated: changes in the amount and architecture of collagen, elastin and GAGs have been described in intrinsic ageing (chronological) and extrinsic ageing (related to the photo-exposition and photo-damage) [18], [20]. In the chronologically aged skin, the rate of collagen synthesis, collagen solubility, density and thickness of collagen bundles all decrease [18], [20] while also the UV exposition has a significant consequences on collagen network and tissue homeostasis [2], [21]. Therefore, in the intrinsic ageing, elastin exhibits numerous age-related changes, including fragmentations and slow degradation of

elastic fibers with a decrease in number and diameter. On the contrary, the photo-exposition generates abnormal localization of fibers in the upper dermis, with an elastotic accumulation [16], [18]. Regarding GAGs and hyaluronic acid (HA), recent studies document that the total level remains constant in the dermis with the ageing. The major age-related change is the increasing avidity of HA. Such intercalated HA may have diminished the ability to take on water of hydration. These events, parallel to the progressive cross-linking of collagen, contributing to dehydration, atrophy and loss of elasticity [17], [20], [22]. However, in photo-aged skin, GAGs and HA increase, with a paradoxical increase of total water, even if photo-damaged skin appears dry and wrinkled. Probably, proteins became more hydrophobic and folded and GAGs are clumped on elastotic material with a minor interaction with water molecules [17], [18], [20].

In the first part of this chapter, in order to evaluate changes and evolution of ECM composition and proprieties during the time, we performed a quantitative assay for quantification of collagen, elastin and GAGs content in our 3D human dermis and skin equivalent. Our results confirmed a dynamic maturation of our model during the assembling phase, with a progressive increase of structural and functional components of ECM.

In the second part of this chapter, among the oxidative stresses, we put the attention on photo-damage UVA-induced both on dermal and epidermal compartment of our organotypic models. In particular, the UVA-induced oxidative stress in epidermal compartment determinates stem cell damage that, in turn, is responsible of epidermal senescence [23], [24], with an irregular pigmentation, wrinkles, laxity, loss of hydration [25]. The penetration of UVA radiations into the skin can initiate detrimental photochemical reactions able to remodel the ECM by increasing matrix-metalloproteinase (MMPs), reducing structural collagen and

affecting cell signaling and phenotype [26], [27]. The capability to restore totally or partially the physiological conditions of the tissue depends on several parameters, including the threshold dose, time exposition, age and type of skin UVA exposed [28]. In this study, we observe the feasibility of using our endogenous human skin equivalent to confirm the well-known photo-protective effect of retinoic acid on UVA induced damages and a powerful crosstalk between dermal and epidermal compartment, by a mutual interaction between fibroblasts and keratinocytes. In fact, the realization of our endogenous full thickness HSE presenting responsive endogenous dermal ECM, biologically active epidermal cells and physiological wettability able to sustain a topical administration [29], recapitulating the complex homeostatic equilibrium and dynamical reciprocity between the cellular and extracellular space, as an essential tool to perform a complete study of *in vitro* photo-repair. Such results suggest a possible regulatory role of the dermis in our 3D-HSE, highlighting that it represents an instructive environment, in which the inductive signals and germinative phenotypes of the basal keratinocytes can be preserved, raising some doubts on the use of exogenous matrices for building-up functional *in vitro* organo-models.

3.2 MATERIALS AND METHODS

3.2.1 3D Human skin equivalent model realization

The development of 3D endogenous HSE were performed by bottom-up tissue engineering strategy widely described in the previous chapter (see chapter 2). Briefly, primary human dermal fibroblasts extracted by human biopsy were sub-cultured into 150 cm^2 tissue flasks in culture medium (Minimum Essential Medium with Earle's salts, Microgem) containing 20% fetal bovine serum (FBS), 100mg/ml L-glutamine, 100 U/ml penicillin/streptomycin (P/S), and 0,1 mM non-essential amino acids) with a density of $8x10^3$ cell/cm^2 and maintained at 37 °C, 5% CO_2 and humidity 90%. Human dermal microtissue precursor (HD-µTP) were produced by seeding HDF of passages 5-9 on gelatin porous microcarriers crosslinked at 4% with D-(+)- Glyceraldehyde (Sigma Aldrich), in a spinner flask (Integra Bioscience) for 9 days and then transferred into the maturation chamber to allow their molding in disc-shaped tissue-construct such as Human Dermis Equivalent (HDE) (1 mm in thickness, 5 mm in diameter) as previously described. Maturation of HDE was carried out until 6 weeks in dynamic conditions by placing the maturation chamber on the bottom of a bioreactor (Bellco) operated at 60 rpm at 37 °C, 5% CO_2 and humidity 90%. The medium was changed every 2 days and at each medium change ascorbic acid (TCI) was added at a concentration of 50µg/ml. At the end of the optimal maturation time, chambers were opened and HDE were extracted and prepared for primary keratinocytes seeding. As described in the chapter 2, human keratinocytes were obtained from biopsy and cultured into 150 cm^2 tissue flasks with a density of $2x10^4$ cell/cm^2 in culture medium KGM_2 (Promocell) composed of 0.1% transferrin, 0.1% epinephrine, 0.1% hydrocortisone,0.1% insulin, 0.1% H-EGF, 0.4% BPE, 5% FBS, 1% P/S and calcium chloride at 0.06 µM and maintained 37 °C, 5% CO_2 and humidity 90%. 3D-HDE were prepared for keratinocytes seeding by a human fibronectin coating for 45

minutes and during this time, keratinocytes were washed and trypsinized. Cells were counted (150,000 cells/samples of 5 mm diameter), seeded on the human dermis models surface and maintained in submerged culture conditions for 6 days in order to allow cell adhesion and proliferation. After 6 days of submerged conditions, the cultures were raised to the air/liquid interface for 14 days in culture medium with a different composition (0.1% transferrin, 0.1% epinephrine, 0.1% hydrocortisone, 0.1% insulin, 1% P/S, without EGF and BPE and with calcium chloride at 1.88 µM) in order to induce and stimulate differentiation and stratification of epidermis.

3.2.2 Quantitative biochemical assay of ECM components in 3D HDE and HSE during the culture time

Quantitative extraction of main components of ECM was performed on our endogenous 3D models (both HDE and HSE) during the time of culture in order to evaluate the contribute of collagen, elastin and GAGs in the ECM composition. These measurements were obtained for our 3D skin system and compared with human breast skin data. 3D-HDE samples were collected at different time of maturation as 4, 5, 6 and 9 weeks of culture, while 3D-HSE samples were collected at the end of air-liquid interface time culture. All data were compared with human breast skin (25 years old) samples. Samples were prepared for protein extraction according to manufacturing procedures, using the extraction assay dye-binding methods designed for the analysis of collagen (Sircol Soluble Collagen Assay), elastin (Fastin Assay) and GAGs (Blyscan Assay) content. All assay kits were purchased from Biocolor, UK.

Sircol soluble collagen assay procedure: The Sircol Assay is a quantitative method of pepsin-acid extraction of soluble collagens. This assay is suitable for monitoring

collagen produced and *in vitro* ECM and recovered from soft tissues, cartilages and fluids.

3D-HDE samples at 4, 5, 6 and 9 weeks of maturation time culture, and 3D-HSE were weighed and then incubated with a pepsin solution 0,1 mg/ml in acetic acid 0,5 M (pepsin-acid extraction buffer) overnight at 4°C to solubilize collagen of ECM. 100 µl of each sample were used for quantitative tests. It was prepared:

- reagent blanks using 100 µl of extraction buffer;
- collagen standards using aliquots containing 10, 20, 30, 40 and 50 µg of the collagen reference standard provided from the kit, and make each standard up to 100 µl using the same extraction buffer;
- test samples using 100 µl of volume of lysed samples

To each tube was added 1 ml of Sircol Dye Reagent in order to fully saturate the collagen molecules within a 100 µl sample volume. Tubes were mixed by inversion and placed in a gentle mechanical shaker for 30 minutes to allow the formation collage-dye complex. Samples were centrifuged at 12000 rpm. for 10 minutes and carefully drained by inversion. 750µl ice-cold Acid-Salt Wash Reagent were added gently on to the collagen-dye pellet to remove unbound dye and then samples were centrifuged again at 12000 rpm for 10 minutes. In order to allow collagen release from collagen-dye complex, 250 µl were added to all samples and mixed with a vortex mixer. When all of the bound dye was dissolved (after 5 minutes), the samples are ready for measurement. Finally, 200 µl of each sample were transferred to individual wells of a 96 micro well plate, and the measurement of absorbance was obtained by setting the microplate reader (Pelkin Elmer) to 555nm. Each sample was normalized with the reagent blanks and it was determined the µg of collagen/mg wet samples using the collagen standards.

Fastin elastin assay procedures: The Fastin Elastin Assay is a quantitative method for the analysis of elastin extracted from mammalian sources by 5,10,15,20-tetraphenyl-21H,23H-porphine tetra-sulfonate (TPPS).

3D-HDE samples at 4, 5, 6 and 9 weeks of maturation time culture and 3D-HSE were weighed and then incubated with 750 µl of 0,25 M oxalic acid at 100°C for 1 h. After the first extraction, samples were centrifuged at 10000 rpm for 10 minutes and liquids were pipetted off and retained for the quantitative analysis. The residual tissue was heated again with 750 µl of 0,25 M oxalic acid at 100°C for 1 h. Up to three heat extractions should be initially used to check that complete solubilization of the tissue elastin has occurred. 100 µl of each sample were used for quantitative tests.

It was prepared:

- reagent blanks using 100 µl of extraction buffer;
- elastin standards using aliquots containing 12,5, 25, 50, 75 µg of the elastin reference standard provided from the kit, and make each standard up to 100 µl using the same extraction buffer;
- test samples using 100 µl of volume of lysed samples

According to kit procedure, to each tube was added 1 ml of an equal volume of Elastin Precipitating Reagent in order to fully saturate the elastin molecules within a 100 µl sample volume. Tubes were mixed by inversion and leaved for 15 minutes to complete precipitation of elastin. Samples were centrifuged at >10000 x g for 10 minutes and liquids were drained. To all samples was added 1 ml of Dye Reagent and were mixed by inversion and leaved for 90 minutes on a gentle shaker. After, test tubes were centrifuged at >10000 x g for 10 minutes. When

liquids were pipetted off, the elastin-dye complex could be observed as a reddish-brown deposit in the bottom and inside lower wall of the tube.

To each tube was added 250 µl of Dye Dissociation Reagent to release the dye into solution with the aid of a vortex mixer. Finally, 200 µl of each sample were transferred to individual wells of a 96 micro well plate, and the measurement of absorbance was obtained by setting the microplate reader (Pelkin Elmer) to 513 nm (blue-green color). Each sample was normalized with the reagent blanks and it was determined the µg of elastin/mg wet samples using the collagen standards.

Blyscan GAGs assay procedures: The Blyscan Assay is a quantitative method for the analysis of sulfated proteoglycans and GAGs. The dye label used in the assay was 1, 9-dimethylmethylene blue and the dye is employed under conditions that provide a specific label for the sulfated polysaccharide component of proteoglycans or the protein free sulfated glycosaminoglycan chains.

3D-HDE samples at 4, 5, 6 and 9 weeks of maturation time culture, and 3D-HSE were weighed and incubated with papain extraction reagent composed of 400 mg sodium acetate (Sigma Aldrich), 200 mg EDTA (Sigma Aldrich), disodium salt (Sigma Aldrich) and 40 mg cysteine HCl (Sigma Aldrich) dissolved in 50 ml of a 0.2 M sodium phosphate buffer, (Na_2HPO_4-NaH_2PO_4), pH 6.4 and 250 µl of papain suspension (Sigma Aldrich), containing 5 mg of the enzyme. 1 ml of Papain extraction reagent was added to test samples and heated at 65° C for 3 h. Samples were centrifuged at 10,000 x g for 10 minutes and supernatants were collected for Blyscan assay protocol. It was necessary:

- reagent blanks using 100 µl of extraction buffer;
- GAGs standards using aliquots containing 1, 2, 3, 4, 5 and 6 µl of the reference standard.

Make each standard up to 100 µl using the same solvent as the Reagent blanks. The standards and the reagent blank are used to produce a calibration curve.

According to kit procedure, to each tube was added 1 ml of an equal volume of Blyscan dye reagent in order to fully saturate the elastin molecules within a 100 µl sample volume. Tubes were mixed by inversion and leaved for 30 minutes on a gentle shaker. During this period a sulphated glycosaminoglycan-dye complex will form and precipitate out from the soluble unbound dye. Test tubes were centrifuged at 12000 rpm for 10 minutes. Carefully, tubes were inverted and drained, and was added 500 µl od Dissociation reagent in order to allow dye release. When all of the bound dye had been dissolved, (usually within 10 minutes), samples were centrifuged at 12000 rpm for 5 minutes to remove foam. 200 µl of test samples were transferred to individual wells of a 96 micro well plate. Avoid rapid pipetting as foaming can cause abnormal absorbance readings setting microplate reader (Pelkin Elmer) to 656 nm. Each sample was normalized with the reagent blanks and it was determined the µg of GAGs/mg wet samples using the collagen standards.

3.2.3 Histological evaluation of ECM components in 3D-HDE and HSE during the culture time

In order to estimate the main components contents of ECM by an ultrastructural analysis, immunofluorescence and histological staining on tissue slices were performed. 3D-HDE samples at 6 weeks of maturation time culture, and 3D-HSE at the end of air-liquid interface culture, were fixed with 10% neutral-buffered formalin fixative for 2–4h at RT and rinsed twice with PBS buffer solution. After the fixation and dehydration procedure, samples were embedded in paraffin to be sectioned and stained with Sirius Red (PSR) and immunolabelled for hyaluronic acid.

Elastin content was estimated by immunofluorescence for α-tropoelastin on frozen section both of 6 weeks 3D-HSE and HSE at the end of air-liquid interface. The samples were fixed in a solution of 4% paraformaldehyde for 30 minutes at RT, rinsed twice with PBS buffer solution and soaked into a sucrose water solution (2M). After 24 h samples were included in Tissue Tek (Killik) in a suitable mold (Peel-A, Ted Pella INC) and submerged in liquid nitrogen vapors for 1 minute and then stored at -80°C. All samples were cut in slices 5 µm in thickness by using a cryomicrotome (Leica CM 1850). The cut was oriented so as to view the cross section of the samples.

Picrosirius red staining

To estimate collagen content, tissue section was stained with Sirius Red (PSR) (Sigma Aldrich) following standard procedure and analyzed by an optical microscope (BX53; Olympus).

Polarized light images of samples stained with PSR alone were acquired with an inverted microscope (BX53; Olympus) with a digital camera (Olympus DP 21). A linear polarizer was placed between the light source and the specimen, while the analyzer was installed in the light path between the specimen and the camera. It is known that the color of collagen fibers stained with PSR and viewed with polarized light depends upon fiber thickness; as fiber thickness increases, the color changes from green to red. For quantitative analyses PSR images were analyzed by using imageJ software. In order to quantitatively determine the proportion of mature (red) and immature (green) collagen fibers, we resolved each image into its hue, saturation and brightness (HSB) components by using ImageJ software “color threshold” function. Only the hue component was retained and a histogram of hue frequency was obtained from the resolved 8-bit hue images, which contain 256 colors. We used the following hue definitions; red

0-51, green 52-120 [29], [30]. The analysis was performed on 20 PSR stained sections of sample. About 5 region of interests (ROIs) were examined for each section.

Immunofluorescence analysis

For the evaluation of GAGs content, an immunofluorescence for hyaluronic acid, the most represented component of GAGs molecules, was performed on paraffin embedded 6 weeks 3D-HDE and on 3D-HSE tissue slices. Histological sections were deparaffinized and permeabilized with 0.2% Triton X-100 (Sigma Aldrich) in PBS and incubated with PBS/BSA (Bovine Serum Albumin, Sigma Aldrich), 6% as blocking solution for 2 h in wet conditions. Sections on slices were incubated with primary anti-hyaluronic acid antibody (1:50, sheep polyclonal, Abcam) overnight at 4°C. Secondary antibody used was 546 Rabbit Anti-Sheep IgG H&L (Abcam). Secondary antibody was diluted 1:500 in PBS/BSA 6%. Nuclei were stained with DAPI (1:10000, Invitrogen) incubated for 15 minutes at RT.

The assessment of elastin content was performed by mean immunofluorescence for α-tropoelastin on frozen section of our samples. Histological section was permeabilized with 0.01% Triton X-100 in PBS/BSA 3% for 1h at room temperature. Subsequently, the slices were incubated with an alkylation reaction solution composed of Tris-buffer 20 mM/DTT 50 mM/Guanidine-HCl 6 M for 15 minutes. Tissue slices were then incubated with iodoacetamide solution 100 mM in order to protect –SH free groups of elastin cysteines. Subsequently, tissue slices were rinsed and incubated with primary antibody anti-α tropoelastin (1:50, policlonal, EPC) for 3 h at RT. The secondary antibody was incubated for 2 h at RT. The secondary antibody used was Alexa Fluor 568 goat-anti rabbit (Life Technologies) was diluted 1:500 in PBS/BSA 3% blocking solution. Nuclei were stained with DAPI and Sytox Green (1:10000, Invitrogen).

3.2.4 Mechanical analysis of 3D HDE and HSE models by means of non-destructive nanoindentations methods

Nano-indentation tests were performed on 3D-HSE at the end of air-liquid interface and on 3D-HDE samples after 4, 5, 6, 9 weeks of maturation by means of Piuma Nano-Indenter (Optics).

Indentation is a versatile, quantitative and non-destructive technique for measurements of the mechanical behavior of tissue [31], [32]. Based on the indentation of surfaces using probes with a well-defined geometry, the elastic and viscoelastic constants of examined materials can be determined by relating indenter geometry and measured load and displacement to parameters which represented stress and deformation [33]. In particular, indentation instruments commercially available have led to the optimization of testing and analyzing methods for deriving materials elastic and plastic proprieties, such as elastic modulus and hardness. For these reasons, the constitutive response of soft tissue and biomaterials differs from that of linearly elastic and isotropic engineering materials. First, the former generally exhibit non-linear stress-strain (σ-ε) behavior [33], [34]; second, their mechanical response is often characterize by a significant time-dependence, which is typically described by empirical parameter viscoelastic models [33], [35], [36]; third, these materials are likely to be both microscopically and microscopically anisotropic, especially in case of biological tissue [33], [37].

Piuma is a displacement-controlled nanoindenter machine including a controller, an optical fiber and a spherical probe. The probe is attached to a spring cantilever that it is connected to the end of optical fiber in order to measure the cantilever deflection. The applied indentation depth (piezo motor movement) and the actual indentation depth are different. The applied indentation depth is a combination of the cantilever deflection and the actual indentation depth; therefore, the actual

indentation depth is calculated by subtracting of the measured cantilever deflection from the displacement of the probe from the point of contact [31]. The analysis of spherical nano-indentation data is generically based on the Hertz model, assuming a linear elastic and isotropic material response [33], [38], [39]. In order to characterize material viscoelastic proprieties and to study the analysis of spherical nano-indentation data, we used the Hertz model and a variant of the nano-epsilon method (εM) [33]. In this method for strain rate viscoelastic material characterization of soft biomaterial (as biological tissue), it was introduced a new definition of indentation stress (σ_{ind}) and strain (ε_{ind}) that allowed us to obtain indentation-stress curved at constant strain rate from load-displacement measurements at constant displacement rate, as follows:

$$\sigma_{ind} = \frac{P}{R\sqrt{h}R} \quad (1)$$

$$\varepsilon_{ind} = \frac{4h}{3R(1-\upsilon^2)} \quad (2)$$

where *P* was the load, *R* the radius of spherical indenter tip, ah *h* was the penetration depth.

The ratio $\sigma_{ind}/\varepsilon_{ind}$ directly returns the sample modulus *E*. Each sample was indented using a cantilever with a stiffness of 59.2 N m^{-1}, the indentation depth was about 10 mm during each indentation test in different areas of the sample. The tip radius was 77 μm and the connected optical fiber measured the cantilever deflection during indentation.

3.2.5 Induction of damage on 3D-HDE and HSE samples

Irritant tests were performed on our 3D human skin platforms following H_2O_2 treatment and UV exposure and the extent of damage was evaluated by mean cytosolic ROS (Reactive Oxygen Species) assay.

Reactive oxygen species (ROS) are chemical compound that are formed upon incomplete reduction of oxygen and includes the superoxide anion (O2–), hydrogen peroxide (H_2O_2) and the hydroxyl radical (HO•). ROS mediate the toxicity of oxygen because of their greater chemical reactivity with other molecules regard to oxygen. In fact, ROS operate in signaling through chemical reactions with specific atoms of target proteins that lead to covalent protein modifications [40]. The effectiveness of our 3D-skin system was tested by hydrogen peroxide treatment as a stress substance, and by UV exposition and cellular damage was evaluated by cytosolic ROS assay. It was used an antioxidant substance as the ascorbic acid and retinoic acid that act as protectant and scavenger of ROS.

Oxidative stress by means of H_2O_2

For stress induced by hydrogen peroxide, samples of 3D-HDE at 6 weeks of maturation, were extracted from maturation chamber the day before the experiment in order to allow contraction of ECM. The day of experiment control samples were incubated with ascorbic acid 250 µM for 2 h. After the incubation, samples were washed with PBS and incubated with 10 µM CM-DCFDA (5--6)-chloromethyl-2,7 dichlorodihydrofluoresceine diacetate, (ROS indicator, Invitrogen) at 37°C for 60 minutes protect from the light. After incubation, the samples were washed in PBS and incubated with H_2O_2 400 µM for 30 minutes in optimal cell condition. Subsequently, samples were incubated with appropriate

medium and maintained at 37°C and finally were collected at 5 minutes from treatment. Samples were divided into three groups:

- Control (not H_2O_2 treated and not protected);
- H_2O_2 (H_2O_2 treated and not protected);
- H_2O_2 Asc. Ac. (H_2O_2 treated and ascorbic acid protected);

Photo-damage by UVA irradiation

For the cellular stress induced by UV light exposition, 3D-HSE samples were exposed to UVA radiations by using a UVA lamp in order to simulate solar exposure. The samples were accommodated in transwell and irradiated in PBS solution for 15 minutes at final power of 20 Joule/cm^2. The UVA lamp (3UVP lamp 115V 60Hz, Thermo Scientific) was mounted on a stable support allowing an exposure distance of 2 cm from the sample surface. Samples sterility was guaranteed by performing irradiation under the biological hood.

Antioxidant and photo-protective compounds

For our experiments 3D-HSE samples were exposed to UVA radiations and retinoic acid solution 1 µM as positive control was used. Treatment with the protectant was performed 4 h before UVA exposure by adding 900 µl retinoic acid in the insert of transwell and 5 µl on the top of epidermal layer for the topic and systemic application and by adding 5µl on the top of epidermal layer for only topically application. To avoid the formation of phototoxic products, immediately before performing UVA irradiation, culture medium was withdrawn and substituted with fresh PBS solution. At the end of 4 h of pre-treatment, samples

were incubated with CM-DCFDA (5--6)-chloromethyl-2,7 dichlorodihydrofluoresceine diacetate, (ROS indicator, Invitrogen) 10 µM at 37°C for 60 minutes protect from the light in order to estimate the rate of oxygen species induced by UV radiations. Samples were divided into three groups:

- Control (not UVA exposed and sunscreen not treated);
- UVA (UVA exposed and sunscreen not treated);
- UVA Ret T&S (UVA exposed and topic&systemic retinoic acid treated);
- UVA Ret Top (UVA exposed and topic retinoic acid treated);

At the end of UVA exposures PBS solution was removed and fresh medium with or without retinoic acid was added.

The UVA-induced damage and the protecting effects of retinoic acid were evaluated 6 and 72 h after UVA exposure for all samples.

Histological analysis

For the evaluation of extent of ROS induced damage, samples were prepared for embedding in Tissue Tek (Killik Bio-optica) after fixation in a solution of 4% paraformaldehyde for 30 minutes at RT and soaked in a sucrose water solution (2M) for 24 h before the inclusion. All samples were cut in slices of 5 µm in thickness by using a cryomicrotome (Leica CM 1850), nuclei stained with 4',6-diamidin-2-fenilindolo (DAPI, 1:10000, Invitrogen). Tissue slices of samples treated with H_2O_2 and UVA exposed were directly closed with 50 % Glycerol solution (Sigma Aldrich).

To quantitatively analysis, images were processed by using ImageJ software and the green signal (ROS indicator excitation at 485 nm) was normalized to the cell number.

For the evaluation of cellular damage UVA-induced on epithelial and dermal compartment of 3D-HSE, mature and immature collagen morphology was assessed by staining 5 µm transverse sample sections with PSR staining (Sigma Aldrich).

All images were acquired with an inverted microscope (BX53; Olympus) with a digital camera (Olympus DP 21). For the PSR images analysis, A linear polarizer was placed between the light source and the specimen, while the analyzer was installed in the light path between the specimen and the camera. Quantitative imaging analyses were performed as previously reported [41].

Immunofluorescences analysis

For immunofluorescences analyses, the 5 µm thick slices were incubated for 3 h at room temperature with primary antibodies followed by incubation with the appropriate secondary antibody for 2 h at RT. The primary monoclonal antibodies used in this study include: anti-matrix metalloproteinase-1 antibody (1:200, polyclonal, Abcam), anti-matrix metalloproteinase-9 antibody (1:200, monoclonal, Abcam), anti-ki67 antibody (1:50, polyclonal, Abcam), anti-p63 monoclonal antibody (1:50, monoclonal, Invitrogen), anti-active Caspase-3 antibody (1:150, monoclonal, Abcam) and anti-keratin 10 antibody (1:500, polyclonal, Covance). The secondary antibodies used were: Alexa Fluor 568 goat anti-rabbit, Alexa Fluor 568 goat anti-mouse, Alexa Fluor 488 goat anti-mouse and goat anti-rabbit (Life Technologies), all secondary antibodies were diluted 1:500 in PBS/BSA 3%. The cell nuclei were detected by DAPI staining (1:10000, Invitrogen) or by Sytox Green staining (1:10000, Invitrogen). The samples were investigated by using optical microscope (BX53; Olympus). To quantitatively analyze MMPs, p63, ki67 and active caspase-3 in each sample, images were processed by using ImageJ software and the signal was normalized to the cell number. Cells were counted by using the

software function “Analyze particles”. The analysis was performed on 3 independent experiments, 30 stained sections for samples were analyzed and 10 regions of interests (ROIs) were chosen.

Second harmonic generation imaging and texture analysis

Sample slices 50 μm thick were prepared for SHG imaging. Samples were investigated by confocal microscopy (TCS SP5 II Leica, Milano, Italy) combined with a MPM where the NIR femtosecond laser beam was derived from a tunable compact mode-locked titanium: sapphire laser (Chamaleon Compact OPO-Vis, Coherent) as widely described in the chapter 2. The SHG images, with a size of 200 x 200 μm, were acquired with a resolution of 12 bit, 1024x1024 pixel by using a 40X N.A. 1.25 objective. To quantitatively assess the collagen-related changes, we performed GLCM texture analysis by using ImageJ plug-in “Texture” on SHG images. The analysis was performed on 3 independent experiments as reported in the previous paragraph. A running neighbor index allowed calculation of a GLCM matrix *per* neighbor index *per* SHG image. In detail, we evaluated the correlation feature; if the correlation fell off sharply with pixel distance, the collagen matrix presented distinct, linear fibrils; if it remained elevated as pixel distance was increased, the collagen matrix showed a less defined fibrillar structure. In this work, we calculated the correlation curve for distances ranging from 1 to 200 pixels (corresponding to 1-40 μm) in the horizontal and vertical direction of each optical section that covered a length of interest of 40 μm. In such spatial windows the distance at which the correlation function fell off represented the correlation length of the texture. In particular the correlation curve was calculated *vs.* the neighbor index and the correlation length was obtained by fitting data with an exponential low [2], [42].

Statistical analysis

Data is expressed, as mean ± SD. Differences between groups were determined using a one-way analysis of variance with ANOVA tests. Significance between groups was established for $p < 0.01$.

3.3 RESULTS AND DISCUSSION

3.3.1 Biochemical, mechanical and histological analysis of 3D-HDE and HSE during the culture time

In order to evaluate main ECM components during the culture time, biochemical quantitative assays were performed both on endogenous 3D-HDE and 3D-HSE, at different weeks of maturation. We quantified the µg of collagen, α-elastin and GAGs for each mg of wet sample. Since primary fibroblasts used for the fabrication of dermal compartment were extracted from breast human biopsy, quantitative analysis was performed also on breast human skin in order to evaluate the efficiency of quantitative test. We assessed by histological evidences that the contribution of epithelial layer was negligible (about 0,004 %) compared to the dermal compartment and we weighted all samples entirely, including the *epithelium*. As showed in the Figure 1, collagen, elastin and GAGs amounts followed a similar trend: all main ECM components increased during the culture time, from 4 to 6 weeks of maturation. These data suggested that fibroblasts of dermal compartment assembled and organized ECM enriching it of structural and elastic proteins during the maturation phase. Furthermore, it was interesting to observe a depletion of collagen and elastin (Figure 1a and b) and an increment of total GAGs in HDE 9 WK samples (Figure 1c). After 14 days of air-liquid interface (HSE 6+3 WK samples) all ECM components levels returned to values similar to HDE 6 WK sample.

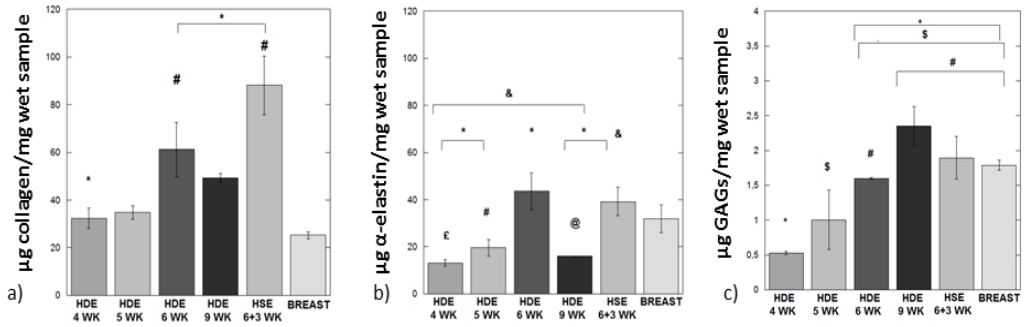

Figure 1. Quantitative assay for main ECM components. Total collagen (a), elastin (b) amd GAGs content in our 3D-HDE and HSE over the time of culture. Breast human skin was used to test the effectiveness of the quantitative assay. (*,&,#, $ p<0.0001).

The increment of ECM components content was confirmed also by histological analysis performed on 5 weeks 3D-HDE and 3D-HSE samples, stained for PSR, in order to evaluate collagen content, and immunolabelled for hyaluronic acid and α-tropoelastin to evaluate GAGs and elastin amount, respectively. The Figure 2 showed the progressive increment of protein content over the time for 5 weeks 3D-HDE and for 3D-HSE at the end of air-liquid interface condition.

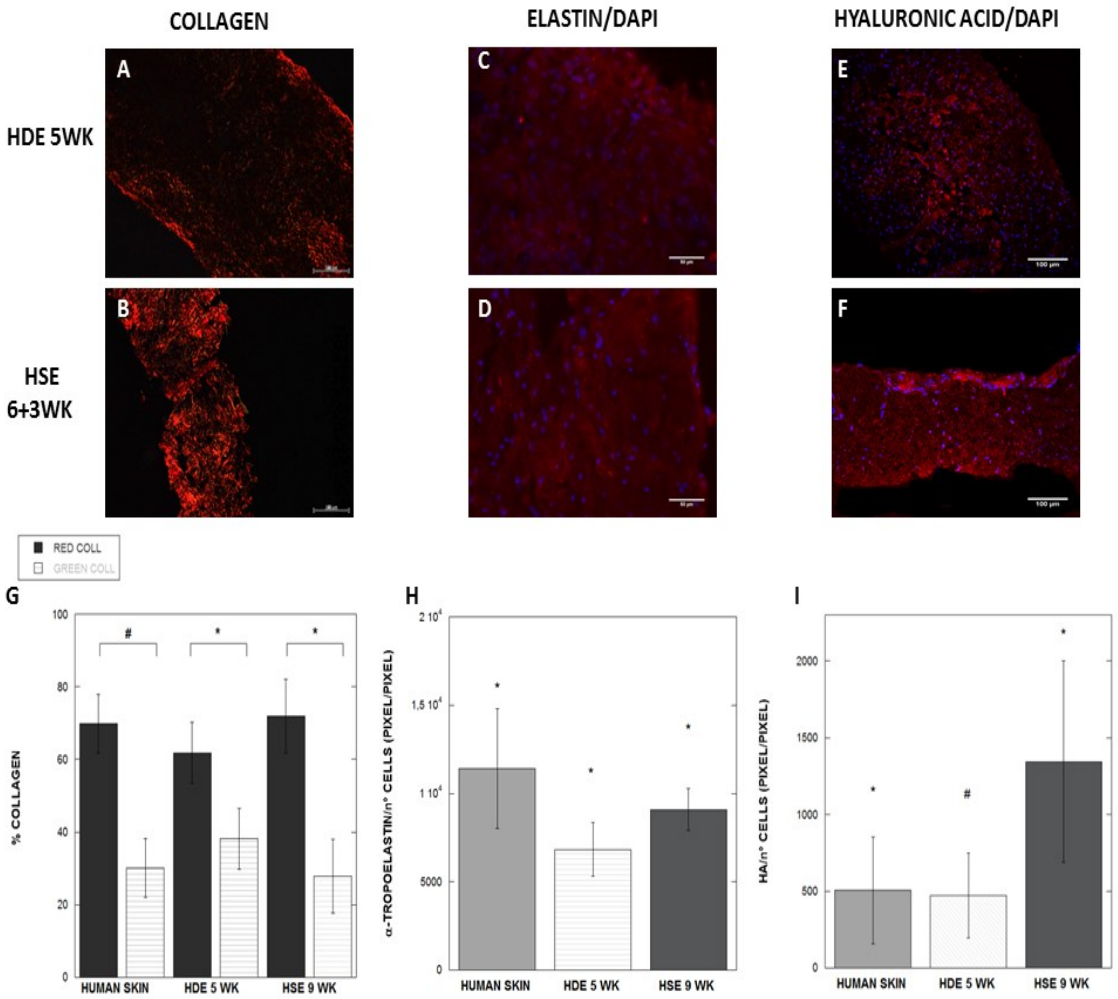

Figure 2. Biochemical quantitative analysis on histological sections of ECM components. Collagen fibers staining with PSR, immunolabelling for α-tropoelastin and hyaluronic acid on 5 weeks 3D-HDE and on 3D-HSE (A and B; C and D; E and F, respectively). Bars in A,B, E, F are 100µm; bars in C, D are 50 µm. Quantitative evaluation by imaging analysis using ImageJ software for each histological section (G, H, I). (*, # p<0.001).

In order to better study the evolution of our samples over the time and the culture conditions, we evaluate also mechanical proprieties of ECM by nano-indentations analysis. The skin behaves as a viscoelastic material, which biomechanical function depends on the concentrations, configurations and type

of components within its matrix, as collagen, elastic fibers and sulfated GAGs [43]. Nano-indentation is a non-destructive technique that achieves measurement of the mechanical behavior of soft tissue [31]. In particular, the probe of Piuma directly in contact with the surface, pushed onto material and then retracted, recording load (*P*) and penetration depth (*h)* over the time (*t*). Among all mechanical tests known, the main limitation of nano-indentation is the inability to obtain information about biomaterial bulk, but despite these handicaps, we employed this method for viscoelastic characterization of our tissues since we were interested to the superficial mechanical proprieties using a non-destructive method, with the possibility to follow the dynamic changes of mechanical characteristics over the time also under sterile conditions, avoiding sacrificing the sample. The observation emerged from quantitative assays and histological analysis, were confirmed by the nano-indentation data (Figure 3) that revealed, as we expected, an increasing of Young's Modulus both of 3D-HDE and 3D-HSE samples analyzed over the time of culture, from 4 to 9 weeks in maturation chamber indicating an assembling *phenomenon* of ECM during the time [44].

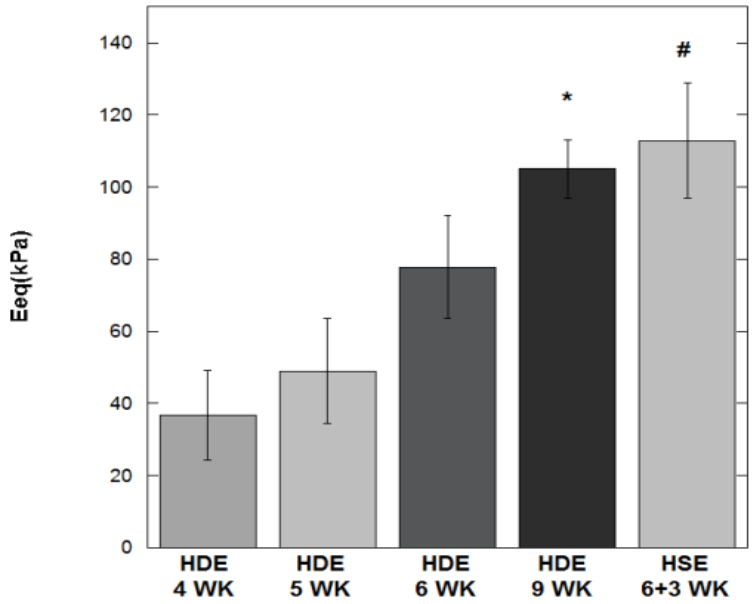

Figure 3. Mechanical proprieties of 3D human dermis and skin equivalent model over the time and the culture conditions. Young's Modulus (E) was expressed in kPa. (*, # indicated not significantly differences).

Taken together, these data suggested an evolution of ECM assembling during the culture period, from 4 weeks to the end of process, at 14 days of air-liquid interface (HSE 6+3 WK). It was interested to observe an increasing trend of ECM components amount that dynamically changed over the time. Quantitative assays showed also a depletion of collagen and elastin content from 6 weeks to 9 weeks in 3D-HDE samples, and, on the contrary, an increase of total GAGs content. These results could be suggested the establishment of a stress condition or of an ageing *phenomenon* for long time culture inside the maturation chamber which probably leaded to a remodeling of ECM. In fact, as it is known from the literature, elastin and collagen fibers represent the major components of the ECM but many degradative mechanisms are thought to operate systemically as a consequence of

a stress conditions or age-related *phenomena* leading to a progressive degradation and fragmentation of the collagenous and elastic fibers network, with significant changes in ECM structure and composition [45] [46]. On the contrary, GAGs increased during the time until reaching the maximum content (about 2,5 µg/mg of wet samples) at 9 weeks, before returning to lower values, similar to those of 5 and 6 weeks HDE samples. This trend might be explained considering the establishment beginning of a stress condition associated to the long-time culture inside the maturation chamber over 6 weeks. In fact, GAGs content and hyaluronic acid amount underwent an increase in pathological conditions, as photo-damage, wound healing, acute and chronical inflammation [17]–[21]. In HSE 6+3 WK samples, all ECM components returned to values close to 5 and 6 weeks of maturation. Probably we could suggest a functional cross-talk between fibroblasts and keratinocytes: keratinocytes of the epithelial compartment participated to ECM assembly triggered by dermal fibroblast by a regulation of protein organization and deposition allowing the improvement of ECM proprieties. The mutual interaction between keratinocytes and fibroblasts and the assembly of basal membrane, could contribute to improvement of ECM composition and organization with a gradual increment of synthesis of matrix constituents [48], [49]. On the other hand, observing data of mechanical proprieties, we could assess that our samples followed not only a dynamic and progressive assembling of ECM components, but also a progressive increasing of tissue stiffness, as revealed by nano-indentation test.

3.3.2 Reactive Oxygen Species (ROS) production in damaged and protected 3D human dermis and skin platforms

Radical oxygen species (ROS) formation is a common start point in many pathways associated with UVA-induced damage [50] and substances with an oxidative effects as hydrogen peroxide [51].

In order to evaluate the effect of oxidative stresses on our dermal and epidermal models, and the effectiveness of our skin system as a testing platform, a cell damage test was performed and the extent of the damage was evaluated by ROS cytosolic assay. We conducted two experiments which we evaluate the effect of two type of oxidative stresses: hydrogen peroxide (H_2O_2) treatment and UV radiations exposition. Cellular response induced by stress stimuli, was evaluated on samples both treated and protected by compounds with a known antioxidant and photo-protective effect, as ascorbic acid and retinoic acid [52], [53]. Inside the molecular mechanism, after oxidation reaction, an antioxidant might be regenerated by reduction, or it might be broken down and therefore need to be replaced ant they allow the chemical conversion of oxygen radicals in less reactive and toxic derivative [53]. Regarding the photo-protectants, we tested retinoic acid, a lipophilic molecule well known for its anti-aging and anti-UVA effects [54].

Oxidative stress induced by H_2O_2 and treatment with antioxidant product on 3D human dermis equivalent model

As shown in Figure 4, analyzing the fluorescence signal given by the presence of cytosolic ROS, a physiological level of intrinsic stress in control samples of HDE was observed. (Figure 4a and b). The intrinsic stress of the sample in basal conditions could be associated to the mechanical action exerted by the grid on the

surfaces of the specimen during the maturation phase. Anyway, the cytosolic ROS signal in control samples was is very low compared to stressed sample with H_2O_2 (Figure 4b and c). Samples exposed to oxidative stress and treated with 250 mM of ascorbic acid showed a lowering of cellular damage compared to stressed and not treated samples, although not entirely comparable to that baseline**.** These data highlighted not only the responsiveness of our 3D human dermis equivalent model to an oxidative insult, but also its effectiveness as a useful testing platform, for several applications and testing compounds.

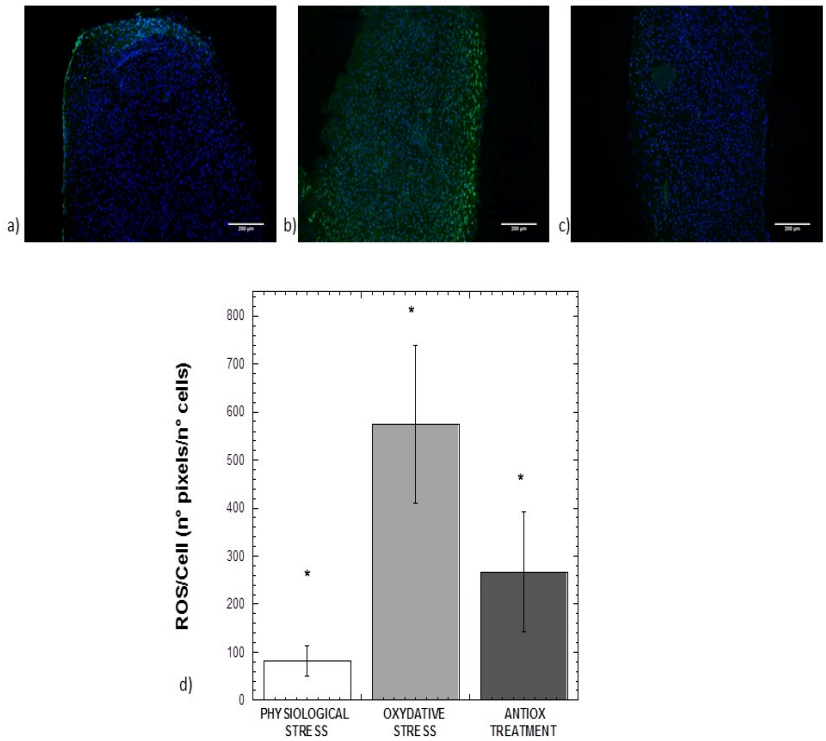

Figure 4. Analysis of the cytosolic ROS signal after treatment with H_2O_2 and antioxidant product: a) intrinsic basal stress in the CTRL sample; b) ROS signal due to cellular damage after treatment with H_2O_2; c) ROS signal following treatment with H_2O_2 and antioxidant ascorbic acid; Nuclei were visible in blue, ROS signal in green; d) Trend of the fluorescence signal of intracellular ROS in the different samples analyzed. (* p<0,001). Bars are 200 µm.

Oxidative stress induced by UVA exposure and treatment with antioxidant product on 3D human skin equivalent platform

We investigated the generation of cytoplasmic ROS induced in photo-exposed and photo-protected samples 5 minutes and 6 h after UVA exposure (Figure 5). Time slots having a duration raging from few minutes to few hours are usually investigated in previous works dealing with oxidative stress damages [55] [56]. Both dermal fibroblasts and epidermal keratinocytes (nuclei stained dye in red) produced a significant increase of ROS (green signal) after 5 minutes of UVA exposure in compare to control samples associated to cellular damage (Figure 5a and b). Quantitative investigations of fluorescent images showed that ROS (Figure 5c) per cells in 3D-HSE not treated with retinoic acid (UVA) 5 minutes and 6 h after UVA irradiation increased respectively 17,096 and 3,842 times compared to the control samples.

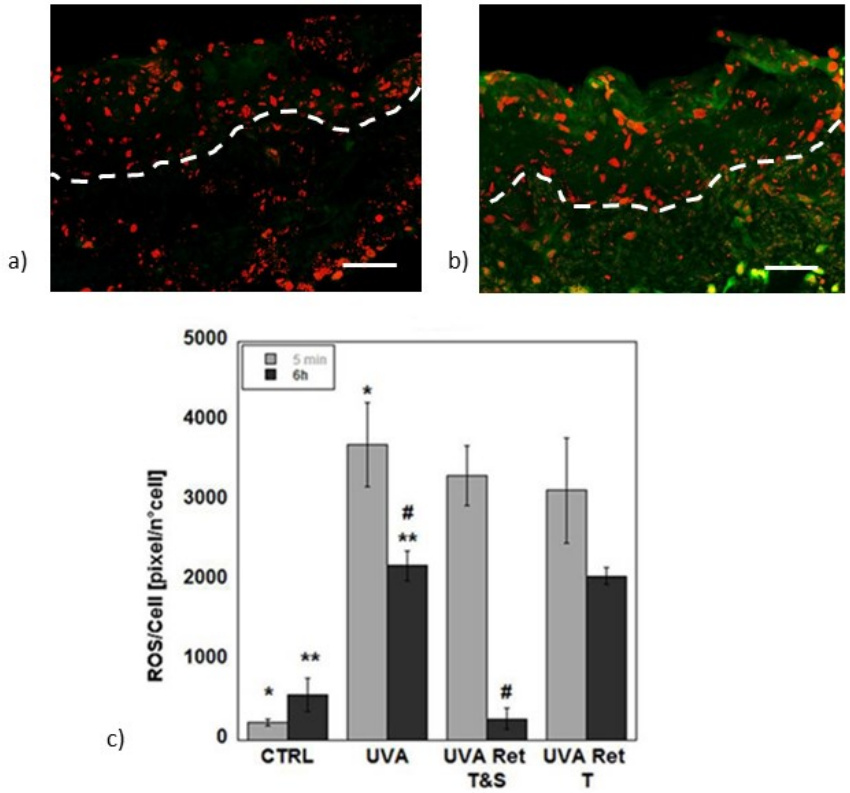

Figure 5. ROS production. ROS production 5 minutes post-irradiation in: (a) 3D-HSE non-irradiated and not treated with retinoic acid (CTRL); (b) 3D-HSE UVA-irradiated and not treated with retinoic acid (UVA). Nuclei are visible in red and ROS signal in green. Bars are 50µm. (c) Quantitative analyses of fluorescent images of ROS assay for cell performed 5 minutes and 6 h post-irradiation; (*, **, #p < 0.01).

In samples treated with retinoic acid, the ROS production decreased only when both topic and systemic treatment (T&S) ($p<0.001$) was applied. Topical application (T) alone was not able to reduce oxidative stress significantly. Topic application was introduced to mimic the application of compounds and formulas on the native skin. The damage UVA-induced is well known to affect more the

cytoplasmic molecule than the structural proteins of the dermis that are likely protected by their amino-acid composition [57].

Early effect of 3D-HSE exposure to UVA was a rise in ROS, which are scavenged by an intrinsic antioxidant defense system as suggested by the decreasing of ROS expression between 5 minutes and 6 h in UVA-exposed samples. These functional tests conducted on our 3D skin systems allowed to evaluate the effectiveness of our models as a testing platform. We tested the cellular response after an oxidative stress induced by H_2O_2 and UVA exposure, and the effect of antioxidant compound on our platform as scavenger substance of reactive oxygen molecules. Our results show not only the cellular response to several types of oxidative stress, but also the effectiveness as testing platform of protective compounds. These evidences pave the way to the possibility to have an *in vitro* skin system useful to investigate the cellular damage induced by an oxidant stress and the effect of protectant compounds, presenting important consequences not only in dermatology but also in cosmetology science with the possibility to investigate *in vitro* cosmetic function previously assessable only *in vivo.*

3.3.3 Effect of UVA photo-degradation on cellular and tissue senescence in our 3D human skin equivalent models

In order to focus the attention on photo-damage UVA exposure-induced, we put the attention on epidermal and dermal response of endogenous human skin model insulted with 20 Joule/cm^2 of UVA radiations. In fact, we observed that the UVA-induced oxidative stress in epidermal compartment induces stem cell damage that, in turn, is responsible of epidermal senescence [23].

Depletion of proliferative activity UVA-induced on 3D-HSE

First of all, we observed that UVA exposure induces a depletion of epidermal proliferation index obtained by the quantification of cellular proliferation by immunolabeling of Ki-67 as a marker of proliferative activity of epithelial cells [58]. The proliferation index was evaluated in photo-exposed and photo-protected samples at 6 and 72 h (Figure 6) In the control samples, proliferating Ki-67 keratinocytes (red signal) were mainly localized at basal layers (Figure 6a and b), while, in photo-exposed samples, the distribution of Ki-67 positive keratinocytes was restricted only at a few basal cells (Figure 6c and d). Meanwhile the Ki-67 signal in the epidermis of T&S and T samples were similar to the control sample in both the time points evaluated (Figure 6e-h). Imaging analysis was performed on immunofluorescent images to evaluate Ki-67 positivity per epidermal cell. A decrease of Ki-67 signal was found in photo-exposed samples compared to the control at both time points. Moreover, both T&S and T samples show the same behavior of the control samples (Figure 6i).

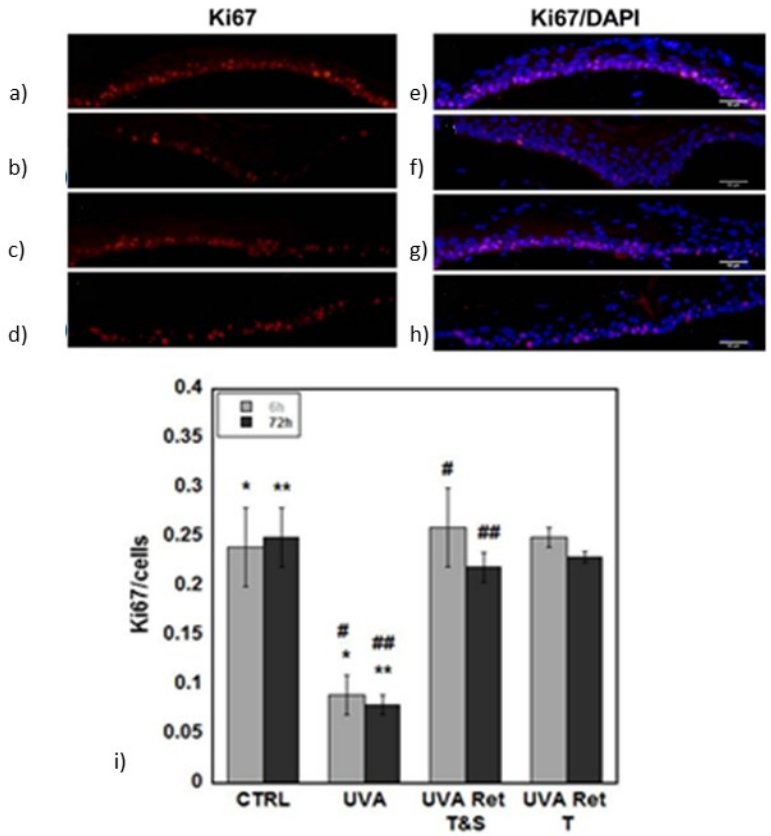

Figure 6. Epidermal proliferation index evaluation. Ki67 immunofluorescences 72 h post-irradiation in: (a, b) 3D-HSE non-irradiated and not treated with retinoic acid (CTRL,); (c, d) 3D-HSE UVA-irradiated and not treated with retinoic acid (UVA).; (e, f) 3D-HSE UVA-irradiated and treated with retinoic acid in topical and systemic application (UVA Ret T&S); (g, h) 3D-HSE UVA-irradiated and treated with retinoic acid in topical application (UVA Ret T). For each sample is reported immunostaining and merge with nuclear staining. Bars are 25 µm. (I) Quantitative analyses of ki67 immunofluorescences performed 6 and 72 h post-irradiation; (*, **, #, ## $p < 0.01$).

Caspase-3 activation by UVA exposure in 3D-HSE

Cellular damage UVA-induced was evaluated also in term of inducing apoptosis. In fact, UVA exposition causes not only the depletion of proliferation rate of epidermal keratinocytes but also the enhancement of apoptotic events. To

determine the activation of caspase-3 during UVA-damage and retinoic acid photo-protection we used antibodies that specifically recognize the cleaved, activated form of caspase-3 (Figure 7). In both modalities of photo-protection treatment, as well as in the control sample, was possible to observe that the immunostained cells were distributed at patches in the transition zone between the granular and cornified layers of the epidermis (Figure 7a). These immunolocalization was described also for native skin suggesting that caspase-3 is activated late during keratinocyte differentiation [59]. On the contrary, in photo-exposed samples the localization of activated form of caspase-3 is evident also in cytosol of basal cells involving more epidermal layers than in photo-protected and control samples (Figure 7b). Quantitative investigations of immunofluorescent images highlight that an early apoptotic stage in photo-exposed samples occurred only 6 h after UVA damage. Consequently, only at this time point it is possible to evaluate the downregulation of caspase-3 due to retinoic acid as shown Figure 7c.

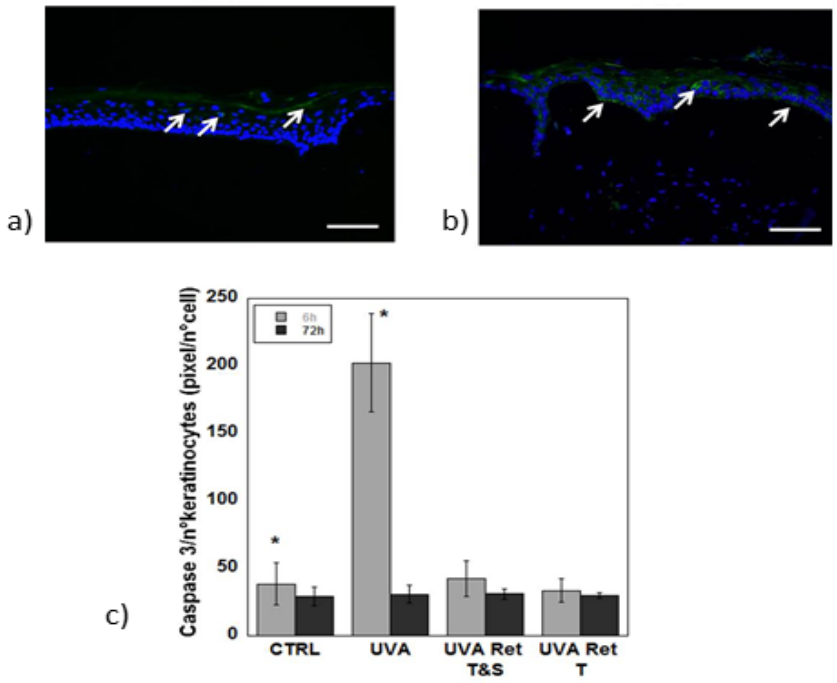

Figure 7. Active-Caspase 3 production. Active Caspase 3 production 72h post-irradiation in: (a) 3D-HSE non-irradiated and not treated with retinoic acid (CTRL); (b) 3D-HSE UVA-irradiated and not treated with photo-protectant (UVA). Nuclei are visible in blue and Caspase 3 signal in green. Bars are 50µm. (c) Quantitative analyses of immunofluorescence of Caspase 3 performed 5 minutes and 6 h post-irradiation; (* $p < 0.01$).

Adult epidermal stem cell depletion by UVA exposure in 3D-HSE

Immunopositivity to p63 in photo-exposed and photo-protected samples was evaluated in order to study its essential role for the proliferative potential of stem cells in stratified epithelia [60] [61]. The distinguishing feature of adult stem cells is their extraordinary capacity to divide prior to the onset of senescence. While stratified epithelia such as skin, prostate, and breast are highly regenerative and account disproportionately for human cancers, genes essential for the proliferative capacity of their stem cells remain unknown. Here we analyzed p63, a gene whose deletion in mice results in the catastrophic loss of all stratified

epithelia. We demonstrated that p63 is strongly expressed in epithelial cells with high clonogenic and proliferative capacity and that stem cells lacking p63 undergo a premature proliferative rundown. Additionally, we showed that p63 is dispensable for both the commitment and differentiation of these stem cells during tissue morphogenesis. Together, these data identify p63 as a key, lineage-specific determinant of the proliferative capacity in stem cells of stratified epithelia. In the epidermis of control samples, p63 was confined to almost all the cells of the basal layer, and gradually decreased in the cells of the suprabasal layer. No p63 expression was found in the granular layer, where cells were immunopositive to K10, and in spinous layer, where terminal cells differentiation occurred (Figure 8a and b). UVA exposure induced a decrease of p63 positive cells in suprabasal layer more than in the basal layer (Figure 8c and d) meanwhile the photo-protected samples shown a distribution of p63 nuclear signal similar to the control sample (Figure 8e-h). Quantitative investigations of immunofluorescent images of photo-exposed samples show significantly lower number of p63-positive epidermal cells than in the control sample. Adult epidermal stem cell maintenance was preserved in photo-protected sample at both the time points evaluated and at both modalities of treatment, confirming the effectiveness of retinoic acid (Figure 8i).

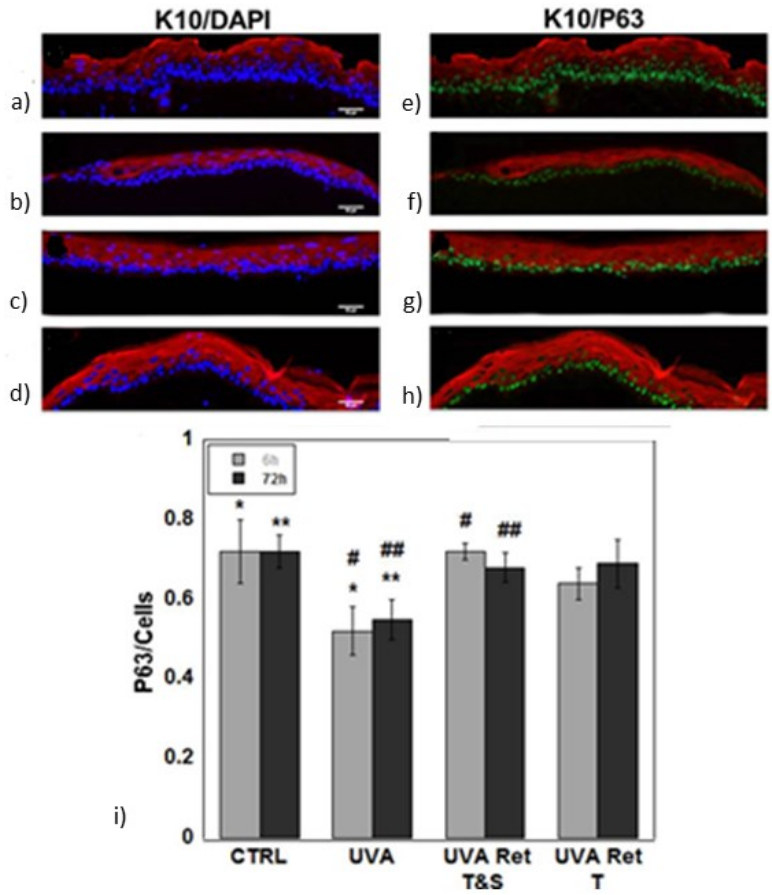

Figure 8. Epidermal stemness index evaluation. P63 (green signal) and K10 (red signal) immunofluorescences 72h post-irradiation in: (a,b) 3D-HSE non-irradiated and not treated with retinoic acid (CTRL); (c, d) 3D-HSE UVA-irradiated and not treated with retinoic acid (UVA); (e, f) 3D-HSE UVA-irradiated and treated with retinoic acid in topical and systemic application (UVA Ret T&S); (g, h) 3D-HSE UVA-irradiated and treated with photo-protectant in topical application (UVA Ret T). DAPI nuclear staining (blue signal) was used for cells-K10 co-localization Bars are 50 µm. (I) Quantitative analyses of P63 immunofluorescences 6 and 72h post-irradiation; (*, **, #, ## $p < 0.01$).

Mutual interaction between MMPs and collagen in dermal compartment of Endo-HSE after UVA exposure

In order to estimate the damage extent in dermal compartment after UVA exposition, immunofluorescence and histochemical analyses were performed evaluating the expression and localization of matrix-metalloproteinase-1 (MMP-1), matrix-metalloproteinase-9 (MMP-9) and collagen type I (coll 1) in the tissue at the two-time points in photo-exposed and photo-protected sample respectively. As shown in the Figure 9, at 72 h after exposition radiations there were high levels of the MMPs and low content of collagen I featured the photo-exposed samples compared to control and photo-protected samples (Figure 9A-N). Indeed MMP-1, a key member of matrix metalloproteinase family in initiating collagen type 1 degradation, and MMP-9, gelatinase able to continue the enzymatic degradation of interstitial collagens, are the major collagenolytic enzymes responsible for collagen destruction in photodamaged native human skin as well as in 3D-HSE UVA-exposed [62]. Quantitative imaging analysis showed that MMP-1 per fibroblast in 3D-HSE irradiated with UVA but not treated with retinoic acid at 6 h and 72 h after UVA irradiation increased respectively 1,8 and 2,2 times compared to the control samples. Our results confirmed the photo-protectant actions of retinoic acid in decreasing the MMP-1 production in both T&S and T photo-protective treatment at 6 and 72h, respectively, compared to UVA exposed samples ($p<0.001$). Moreover, not statistically differences were reported in photo-protected sample at 6 and 72 h compared to the control samples (Figure 9O). Upregulation of MMP-9 in the photo-exposed samples at 6 and 72 h was reported respectively 1.9 and 2.2 times compared to the control. MMP-9 production response in photo-protected sample was pushed down to the values of the control in both time points evaluated in the two different treatments performed Figure 9P). It is interesting to observe that the collagen I (mature collagen in red)

stained with PSR detected in photo-exposed samples decreases of 1.6 and 1.5 time, respectively, compared to control samples. On the contrary in the photo-protected sample at both modalities of treatment, the retinoic acid preserved the collagen I degradation from enzymatic cleavage maintaining the amount of collagen I at same level of controls (Figure 9Q).

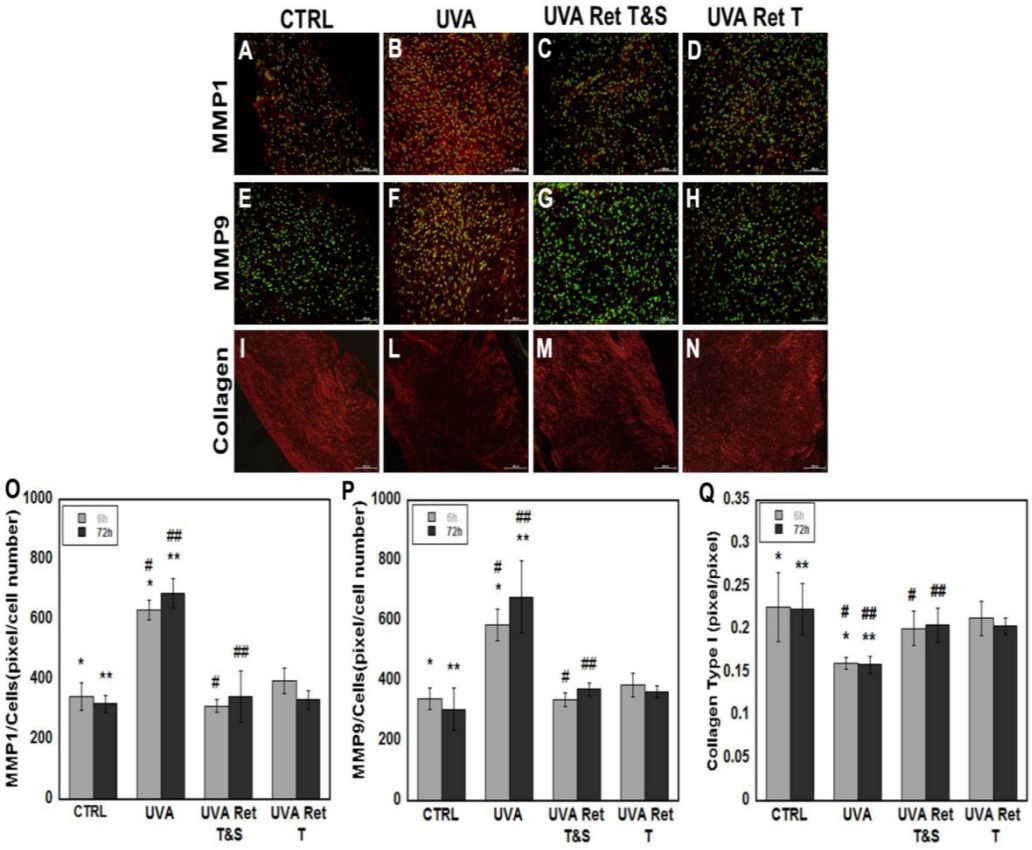

Figure 9. MMPs and endogenous collagen I productions. (A-D) MMP-1 immunofluorescences in all type of samples investigated 72 h post-irradiation; (E-H) MMP-9 immunofluorescences in all type of samples investigated 72 h post-irradiation; (I-N) Collagen I histochemical staining (Picro Sirius Red) at linear light polarized of all samples investigated 72h post-irradiation. Sytox Green staining was used in immunofluorescent images. Bars are 100µm for all images. (O-Q) Quantitative analyses of immunofluorescences and histochemical staining performed 6 and 72 h post-irradiation; (*, **, #, ## $p < 0.01$).

To study collagen remodeling after UVA exposure the unstained collagen structure was visualized by exploiting SHG. By performing grey-level co-occurrence matrix (GLCM) texture analysis, we evaluated the correlation length as a parameter indicating the roughness of the collagen matrix [2], [63], [64]. Rough textures, or low correlation length, is synonymous of fine structure, with well-defined collagen bundles and narrow distribution of the bundle diameter. This is the condition of young and healthy dermis. Ageing, and photoaging, induces collagen degeneration, causing changes in the textural features of the collagen matrix. As a consequence, correlation length tends to increase because of collagen matrix coarsening [62]. SHG imaging was performed on treated and on non-treated Endo-HSE in order to highlight the responsiveness and structural changes in collagen organization. All the samples were observed at the two-time points, but only images at 72h are shown (Figure 10A-D).

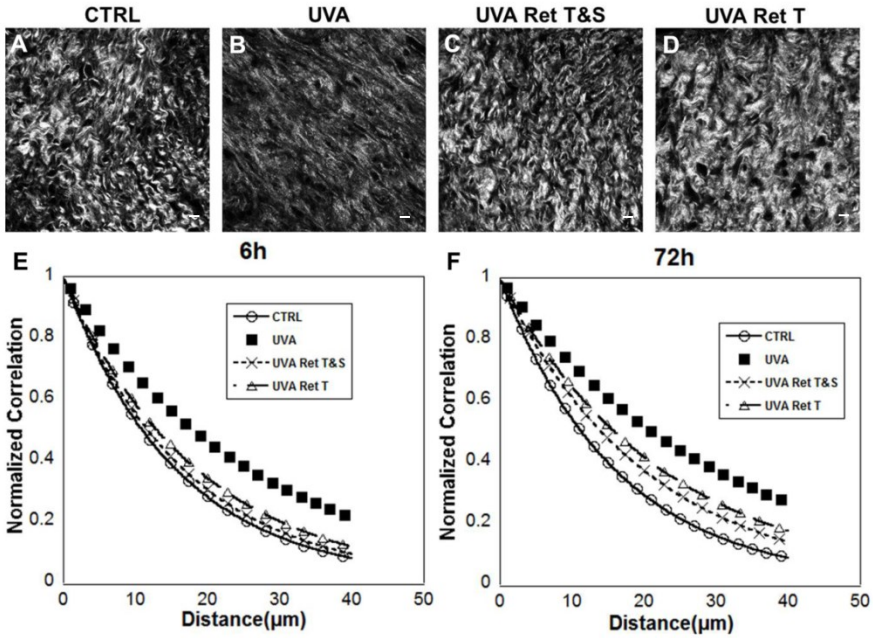

Figure 10. SHG imaging and GLCM analyses. (A–D) SHG images of 3D-HSE 72h post-irradiation show the morphology of collagen organization in: (A) non irradiated and not treated with retinoic acid samples (CTRL); (B) UVA-irradiated and not treated with retinoic acid samples (UVA); (C) UVA-irradiated and treated with photo-protectant in topical and systemic application (UVA Ret T&S); (D) UVA-irradiated and treated with photo-protectant in topical application samples (UVA Ret T); Bars are 25 µm. (E,F) GLCM analyses on SHG images allow quantification of the coarsening collagen network in 3D-HSE, 6 and 72 h post-irradiation.

By comparing the SHG images of photo-exposed 3D-HSE samples it is possible to note the different organization of the endogenous collagen between control and photo-protected samples. In detail, in all images is possible to detect an intense SHG signal indicating a dense matrix, with tight collagen bundles. In particular, in the photo-exposed samples, the fibrils show marked clumping, indicating a loss of the fine structure and structural organization, while the samples treated with retinoic acid have a collagen structure very similar to the control. In order to make

such an observation objective, the correlation curve was calculated at both time points for all samples and its behavior was reported (Figure 10E-F). UVA exposed samples but non-treated with retinoic acid were characterized by the highest correlation values, indicating a collagen matrix coarsening due to UVA exposure. In contrast, the photo-protected samples presented correlation curves very similar to those of the control. The correlation lengths calculated in a window of 40 µm is reported in Table 1: according to the behavior of the correlation curve, photo-exposed samples presented the highest correlation length at both time points compared to the control ($p < 0.01$). Moreover not statistically differences were present in the correlation length of T&S and T retinoic acid treatments compared to the controls.

Table 1. Fitting parameters from normalized correlation curves

Type of treatment	Correlation lenght ± SD (µm)	
	6 h	72 h
CTRL	15.74 ± 1.69	16.25 ±3.44
UVA	25.85± 6.66	30.18±5.02
UVA Ret T&S	16.81±4.17	20.19±3.44
UVA Ret Top	17.01±2.61	18.83±3.85

Table 1.: Values represent average ± SD of correlation length for the following samples: samples non-UVA-irradiated and not treated with photo-protectants (CTRL); samples UVA-irradiated and not treated with photo-protectants (UVA); samples UVA-irradiated and treated with photo-protectant in topical and systemic application (UVA Ret T&S); samples UVA-irradiated and treated with photo-protectant in topical application (UVA Ret T).

In particular, these data highlighted UVA radiations effects associated to cellular damage on dermal and epidermal compartment. The effect of cellular damage UVA-induced was evaluated on our 3D endogenous skin equivalent models, which showed the advantage to present a dermis compartment composed of fibroblasts that are embedded in their own matrix presenting several of the complex macromolecules that characterize the native ECM [58].

This fundamental feature makes the dermis not a merely “passive” matrix holding cells and tissues in place, but a dynamic repository for morphogens, cytokines and growth factors, which *in vivo* regulate diverse cellular processes. Such unique feature affects also the development of epidermis that, in contrast to that of HSE model based on fibroblast populated collagen, is characterized by a convoluted profile of DEJ and superior barrier epithelial functions correlate with higher density of p63-positive cells with a germinative potential [65].

Moreover we immunoquantified p63, Ki67 and caspase 3 in the epidermal layers in order to investigate the effect of UVA on cellular senescence [59], [60] . We found that p63 and Ki67 were downregulated in UVA samples and that the T and T&S treatments with the retinoic acid maintaining the level of p63 and Ki67 to those of the control. The UVA-response caused the depletion of staminal and proliferative potential of both the basal cells and a subset of daughter cells locate in suprabasal epidermal layer. Meanwhile the caspase 3 was up-regulated only at short time point of UVA exposure, suggesting an attempt of a rapid restoration in basal cells of epidermal tissue. T and T&S application of retinoic acid was able to restore the situation of control samples. These findings are compatible with the hypothesis that, in proliferating basal stem cell pool, cellular senescence is important for the response to single UVA exposure in order to cope a repair mechanism that sacrifices the germinative capability of basal stem cells through

p63 and Ki67 downregulation. Our model potentially allows to investigate several *phenomena* involving germinative cells and here, for the first time, we quantified the early induction of cellular senescence after UVA exposure and the cellular and structural damage both in dermis and epidermal compartment. In fact, we found that the combined production of the MMP9 and MMP1 by fibroblasts leads to a strong degradation of collagen in photo-exposed samples, while due to the protective action of retinoic acid both in T and T&S samples, collagen degradation is preserved. Moreover, in accordance with a study performed *in vivo* on photo-aged skin [2], [68] we quantify the collagen structure by using GLCM texture analysis and evaluate the difference between the denser and fine structure of collagen fibrils in the not exposed sample, and the loss of the fine structure and structural organization of the photo-exposed samples. Taken together, these evidences lead the Endo-HSE an effective upgraded alternative at the *in vitro* platform currently used. Indeed, here we demonstrate for the first time *in vitro* that UVA-induced cellular and extracellular senescence is reflected in the parallel decline of epidermal germinative potential and collagen network assembly.

3.4 CONCLUSIONS

In this chapter, we investigated the different uses and applications of our 3D tissue model as a responsive system that reacts to external stimuli and a useful platform for testing compound in a complex 3D environment. The presence of the cell-synthesized ECM organized in a 3D fashion represented a more suitable system able to mimic *in vitro* damages and regeneration of tissue and confirms that in the dermis reside the solution to contrast profound change in skin structure such as wrinkle and laxicity. Due to its morphological and functional features, our human skin equivalent is a unique tool to study effects on tissue

homeostasis *in vitro* in terms of exhaustion of staminal and proliferative potentials in the epidermis as well as of ECM remodeling in the dermis. We demonstrated that our models could be degraded by enzymatic digestion in order to quantify ECM components content, and that there was a gradual progressive assembly of ECM structural elements during the time of culture, and that long-time culture could establish stress *phenomena* and structural changes of ECM organization and composition. These data suggest that our system dynamically changed over the time. Moreover, the single oxidative stress (hydrogen peroxide and UVA radiations) can contribute to cellular damage and to the depletion of epidermal stem cell, induces ROS production in the entire tissue and through the MMPs action can remodel the collagenous network decreasing both the collagen content and its structural quality. The development of such model might as a realistic tool to lead to the possibility of studying *in vitro* the effects of variations in human skin (e.g. variation due to aging) on selected aspects of both cellular and extracellular components.

3.5 REFERENCES

[1] S. L. K. Bowers, I. Banerjee, and T. A. Baudino, "The extracellular matrix: At the center of it all," *J. Mol. Cell. Cardiol.*, vol. 48, no. 3, pp. 474–482, Mar. 2010.

[2] G. Imparato *et al.*, "A novel engineered dermis for *in vitro* photodamage research: A dermis equivalent for investigating UVA damage *in vitro*," *J. Tissue Eng. Regen. Med.*, p. n/a-n/a, 2016.

[3] Y. S. Zhang and A. Khademhosseini, "Seeking the right context for evaluating nanomedicine: from tissue models in petri dishes to microfluidic organs-on-a-chip," *Nanomed.*, vol. 10, no. 5, pp. 685–688, Mar. 2015.

[4] Y. Sasai, M. Eiraku, and H. Suga, "*In vitro* organogenesis in three dimensions: self-organising stem cells," *Development*, vol. 139, no. 22, pp. 4111–4121, Nov. 2012.

[5] A. El Ghalbzouri, E. Lamme, and M. Ponec, "Crucial role of fibroblasts in regulating epidermal morphogenesis," *Cell Tissue Res.*, vol. 310, no. 2, pp. 189–199, Nov. 2002.

[6] S. MacNeil, "Progress and opportunities for tissue-engineered skin," *Nature*, vol. 445, no. 7130, pp. 874–880, Feb. 2007.

[7] V. Moulin, D. Garrel, F. A. Auger, M. O'Connor-McCourt, G. Castilloux, and L. Germain, "What's new in human wound-healing myofibroblasts?," *Curr. Top. Pathol. Ergeb. Pathol.*, vol. 93, pp. 123–133, 1999.

[8] M. Varkey, J. Ding, and E. E. Tredget, "Differential collagen-glycosaminoglycan matrix remodeling by superficial and deep dermal fibroblasts: potential therapeutic targets for hypertrophic scar," *Biomaterials*, vol. 32, no. 30, pp. 7581–7591, Oct. 2011.

[9] S. Muffler *et al.*, “A stable niche supports long-term maintenance of human epidermal stem cells in organotypic cultures,” *Stem Cells Dayt. Ohio*, vol. 26, no. 10, pp. 2506–2515, Oct. 2008.

[10] D. Janson, G. Saintigny, C. Mahé, and A. El Ghalbzouri, “Papillary fibroblasts differentiate into reticular fibroblasts after prolonged *in vitro* culture,” *Exp. Dermatol.*, vol. 22, no. 1, pp. 48–53, Jan. 2013.

[11] A. El Ghalbzouri, S. Commandeur, M. H. Rietveld, A. A. Mulder, and R. Willemze, “Replacement of animal-derived collagen matrix by human fibroblast-derived dermal matrix for human skin equivalent products,” *Biomaterials*, vol. 30, no. 1, pp. 71–78, Jan. 2009.

[12] K. Boehnke, N. Mirancea, A. Pavesio, N. E. Fusenig, P. Boukamp, and H.-J. Stark, “Effects of fibroblasts and microenvironment on epidermal regeneration and tissue function in long-term skin equivalents,” *Eur. J. Cell Biol.*, vol. 86, no. 11–12, pp. 731–746, Dec. 2007.

[13] D. Larouche, K. Cuffley, C. Paquet, and L. Germain, “Tissue-Engineered Skin Preserving the Potential of Epithelial Cells to Differentiate into Hair After Grafting,” *Tissue Eng. Part A*, vol. 17, no. 5–6, pp. 819–830, Mar. 2011.

[14] H. Fernandes, L. Moroni, C. van Blitterswijk, and J. de Boer, “Extracellular matrix and tissue engineering applications,” *J. Mater. Chem.*, vol. 19, no. 31, p. 5474, 2009.

[15] A. M. Pizzo, “Extracellular matrix (ECM) microstructural composition regulates local cell-ECM biomechanics and fundamental fibroblast behavior: a multidimensional perspective,” *J. Appl. Physiol.*, vol. 98, no. 5, pp. 1909–1921, Jan. 2005.

[16] D. Rossetti *et al.*, “A novel anti-ageing mechanism for retinol: induction of dermal elastin synthesis and elastin fibre formation: Retinol induces elastin synthesis,” *Int. J. Cosmet. Sci.*, vol. 33, no. 1, pp. 62–69, Feb. 2011.

[17] J.-H. Oh *et al.*, “Intrinsic aging- and photoaging-dependent level changes of glycosaminoglycans and their correlation with water content in human skin,” *J. Dermatol. Sci.*, vol. 62, no. 3, pp. 192–201, Jun. 2011.

[18] J. M. Waller and H. I. Maibach, “Age and skin structure and function, a quantitative approach (II): protein, glycosaminoglycan, water, and lipid content and structure,” *Skin Res. Technol. Off. J. Int. Soc. Bioeng. Skin ISBS Int. Soc. Digit. Imaging Skin ISDIS Int. Soc. Skin Imaging ISSI*, vol. 12, no. 3, pp. 145–154, Aug. 2006.

[19] E. F. Bernstein, C. B. Underhill, P. J. Hahn, D. B. Brown, and J. Uitto, “Chronic sun exposure alters both the content and distribution of dermal glycosaminoglycans,” *Br. J. Dermatol.*, vol. 135, no. 2, pp. 255–262, Aug. 1996.

[20] M. Gniadecka, O. F. Nielsen, S. Wessel, M. Heidenheim, D. H. Christensen, and H. C. Wulf, “Water and protein structure in photoaged and chronically aged skin,” *J. Invest. Dermatol.*, vol. 111, no. 6, pp. 1129–1133, Dec. 1998.

[21] T. Quan, E. Little, H. Quan, Z. Qin, J. J. Voorhees, and G. J. Fisher, “Elevated Matrix Metalloproteinases and Collagen Fragmentation in Photodamaged Human Skin: Impact of Altered Extracellular Matrix Microenvironment on Dermal Fibroblast Function,” *J. Invest. Dermatol.*, vol. 133, no. 5, pp. 1362–1366, May 2013.

[22] R. Stern and H. I. Maibach, “Hyaluronan in skin: aspects of aging and its pharmacologic modulation,” *Clin. Dermatol.*, vol. 26, no. 2, pp. 106–122, Apr. 2008.

[23] U. Panich, G. Sittithumcharee, N. Rathviboon, and S. Jirawatnotai, “Ultraviolet Radiation-Induced Skin Aging: The Role of DNA Damage and Oxidative Stress in Epidermal Stem Cell Damage Mediated Skin Aging,” *Stem Cells Int.*, vol. 2016, p. 7370642, 2016.

[24] Q. Li *et al.*, “FOXA1 mediates p16INK4a activation during cellular senescence,” *EMBO J.*, vol. 32, no. 6, pp. 858–873, Feb. 2013.

[25] Y. R. Helfrich, D. L. Sachs, and J. J. Voorhees, “Overview of skin aging and photoaging,” *Dermatol. Nurs.*, vol. 20, no. 3, p. 177–183; quiz 184, Jun. 2008.

[26] C. Battie, S. Jitsukawa, F. Bernerd, S. Del Bino, C. Marionnet, and M. Verschoore, “New insights in photoaging, UVA induced damage and skin types,” *Exp. Dermatol.*, vol. 23 Suppl 1, pp. 7–12, Oct. 2014.

[27] K. Biniek, K. Levi, and R. H. Dauskardt, “Solar UV radiation reduces the barrier function of human skin,” *Proc. Natl. Acad. Sci.*, vol. 109, no. 42, pp. 17111–17116, Oct. 2012.

[28] M. Meloni, A. Farina, and B. de Servi, “Molecular modifications of dermal and epidermal biomarkers following UVA exposures on reconstructed full-thickness human skin,” *Photochem. Photobiol. Sci. Off. J. Eur. Photochem. Assoc. Eur. Soc. Photobiol.*, vol. 9, no. 4, pp. 439–447, Apr. 2010.

[29] G. Imparato, F. Urciuolo, C. Casale, and P. A. Netti, “The role of microscaffold properties in controlling the collagen assembly in 3D dermis equivalent using modular tissue engineering,” *Biomaterials*, vol. 34, no. 32, pp. 7851–7861, Oct. 2013.

[30] S. K. Nadkarni *et al.*, “Measurement of Collagen and Smooth Muscle Cell Content in Atherosclerotic Plaques Using Polarization-Sensitive Optical Coherence Tomography,” *J. Am. Coll. Cardiol.*, vol. 49, no. 13, pp. 1474–1481, Apr. 2007.

[31] P. R. Moshtagh, B. Pouran, N. M. Korthagen, A. A. Zadpoor, and H. Weinans, “Guidelines for an optimized indentation protocol for measurement of cartilage stiffness: The effects of spatial variation and indentation parameters,” *J. Biomech.*, vol. 49, no. 14, pp. 3602–3607, Oct. 2016.

[32] N. E. Kurland, Z. Drira, and V. K. Yadavalli, “Measurement of nanomechanical properties of biomolecules using atomic force microscopy,” *Micron*, vol. 43, no. 2–3, pp. 116–128, Feb. 2012.

[33] G. Mattei, G. Gruca, N. Rijnveld, and A. Ahluwalia, “The nano-epsilon dot method for strain rate viscoelastic characterisation of soft biomaterials by spherical nano-indentation,” *J. Mech. Behav. Biomed. Mater.*, vol. 50, pp. 150–159, Oct. 2015.

[34] S. J. Hollister, C. G. Jeong, J. J. Schwiedrzik, A. G. Mitsak, H. Kang, and F. Migneco, “Nonlinear Elastic Scaffold Design, Modeling and Fabrication for Soft Tissue Engineering,” in *Advances on Modeling in Tissue Engineering*, vol. 20, P. R. Fernandes and P. J. Bártolo, Eds. Dordrecht: Springer Netherlands, 2011, pp. 35–53.

[35] M. Galli, K. S. C. Comley, T. A. V. Shean, and M. L. Oyen, “Viscoelastic and poroelastic mechanical characterization of hydrated gels,” *J. Mater. Res.*, vol. 24, no. 03, pp. 973–979, Mar. 2009.

[36] M. Galli, E. Fornasiere, J. Cugnoni, and M. L. Oyen, “Poroviscoelastic characterization of particle-reinforced gelatin gels using indentation and homogenization,” *J. Mech. Behav. Biomed. Mater.*, vol. 4, no. 4, pp. 610–617, May 2011.

[37] Z.-W. Chen, P. Joli, and Z.-Q. Feng, “Anisotropic hyperelastic behavior of soft biological tissues,” *Comput. Methods Biomech. Biomed. Engin.*, vol. 18, no. 13, pp. 1436–1444, Oct. 2015.

[38] J. S. Field and M. V. Swain, “Determining the mechanical properties of small volumes of material from submicrometer spherical indentations,” *J. Mater. Res.*, vol. 10, no. 01, pp. 101–112, Jan. 1995.

[39] W. C. Oliver and G. M. Pharr, “Measurement of hardness and elastic modulus by instrumented indentation: Advances in understanding and

refinements to methodology," *J. Mater. Res.*, vol. 19, no. 01, pp. 3–20, Jan. 2004.

[40] B. D'Autréaux and M. B. Toledano, "ROS as signalling molecules: mechanisms that generate specificity in ROS homeostasis," *Nat. Rev. Mol. Cell Biol.*, vol. 8, no. 10, pp. 813–824, Oct. 2007.

[41] L. Rich and P. Whittaker, "Collagen and picrosirius red staining: a polarized light assessment of fibrillar hue and spatial distribution," *Braz J Morphol Sci*, vol. 22, no. 2, pp. 97–104, 2005.

[42] S. Mukherjee, A. Date, V. Patravale, H. C. Korting, A. Roeder, and G. Weindl, "Retinoids in the treatment of skin aging: an overview of clinical efficacy and safety," *Clin. Interv. Aging*, vol. 1, no. 4, pp. 327–348, 2006.

[43] F. H. Silver, J. W. Freeman, and D. DeVore, "Viscoelastic properties of human skin and processed dermis," *Skin Res. Technol. Off. J. Int. Soc. Bioeng. Skin ISBS Int. Soc. Digit. Imaging Skin ISDIS Int. Soc. Skin Imaging ISSI*, vol. 7, no. 1, pp. 18–23, Feb. 2001.

[44] F. Martorina, C. Casale, F. Urciuolo, P. A. Netti, and G. Imparato, "*In vitro* activation of the neuro-transduction mechanism in sensitive organotypic human skin model," *Biomaterials*, vol. 113, pp. 217–229, Jan. 2017.

[45] M. J. Sherratt, "Tissue elasticity and the ageing elastic fibre," *AGE*, vol. 31, no. 4, pp. 305–325, Dec. 2009.

[46] E. C. Naylor, R. E. B. Watson, and M. J. Sherratt, "Molecular aspects of skin ageing," *Maturitas*, vol. 69, no. 3, pp. 249–256, Jul. 2011.

[47] E. Papakonstantinou, M. Roth, and G. Karakiulakis, "Hyaluronic acid: A key molecule in skin aging," *Dermatoendocrinol.*, vol. 4, no. 3, pp. 253–258, Jul. 2012.

[48] H. Smola, H. J. Stark, G. Thiekötter, N. Mirancea, T. Krieg, and N. E. Fusenig, "Dynamics of basement membrane formation by keratinocyte-fibroblast

interactions in organotypic skin culture," *Exp. Cell Res.*, vol. 239, no. 2, pp. 399–410, Mar. 1998.

[49] F. Duplan-Perrat *et al.*, "Keratinocytes influence the maturation and organization of the elastin network in a skin equivalent," *J. Invest. Dermatol.*, vol. 114, no. 2, pp. 365–370, 2000.

[50] R. Bosch *et al.*, "Mechanisms of Photoaging and Cutaneous Photocarcinogenesis, and Photoprotective Strategies with Phytochemicals," *Antioxid. Basel Switz.*, vol. 4, no. 2, pp. 248–268, Mar. 2015.

[51] J. W. Zmijewski, S. Banerjee, H. Bae, A. Friggeri, E. R. Lazarowski, and E. Abraham, "Exposure to hydrogen peroxide induces oxidation and activation of AMP-activated protein kinase," *J. Biol. Chem.*, vol. 285, no. 43, pp. 33154–33164, Oct. 2010.

[52] L. J. Machlin and A. Bendich, "Free radical tissue damage: protective role of antioxidant nutrients," *FASEB J. Off. Publ. Fed. Am. Soc. Exp. Biol.*, vol. 1, no. 6, pp. 441–445, Dec. 1987.

[53] A. Meister, "Glutathione-ascorbic acid antioxidant system in animals," *J. Biol. Chem.*, vol. 269, no. 13, pp. 9397–9400, Apr. 1994.

[54] G. J. Fisher and J. J. Voorhees, "Molecular mechanisms of photoaging and its prevention by retinoic acid: ultraviolet irradiation induces MAP kinase signal transduction cascades that induce Ap-1-regulated matrix metalloproteinases that degrade human skin *in vivo*," *J. Investig. Dermatol. Symp. Proc.*, vol. 3, no. 1, pp. 61–68, Aug. 1998.

[55] C. Marionnet, C. Pierrard, F. Lejeune, J. Sok, M. Thomas, and F. Bernerd, "Different Oxidative Stress Response in Keratinocytes and Fibroblasts of Reconstructed Skin Exposed to Non Extreme Daily-Ultraviolet Radiation," *PLoS ONE*, vol. 5, no. 8, p. e12059, Aug. 2010.

[56] A. Svobodová, A. Zdarilová, J. Malisková, H. Mikulková, D. Walterová, and J. Vostalová, “Attenuation of UVA-induced damage to human keratinocytes by silymarin,” *J. Dermatol. Sci.*, vol. 46, no. 1, pp. 21–30, Apr. 2007.

[57] R. E. B. Watson, N. K. Gibbs, C. E. M. Griffiths, and M. J. Sherratt, “Damage to skin extracellular matrix induced by UV exposure,” *Antioxid. Redox Signal.*, vol. 21, no. 7, pp. 1063–1077, Sep. 2014.

[58] T. Tumbar, “Defining the Epithelial Stem Cell Niche in Skin,” *Science*, vol. 303, no. 5656, pp. 359–363, Jan. 2004.

[59] M. Weil, M. C. Raff, and V. M. Braga, “Caspase activation in the terminal differentiation of human epidermal keratinocytes,” *Curr. Biol. CB*, vol. 9, no. 7, pp. 361–364, Apr. 1999.

[60] M. Senoo, F. Pinto, C. P. Crum, and F. McKeon, “p63 Is essential for the proliferative potential of stem cells in stratified epithelia,” *Cell*, vol. 129, no. 3, pp. 523–536, May 2007.

[61] M. I. Koster and D. R. Roop, “The role of p63 in development and differentiation of the epidermis,” *J. Dermatol. Sci.*, vol. 34, no. 1, pp. 3–9, Feb. 2004.

[62] M. Brennan *et al.*, “Matrix metalloproteinase-1 is the major collagenolytic enzyme responsible for collagen damage in UV-irradiated human skin,” *Photochem. Photobiol.*, vol. 78, no. 1, pp. 43–48, Jul. 2003.

[63] S. Wu, H. Li, H. Yang, X. Zhang, Z. Li, and S. Xu, “Quantitative analysis on collagen morphology in aging skin based on multiphoton microscopy,” *J. Biomed. Opt.*, vol. 16, no. 4, p. 040502, Apr. 2011.

[64] C. B. Raub *et al.*, “Noninvasive assessment of collagen gel microstructure and mechanics using multiphoton microscopy,” *Biophys. J.*, vol. 92, no. 6, pp. 2212–2222, Mar. 2007.

[65] C. Casale, G. Imparato, F. Urciuolo, and P. A. Netti, “Endogenous human skin equivalent promotes *in vitro* morphogenesis of follicle-like structures,” *Biomaterials*, vol. 101, pp. 86–95, Sep. 2016.

[66] W. M. Keyes, Y. Wu, H. Vogel, X. Guo, S. W. Lowe, and A. A. Mills, “p63 deficiency activates a program of cellular senescence and leads to accelerated aging,” *Genes Dev.*, vol. 19, no. 17, pp. 1986–1999, Sep. 2005.

[67] A. B. Truong, M. Kretz, T. W. Ridky, R. Kimmel, and P. A. Khavari, “p63 regulates proliferation and differentiation of developmentally mature keratinocytes,” *Genes Dev.*, vol. 20, no. 22, pp. 3185–3197, Nov. 2006.

[68] R. Cicchi *et al.*, “Scoring of collagen organization in healthy and diseased human dermis by multiphoton microscopy,” *J. Biophotonics*, vol. 3, no. 1–2, pp. 34–43, Jan. 2010.

Chapter 4
Scale-up strategy for skin models production

4.1 INTRODUCTION

TE products applied in pharmaceutical research as test systems offer possibilities for closing the gap between animal testing and administration of drugs to human subjects in clinical trials. The biological complexity of 3D tissue entails high requirements regarding applicable culture technique [1]. The development of the system biotechnology and its application in the industrial process open new horizons to industrial biotechnology. Improvements of yields and consistent products are the key mission in industrial process [2] and in an industrial prospective, the main difficult in a scale-up strategy of a bioprocess is the transition from the microscale to the large-scale production without compromising the quality and the effectiveness of products. We developed an accurate working plan and specific criterions to improve our bioprocess control and to ensure the good quality of our skin systems.

The complexity of biological systems, from individual proteins to whole cells, makes it exceedingly difficult to predict their behavior under not ideal conditions. A bioprocess includes several unit operations, and the single complexity of a manufacturing scale could affect the performance of an individual operation [3], [4]. Concerning the scale-up of a bioprocess from bench scale to large production scale, the main aims are product yield and quality and both requirements are a "net results from several independent, but interrelated, steps" [5]. Indeed, bioprocess complexity increased when whole bioprocess is considered as a set of multiple interacting variables between individual unit operations. Microscale processing techniques offer the potential to speed up the fabrication of products

in a more controlled manner, from the numbers of products fabricated to the costs [4]. First of all, in a scale-up procedure of a bioprocess, it is fundamental determining a scale-down approach, since the only safe method is to study all different steps separately, but under conditions comparable with the ones in the production scale. [5]. In this context, two significant industrial problems related to a biological process can be identified: batch variations and the lack of reproducibility. These problems are caused by a multitude of factors and it is necessary to introduce an accurate methodology to support the scale-up [6]. The improvement of a bioprocess is developed in three fundamental stages: laboratory scale, where basic screening procedures are carried out; a working plan, where the optimal operating conditions are ascertained; and the plant scale, where the process is brought to economic fruition [7]. According to conventional scale-up strategies, in a manufacturing process, when specific parameters are maintained constant, others parameters cannot be controlled and may changes substantially in unexpected way [7]–[9] causing undesired effects on the yield and quality of products [7]. The productivity of a bioprocess generally depends on two elements: cell lines and process control. In particular, the process control is defined as the providing a near optimal environment to produce a desired product. The scope of bioprocess control theoretically includes not only the sequence of single steps but also product recovery including pre-incubation operations, sterilization, cell culture and environment [3]. Among several strategies employed to improve the productivity of an industrial bioprocess, one effective method applied to accelerate the development and the yield is the possibility of operating many big bioreactors in parallel working at the maximal capacity [4]. It is known that the parallelization and the automation of high-throughput cell cultivations in small-scale bioreactor system is an important topic to increase the production controlling all process conditions [10]. In this last

chapter, we described an innovative scale-up strategy in order to optimize the production of human skin models as a platform commercially available for cosmetic testing and several applications. Firstly, we conducted a characterization of the best gold standard skin models and a comparison with our 3D human skin equivalent platforms to better understand the structure and the composition of competitive skin models commercially available. Subsequently, we described methods to improve the productivity of our tissue process with the prospect of achieving a start-up by the parallelization of our bioprocess using many bioreactors working at maximal capacity with the aim of increasing volumes, cells and number of tissues produced for month.

Phenion Full-Thickness skin model fabricated by Henkel and EpiDerm 312X FT produced by MatTek Corporation, were purchased and studied by means of histological and morphological analysis. The Phenion Full-Thickness skin model is a 3D tissue-construct that simulates histological and physiological properties of human skin. Different cell types, build up a dermal and epidermal compartment: fibroblasts, growing inside a spongy scaffold composed of collagen-GAGs mixture, form the connective tissue as basis for overlying epithelial cell layers mimicking *in vivo* conditions. This skin model is a useful *in vitro* test system employed for the study of the effects of active compounds following topical or systemic application, in order to study genotoxicity, corrosion and percutaneous adsorption [11], [12] (http//www.henkel_adhesives.de/de/content_data/247926_Flyer_Phenion_FT_Skin_Models). EpiDerm 312X FT skin model produced by MatTek Corporation, is an engineered skin system composed of normal human epidermal keratinocytes (NHEK) and normal human dermal fibroblasts (NHFB) cultured to form a multilayered model of the human dermis and epidermis. The dermal compartment consists of a collagen matrix containing viable normal human dermal fibroblasts (NHDF), while the epidermal compartment was composed of

human keratinocytes adequately differentiated in spinous, granular and cornified layers analogous to those found *in vivo* counterpart [11], [12] (http//www.mattek.com/products/epidermft/). The principal applications of this skin system are irritation and corrosion tests, photo/genotoxicity, transdermal drug delivery.

With this assumptions, after this characterization, we set up an accurate strategy for the realization of endogenous 3D human skin models in large scale with the aim to make them commercially available as a functional platform for cosmetics testing. Our scale-up strategy is based on i) the improvement of tissue production both through the parallelization of the entire bioprocess; ii) the use of higher instruments and devices for increasing the capacity, volumes and quantity; iii) the introduction of a meticulous working plan and several check points in each critical phase of our tissue process in order to guarantee the control on yield and quality products.

Finally, we obtained a safety and standardized protocols to ensure about 200 tissue products per month available for several tests and applications as useful alternative to animal testing.

4.2 MATERIALS AND METHODS

4.2.1 Characterization of commercially available gold standards models and comparison with our endogenous 3D human skin platform

First of all, in order to assess the characterization in terms of morphology and composition of the best skin models commercially available, we purchased two type of gold standard skin models, Phenion Full-Thickness skin model by Henkel and EpiDerm 312X FT (Full Thickness) by MatTek Corporation. We conducted a morphological analysis on Phenion by SHG imaging in order to study its configuration and composition. With the aim to evaluate the effective functionality of EpiDerm 312X FT as a screening platform for cosmetic testing, we performed an irritation test and a macroscopic analysis through the stereomicroscope (Olympus) and histological analysis in order to obtain a useful comparison between our endogenous 3D human skin platform and the best competitor skin model commercially available.

Irritation test for cellular viability of EpiDerm 312X FT skin model

With the aim to evaluate the functionality and the viability of EpiDerm 312X FT purchased from MatTek Corporation, an irritation test was performed according to MatTek Corporation procedures and protocol (*in vitro* EpiDerm skin irritation test).

Basic Procedure. On the day of receipt, EpiDerm 312X FT tissues were conditioned by incubation to release transport-stress related compounds and debris overnight. After pre-incubation, tissues are topically exposed to the test chemicals for 60 min. Preferably, 3 tissues are used per test chemical (TC) and for the positive control (PC) and negative control (NC). Tissues are then thoroughly rinsed, blotted to remove the test substances, and transferred to fresh medium. A viability test

MTT assay was performed by transferring the tissues to 24-well plates containing MTT medium (1 mg/ml). After a 3h MTT incubation, the blue formazan salt formed by cellular mitochondria was extracted with 2 ml/tissue of isopropanol (extracting solution) and the optical density of the extracted formazan was determined using a spectrophotometer at 570 nm. Relative cell viability was calculated for each tissue as % of the mean of the negative control tissues. Skin irritation potential of the test material is predicted if the remaining relative cell viability is below 50%. According to the EU and GHS classification (R38/ Category 2 or no label), an irritant compound is predicted if the mean relative viability of three individual tissues exposed to the test substance is reduced below 50% of the mean viability of the negative controls (see Table 1).

We tested the responsiveness of samples to irritant compound using a solution of SDS (sodium dodecylsulfate, Fluka) 5% in dH_2O (defined as irritant substance), and PBS 1X (Microtech) as negative control.

In vitro result	*In vivo* prediction
mean tissue viability ≤ 50%	Irritant (I), (R38 or GHS category 2)
mean tissue viability > 50%	non-irritant (NI)

Table 1. Criterions for irritant compounds classification.

Step 1

30 µl of the test substance were added into 0.3 ml of dH_2O. The test was performed in a transparent, preferably glass test-tube to avoid any reaction with plastic during the incubation time. The mixture was incubated in the incubator (37°C, 5 % CO_2, 95% RH) for 60 min. At the end of the exposure time, the mixture was shaken and it was evaluated the presence and intensity of the staining.

Step 2

At the end of treatment, samples were washed with PBS 1X and incubated for 3 h incubation in culture media with MTT (37°C, 5% CO_2, 95% RH). After the 3 h incubation, the tissues were rinsed and extracted using 2 ml of isopropanol and the optical density (OD) was measured at 570 nm. The real MTT OD (unaffected by interference with the colored test materials) was calculated using following formula:

$$\boldsymbol{OD = OD\ colored\ tissue\ (MTT\ assay) - OD\ colored\ tissue\ (no\ MTT\ assay)}$$

Histological analysis

For characterization of microscopic structure of exogenous 3D skin model, and comparison with our 3D skin platform, morphological analysis on histological section was performed both on EpiDerm 312X FT and our 3D HSE skin model. On the day of receipt, EpiDerm 312X FT samples were removed from agarose support and placed in a 12 well plate and maintained in culture medium at 37°C for 24 h. Subsequently, samples were fixed with 10% neutral-buffered formalin fixative for 2–4 h at RT and rinsed twice with PBS buffer solution. After the fixation and dehydration procedure, samples were embedded in paraffin to be sectioned and stained. 7 µm transverse sections of samples were stained using hematoxylin-eosin (Bio Optica) solutions and Picro Sirius Red (PSR) (Sigma Aldrich) following standard procedure and analyzed by an optical microscope (BX53; Olympus). Polarized light images of samples stained with PSR alone were acquired with an inverted microscope (BX53; Olympus) with a digital camera (Olympus DP 21). A linear polarizer was placed between the light source and the specimen, while the analyzer was installed in the light path between the specimen and the camera. It is known that the color of collagen fibers stained with PSR and viewed with

polarized light depends upon fiber thickness; as fiber thickness increases, the color changes from green to red [13], [14].

Collagen structure by Second Harmonic Generation imaging

For the Second Harmonic Generation (SHG) imaging (see chapter 2), at the time of receipt, Phenion and EpiDerm 312X FT samples were removed from agarose support and placed in a 12 well plate and maintained in culture medium at 37°C for 24 h. Subsequently, samples were fixed in 4% paraformaldehyde for 30 min at RT, washed in PBS and observed in their 3D structure. SHG imaging were performed using a Confocal Leica TCS SP5 II femtosecond laser scanning system (Leica), coupled to a tunable compact mode-locked Ti:sapphire laser (Chamaleon Compact OPO-Vis, Coherent) (for details see the chapter 2). Nuclei were stained with Sytox Green (1:10000, Invitrogen).

Contact angle measurements

In order to estimate surface proprieties and wettability of our 3D endogenous HSE and EpiDerm 312X FT, contact angle measurements were performed on samples.
In particular, human skin *stratum corneum*, (the outer layer of the *epithelium*) is a complex of proteins, water-soluble components and lipids, and it acts as a primary barrier to transdermal diffusion for most substances and it is responsible for the physicochemical properties of the human skin surface. The main function of the skin is to minimize water loss entry of foreign matter [15]. For these reasons, the study of superficial properties and their modification (for example induced by cosmetics or surfactants treatments) is a central focus of cutaneous, cosmetic and pharmaceutical research. The human skin-wetting process is the main factor of its protective and barrier functions: minimizing water loss and preventing the entry of foreign matter and chemicals [15], [16]. Contact angle measurements were performed by means of the static, sessile, optical contact angle drop method with

Attension Theta optical tensiometer (Biolin Scientific). An amount of 1.5 ml of MilliQ water was dropped on dry samples at 3 ml s^{-1} dispense rate. The plateau value of the contact angle was reached after 1 min and five images were recorded and analyzed by Young Laplace fitting method for every drop.

4.2.2 Scale-up of 3D human skin equivalent multistep tissue process

In order to obtain endogenous human skin models as effective and useful testing platform, responsive to external stimuli and to testing molecules and compounds (see Chapter 3) we set up a multistep process according to a bottom-up approach and we introduced several check points to ensure the good manufacture of our skin systems step by step, from primary extracted fibroblasts, to final 3D human skin models. The main phases of fabrication of 3D endogenous HSE was widely described in the chapter 2, performed by a multistep bottom up approach.

3D Human skin equivalent model realization

As widely explained in the chapter 2, 3D endogenous HSE were fabricated by bottom-up approach. Briefly, primary human dermal fibroblasts extracted by human biopsy (they were obtained by "Azienda Ospedaliera di Rilievo Nazionale e di Alta Specializzazione (AORN) A. Cardarelli/Santobono/Pausillipon at Urology and Biotechnology Centre-AORN" according to the project "Realization of human skin equivalent *in vitro*" after approval of ethical committee") were sub-cultured into 1720 cm^2 tissue HYPER*flasks* (Corning) with a density of $8x10^3$ cell/cm^2 in order to improve cell number and reduce risks of contamination. Cells were and maintained in culture medium (Minimum Essential Medium with Earle's salts, Microgem) containing 20% fetal bovine serum (FBS), 100 mg/ml L-glutamine, 100 U/ml penicillin/streptomycin (P/S), and 0,1 mM non-essential amino acids at 37 °C, 5% CO_2 and humidity 90%. Human Dermal microTissue Precursor (HD-µTP)

were obtained by seeding HDF (passages 5-9) on gelatin porous microcarriers crosslinked at 4% with D-(+)- Glyceraldehyde (Sigma Aldrich), in a spinner flask (Integra Bioscience) for 9 days. Each spinner flask was initially loaded with 9.5 x 10^6 HDF and 172 mg of microbeads, corresponding to 10 cells/beads. Spent 9 days in dynamic culture, HD-µTP were transferred into the maturation chamber to allow their molding in disc-shaped tissue-construct such as Human Dermis Equivalent (HDE) (1 mm in thickness, 5 mm in diameter) as previously described in the chapter 2. Maturation of HDE was carried out until 6 weeks in dynamic conditions by placing the maturation chamber on the bottom of a bioreactor (Bellco) operated at 60 rpm at 37°C, 5% CO_2 and humidity 90%. The medium was changed every 2 days and ascorbic acid (TCI) was added at a concentration of 50 µg/ml. At the end of 6 weeks of maturation, chambers were opened and HDE were extracted and prepared for primary keratinocytes seeding. As described in the chapter 2, human keratinocytes were obtained from biopsy and cultured into 150 cm^2 tissue flasks with a density of $2x10^4$ cell/cm^2 in culture medium KGM_2 (Promocell) supplemented with 0.1% transferrin, 0.1% epinephrine, 0.1% hydrocortisone,0.1% insulin, 0.1% H-EGF, 0.4% BPE, 5% FBS, 1% P/S and calcium chloride at 0.06 µM and maintained 37 °C, 5% CO_2 and humidity 90%. 3D-HDE were prepared for keratinocytes seeding by a human fibronectin coating for 45 min and during this time, keratinocytes were washed and trypsinized. Cells were counted (150,000 cells/samples of 5 mm diameter), seeded on the human dermis models surface and maintained in submerged culture conditions for 6 days in order to allow cell adhesion and proliferation. After 6 days of submerged conditions, the cultures were raised to the air-liquid interface for 14 days in culture medium with a different composition (0.1% transferrin, 0.1% epinephrine, 0.1% hydrocortisone, 0.1% insulin, 1% P/S, without EGF and BPE and with calcium chloride at 1.88 µM) in order to induce and stimulate differentiation and

stratification of epidermis thanks to the contact to the air and to the high concentration of $CaCl_2$ [17], [18].

Quality control check point of cell cultures

In order to evaluate the good conditions of extracted primary dermal fibroblasts, cells were amplified in HYPER*flasks* of 1720 cm^2 and controlled during the amplification to avert any contamination and such a trans-differentiation in activated contractile fibroblasts [19], [20].

The modulation of the fibroblast into the modified fibroblast, as myofibroblasts, has been the object of several studies and seems to be caused by several agents or stimuli that trigger the evolution of the fibroblast into the proto-myofibroblast, and then, in activated myofibroblast [21]. Contractile fibroblasts are involved in wound healing and fibrocontractive disease, and they represent key players in the physiological reconstruction of connective tissue after injury and in generating the pathological tissue deformations that characterize fibrosis [19] [22]. The density of seeding ($8x10^3$ cells/cm^2) and several external stimuli can trigger the activation of fibroblasts transition in contractile modified fibroblasts: it is well established that the first changes that fibroblasts undergo during myofibroblastic modulation are the acquisition of a spindle shaped thanks of stress fibers composed of cytoplasmic actin. Contractile fibroblasts are positive for α-smooth muscle actin (α-SMA) and in a first phase, they do not secrete collagen [21].

During the culture period, fibroblasts were controlled in shape and in time of cellular generation, following this formula at each trypsinization. Only if cells conserved a time generation of 0.46, they were used for 3D-HSE fabrication.

$$Doubling\ time = \frac{\log(final\ cell\ concentration) - \log(initial\ cell\ concentration)}{log2\ x\ duration}$$

Quality control check point of HD-µTP

The second quality control was performed on HD-µTPs at 9^{th} days of dynamic culture in spinner flask both on 3D samples and on histological sections in order to evaluate collagen deposition and the expression of α-SMA as marker of transition in contractile fibroblasts.

Collagen structure by Second Harmonic Generation imaging

For collagen assessment, samples taken from spinner flask were washed in PBS and then fixed with paraformaldehyde solution 4% for 20 min at RT and rinsed twice with PBS. After fixation procedure, samples of 3D HD-µTP were observed to evaluate collagen deposition by Second Harmonic Generation (SHG) imaging as explained in the chapter 2.

Immunolabelling

The expression of α-SMA was evaluated performing an immunofluorescence directly on 3D fixed HD-µTP. Samples were washed in PBS and fixed with paraformaldehyde solution 4% for 20 min at RT and rinsed twice with PBS. Samples were incubated with histoblock solution at 3% of bovine serum albumine (BSA, Sigma Aldrich), 3% of FBS and 0,001 % Triton-X100 (Sigma-Aldrich) for 1 h at RT. Subsequently, samples were incubated with primary antibody anti α-SMA (monoclonal, 1:100, Abcam) for 2 h at RT. Secondary antibody used was Alexa Fluor donkey anti-mouse 546 (1:500, Life Technologies). Nuclei were stained with 4',6-diamidin-2-fenilindole (DAPI, 1:10000, Invitrogen).

Quality control check point of 3D human dermis and skin equivalent

These quality checks were performed on 3D-HDE after 6 weeks of maturation time culture and on the final products (3D-HSE) after 14 days at air-liquid culture condition. We compared good and poor quality samples in order to evaluate the manufacture of our product during the tissue process. For human dermis and skin models characterization, morphological analysis was performed on histological section of samples during the maturation phase in bioreactor culture system. Samples were fixed with 10% neutral-buffered formalin fixative for 2–4 h at RT and rinsed twice with PBS buffer solution. After the fixation and dehydration procedure, samples were embedded in paraffin to be sectioned and stained. 5 µm transverse sections of samples were stained using hematoxylin-eosin (Bio Optica) solutions, analyzed by an optical microscope (BX53; Olympus).

Quality control check point of Fetal Bovine Serum and culture media by streaking agar plate

FBS was one of the leading cause of bacterial contaminations [23], [24]. Since FBS was used at 20% in fibroblasts growth medium, in order to avoid any risk of contaminations, FBS purchased from Sigma Aldrich was thawed at 4°C overnight and an aliquot of about 2 ml were taken from the bottle. A sterile cotton bud was immersed in FBS aliquot and then a streaking on BHI (Brain Heart Infusion) agar plate (BD Falcon) was performed. The same procedure was performed also for culture media of extracted primary cells and of spinner flasks during the different phases of tissue process. The plate was leaved at 37°C for 48 h. Any bacterial contamination was visible on the plate by the formation of colonies distributed along the streaking.

Mycoplasma detection assay

Mycoplasmas are important tissue culture contaminants that exist in close association with the host cell membrane. This infection causes structural damage and changes in host cell metabolism which can interfere with experiments or result in the loss of the infected cell line [25]. In fact, the contamination of cell cultures by mycoplasmas remains a major problem in cell culture. Mycoplasmas can produce a virtually unlimited variety of effects in the cultures they infect [26]. Constant monitoring of cells is therefore imperative [25]. There are several procedures to detect mycoplasma contaminations, such as cultivation in appropriate media, immunofluorescence, or measurement of uridine-uracil incorporation ratio, and fluorescent staining by DNA-binding dyes such as DAPI and Hoechst 33258 [25]. We performed a mycoplasma detection assay (ApplyChem) based on the amplification by PCR of ribosomal subunit of RNA 16S on supernatant aliquots of FBS, of culture medium of primary fibroblast and keratinocytes extracted from biopsy, and on culture media withdraw from spinner flasks at each critical phase of tissue process: before HD-µTP molding, at 9th day of culture, and at 2 and 4 weeks of maturation phase of 3D-HDE tissues.

Procedure. According to manufacturing procedure, samples were prepared to the assay transferring 0.5-1.0 ml cell culture supernatant into a 2 ml centrifuge tube. To pellet cellular debris, samples were centrifuged at 250 xg briefly. Subsequently, supernatants were transferred into a fresh sterile tube and centrifuged at 15000-20000 xg for 10 min to sediment Mycoplasma. Carefully the supernatant was decanted in order to keep the pellet (not always visible). Pellet was re-suspended in 50 µl of the Buffer Solution (provided by the kit), mixed thoroughly with a micropipette and heated to 95°C for 3 min. The test sample could be stored at this stage at -20°C for later use.

For the PCR amplification, we prepared the reaction mixture in a PCR tube by combining the reagents in a specific ratio, as shown in Table 2.

Reagents	Volume
H_2O	35 µl
Reaction Mix	10 µl
Test sample	5 µl

Table 2. PCR amplification reagents

Before of loading samples, mineral oil was added (approximately 40 µl) to avoid the evaporation of the reaction mixture. All tubes were placed in DNA thermal cycler and parameters were set for the following conditions (see the Table 3).

94°C	30 secs.	
94°C	30 secs.	36 cycles
60°C	120 secs.	
72°C	60 secs.	
72°C	4 min.	
4 - 8°C	Cool down and hold	

Table 3. Thermal cycler parameters

For electrophoresis, 2% Agarose was prepared (Sigma Aldrich), enriched with about 6 µl of ethidium bromide (Sigma Aldrich) as intercalating agent of DNA, emits a fluorescence when exposed to UV light. 20 µl of all PCR products, including negative control (only Buffer solution) and positive control (1 µl of

Positive Template Control, provided by the kit) were added to the gel agarose electrophoresis. The size of DNA fragments amplified using the specific primers in this kit is 270 bp. Amplification products were observed with ChemiDoc XRS System (Biorad), and images were acquired with Quantity One software.

Industrialization and working plan set up of all tissue process operations to allow a large-scale production

In order to improve the bioprocess productivity and ensure endogenous 3D-HSE fabrication in large scale for the commercial availability, we set up an accurate strategy plan for the scale up of tissue process. This method allowed to guarantee the complete control on yield and quality products, and in the same time, to increase the productivity by means of the parallelization of our bioprocess obtaining a safety and standardized protocols to ensure about 200 tissue products per month available for several tests and applications.

First of all, to increase the productivity, we employed all tools and procedures to improved volumes, cell numbers, amount of tissue produced using big bioreactors (Bellco) of 500 ml working in parallel at the maximal capacity; second, in order to control all steps of tissue process; we purchased both of small and big incubator (Esco AirFlow and Thermo Scientific, respectively) to start tissue production in series. We optimized our bioprocess identifying 5 phases of bioprocess and for each phase we characterized main critical points that could compromise the manufacture quality of tissue system.

We developed a weekly program for each laboratory operation related to a single tissue process phase, ensuring the best organization in order to obtain a constant number of tissue models each month.

4.3 RESULTS

4.3.1 Characterization of Phenion Full-Thickness skin model by Henkel by SHG imaging

The equivalent skin samples Phenion Full-Thickness skin model were purchased from Henkel in order to study the characteristics and the composition of one of the most important skin model competitor commercially available. The dermal compartment is obtained starting from a mixture of reconstituted bovine collagen and glycosaminoglycans that formed a sponge, and human fibroblasts (Normal Human Fibroblast) extracted from biopsy. The epidermis is produced from a population of epithelial cells seeded on the dermal surface and made adequately differentiate into a multilayered *epithelium* in air-liquid interface [27]. The entire system is sent in a 24 well plate, and each skin models is set on a polycarbonate filter and embedded in a mixture solution of agarose and culture medium. At the time of delivery Petri dishes were filled with the ready-to-use ALI-medium provided with the skin models and samples were removed from the agarose, resting on filter paper in order to ensure the air-liquid culture condition (Figure 1a). Samples were maintained in this culture configuration for 24 h at 37°C and subsequently were fixed in paraformaldehyde 4% for 20 min in order to perform a SHG imaging.

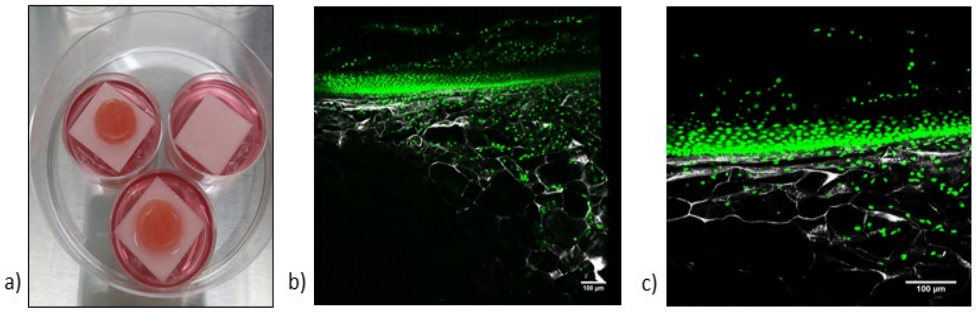

Figure 1. Characterization of Phenion Full-Thickness skin model. a) Phenion skin models at the time of receipt laying on filter paper to recreate the air-liquid culture condition; tissue model composition with cells in green and scaffold in grey by tile scan function and conventional acquisition (b and c respectively). Bars are 100 µm.

As shown in Figure 1b and c, Phenion Full-Thickness skin model was composed of a spongy matrix, made of a mixture of reconstituted collagen and GAGs which confers a porous structure to the scaffold. Fibroblasts did not deeply penetrate into the spongy matrix, and they were distributed in the upper part of the dermal compartment (about 10 µm). Keratinocytes, distributed on the top of the dermis, composed a high cellularized *epithelium* scarcely differentiated: in fact, as better seen in Figure 1c, the *epithelium* was rich of cells in all its layers without an adequate stratification, since the upper stratum of epidermis were highly cellularized. These data highlighted the limitations of this skin model related to the scarce complexity both of dermal and epidermal compartment. The dermis was lack of an endogenous well organized ECM, and of homogeneity in cell distribution, while the epidermis is not adequately differentiated and stratified.

4.3.2 EpiDerm 312X FT skin model by MatTek Corporation and comparison with our endogenous 3D human skin platform

In order to assess the morphology and the composition of another gold standard skin model, we purchased the EpiDerm 312X FT skin model by MatTek Corporation. Samples were shipped in a 12 well plate and embedded in a mix solution of agarose and culture medium in a similar configuration of Phenion Full-Thickness skin model. On the day of receipt, samples were removed from agarose and leaved in polycarbonate filter to ensure the air-liquid interface condition. After 24 h, we conducted an irritation test, to evaluate the effective functionality of model as a screening platform for cosmetic testing, and a macroscopic analysis through the stereomicroscope (Olympus) and histological analysis in order to obtain a morphological characterization and a useful comparison between our endogenous 3D human skin platform and the best competitor skin model commercially available.

Irritation test

To test the cell viability and the models response to an irritant compound, an irritation test was performed using 5% SDS as irritant substance and PBS 1X as a control solution. Irritant compound was put in contact with samples for 60 min and subsequently a MTT assay to assess cell viability was conducted. As shown in Fugure 2b after MTT test, the purple color of control sample (treated with PBS 1X) denoted a higher cell viability compared to samples treated with the irritant compound. After solubilization of formazan with isopropanol, the absorbance of the supernatant was read at 570 nm and the relative cell viability was calculated: the relative viability of the samples treated with PBS 1X was equal to 100%; while the viability of samples treated with SDS 5 % was equal to 33% (Figure 2c).

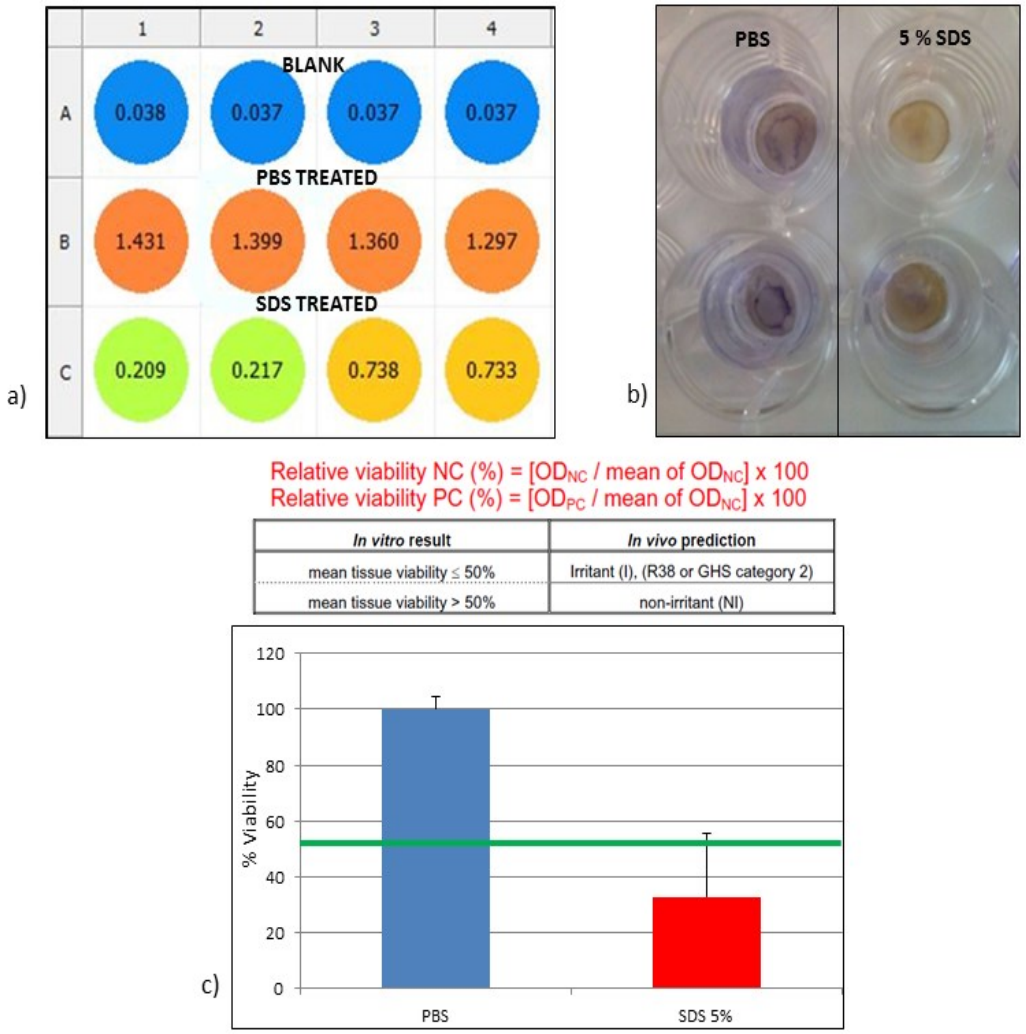

Figure 2. Irritation test on 3D skin equivalent EpiDerm 312X FT. a) Absorbance reading of MTT test for cell viability at 570 nm; b) MTT assay after the treatment with PBS and 5% SDS; c) relative cell viability calculated according to the manufacturing procedure.

Histological characterization

In order to characterize the structure and the morphological composition of exogenous 3D EpiDerm 312X FT skin model, histological analysis of tissue slides was performed. The simple composition of ECM was highlighted from H&E staining of 7 μm paraffin-embedded tissue slices as shown in Figure 3. In fact, the ECM network was less cellularized than endogenous ECM of our 3D–HSE counterpart. PSR staining showed several green, thin and immature collagen fibers, typical of reconstituted collagen used for the realization of dermal compartment. This structural organization was confirmed also by SHG images, which showed a diffuse grey signal without collagen organization in fibers or bundles (Figure 3g).

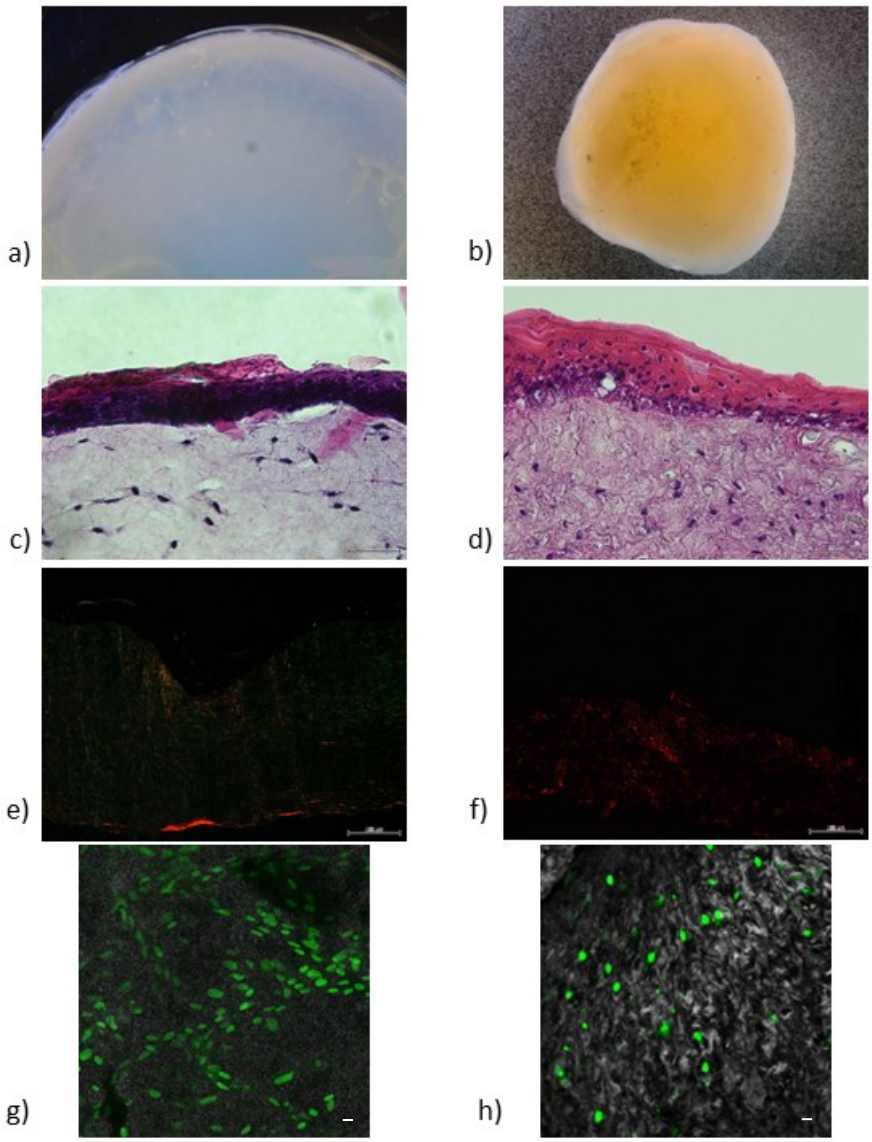

Figure 3. Comparison between our endogenous 3D human skin system and EpiDerm 312X FT skin model by MatTek Corporation. Images acquired at stereomicroscope (Olympus) of entire superficial features of EpiDerm 312 X FT (a) and 3D human skin equivalent (b); and H&E staining of paraffin embedded tissue of EpiDerm 312X FT and 3D-HSE (c and d respectively); PSR staining of embedded tissue slices of and EpiDerm 312X FT and 3D -HSE (e and f respectively); SHG images of collagen signal of ECM (endogenous 3D HSE in g and EpiDerm 312X FT in h). Nuclei were stained with Sytox Green. Bars in c-f) are 100 µm, bars in g-h) are 25 µm.

Thanks to morphological and histological analysis, differences between our 3D-skin system and EpiDerm 312X FT skin model became evident. Our 3D skin system appeared compact shaped, resistant to pressure and tension, with a compact network of endogenous ECM that primary fibroblasts assembled and secreted themselves spontaneously during the maturation phase in dynamic culture conditions. 3D EpiDerm 312X FT was made by reconstituted bovine collagen type I mixed with a primary fibroblasts and human keratinocytes seeded on the dermis surface, but the exogenous ECM is a simple system without any complexity and architecture. Our endogenous 3D human skin model was obtained with an innovative approach that allow and stimulate primary fibroblasts to produce endogenous ECM in a dynamic culture system. In fact, the endogenous ECM was rich of collagen, elastic fibers and glycosaminoglycans produced by cells: the dermis compartment recapitulated all features of human counterpart in term of morphology, function and organization. In the same time, in order to obtain the epidermal layer, primary keratinocytes were seeded on dermis compartment, mixed to a population of melanocytes that gave to our skin model the typical light brown color with spot of dark brown pigment (Figure 3a and b). PSR staining and SHG signal confirmed the presence of immature and thin collagen fibers not assembled in a consistent ECM for EpiDerm 312X FT skin model compared to ECM of our model. The ability our human skin equivalent in representing a more physiological and cell-instructive environment was probably due to the endogenous nature of HDE [28]. Indeed, HDE are composed of an intricate complex of cells and cell-synthesized matrix, which resembles the structure and the physiology of its *in vivo* counterpart. Histological analyses highlighted that human dermal fibroblasts actively produced and correctly assembled ECM components, and they showed a typical elongated morphology and were

embedded in their own ECM. Finally, we assessed that our 3D skin system mimics more closely the morphology of native human skin.

Wettability of samples

In order to further investigate the functionality of the model, we evaluated the surface wettability, which is strictly correlated with the barrier properties of the skin, by measuring its contact angle [29]. We found that our 3D organotypic tissue HDE presented a value of 83.1± 4.3, while exogenous skin model a value of 66.2 ± 8.5 (Figure 4). Such results suggested that the physiological barrier function of the skin was better recapitulated on our human skin equivalent model. These data suggested that there is a functional crosstalk between fibroblasts and ECM components secreted by cells themselves and keratinocytes of epidermal compartment, and that the complexity of ECM and its organization could stimulate and trigger the keratinocytes differentiation and stratification. [30], [31].

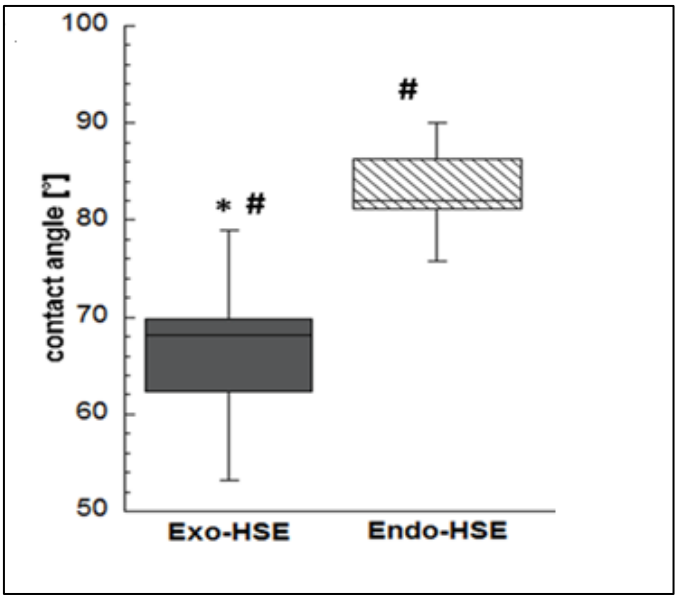

Figure 4. Contact angle measurement. Wettability properties by contact angle measurement on EpiDerm 312X FT skin model (exogenous skin model) and our endogenous 3D-HSE (Endo-HSE). (All bars are 200 mm; *, #p < 0.001).

We investigated the main morphological differences between our model and the best competitor models commercially available, Phenion Full-Thickness skin model and EpiDerm 312X FT skin model purchased from Henkel and MatTek Corporation respectively. The morphological characterization on histological sections revealed the complexity of our 3D human skin models, which is characterized by a compact endogenous ECM secreted and assembled by dermal fibroblasts during the culture period of the maturation phase. Thanks to loading of HD-μTP in the maturation chamber, tissue precursors aggregated for the realization of dermal compartment. In fact, the dermis of our models was composed of a homogenous cellular population embedded in a complex ECM enriched of collagen fibers and elastic components that gave support to the tissue system mimicking the native counterpart (as seen in Figure 3).

4.3.3 Industrialization of 3D human skin equivalent models production

The improvement of productivity and development of our 3D skin tissues was obtained by setting up a laboratory fully dedicated to the sole production of skin models. Tissue process already applied for the development of skin models in small-scale was achieved employing several methods and instruments useful to increase the cell numbers, culture media volumes, HD-µTP and 3D HSE models fabricated. In order to transfer the production from the small scale to the large scale, we purchased large instruments and devices to maximize the production.

Figure 5. Improvement of skin models production. a) small bioreactor used for tissue production in small scale; b) big bioreactor employed for the fabrication of dermal tissues; c) small incubator for cells cultivation and amplification (d); industrial incubator for the development of HD-µTP (f) and skin tissue (g) in large scale.

In particular, the transition from the small scale to the large scale it has involved the use of big bioreactors (Bellco), able to accommodate 4 maturation chambers with a maximal capacity of 500 ml of cell culture medium, substituting small bioreactors (Bellco), used hitherto able to accommodate only one maturation chamber in a maximal volume of 120 ml, as shown in Figure 5a and b. The use of big bioreactor working in parallel at the maximal capacity allowed us to increase the production of 3D skin models, since each big bioreactor accommodated 4 maturation chambers, containing 7 skin models draw each. In addition to the employment of big bioreactors, we purchased two type of incubators: a small conventional incubator (Esco AirFlow) of 75 L, for the maintenance and the amplification of cell cultures used in our tissue process (dermal fibroblasts and keratinocytes) (Figure 5c and d); and an industrial incubator (Thermo Scientific) of 680 L, for the fabrication of HD-µTP and of dermal skin models (Figure 5e, f and g, respectively) with the possibility of start multiple tissue process in parallel to intensify the productivity. For the sterilization of tools and instruments, a big industrial autoclave (Falc), with 4 preset sterilization cycles and 1 manual sterilization cycle was purchased, and two different cell culture hoods (Esco AirFlow), were used in order to separate the cell extraction activities from others producers of the tissue process, reducing drastically the risk of contaminations (in Figure 6).

a)  b) 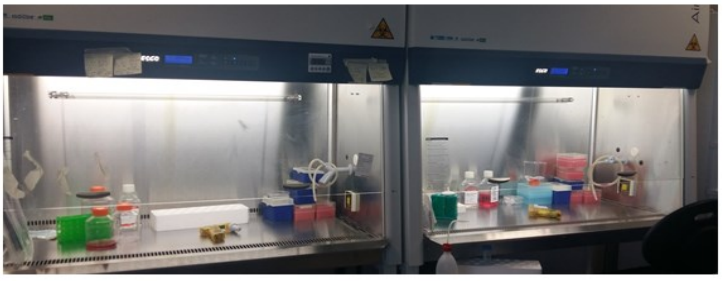

Figure 6. Instruments employed for the industrialization of human skin equivalents production. a) large autoclave for the sterilization of big bioreactors and big spinner flasks; b) cell culture hoods for cell extraction from human biopsy and all other phases of tissue process.

All these measures employed to produce skin models in large scale, were applied to intensity and enhance the productivity in two manners: on the one hand, by the purchasing of instruments with a greater capacity and higher dimensions, and on the other, by the production of skin tissue models in series, using big bioreactors working in parallel at their maximal capacity of 4 chambers and 7 dermal tissues for chamber. In this way, we increase not only the total cell number for each tissue process, but also HD-µTP obtained and final 3D-HSE fabricated for month.

4.3.4 Organization planning to improve human skin models production

To improve the productivity of our tissue process, we introduced crucial check points in each critical phase of bioprocess and we defined an accurate organization plan of laboratory activity during the work week. This plan allowed to guarantee a continuous productions of tissue models in large scale, ensuring good manufacturing products with the maximum yield [3], [32]. The improvement of tissue production was obtained by defining the specific sequence of single steps of

tissue process and by programming each activity and operation for each day of work week. This accurate program allowed to ensure a perfect activity organization and the production of a constant number of tissue every month, with the purpose of sustaining the market requirements and competing with other skin models commercially available.

As shown in the first scheme, in Figure 7a, we divided the whole tissue process in 5 main phases, which included critical steps:

A. Fabrication of HD-µTP;

B. Loading of HD-µTP after 9 days in dynamic culture conditions;

C. Preparation of 3D-HDE after 6 weeks of maturation phase;

D. Keratinocytes seeding on 3D-HDE in order to obtain final 3D-HSE;

E. End of air-liquid interface culture condition and realization of 3D-HSE as final products of our bioprocess

The subdivision of the process in these main phases allowed us to set up an accurate organization plan of the work week. In the second scheme, in Figure 7b, we set up a weekly working program with the purpose of standardizing each laboratory activities to better control and improve the sale-up of tissue production. The laboratories activities were divided by hours of work of an individual operator considering all operations related to every step of tissue process, as change culture media, (referring both to culture cells, spinner flasks and bioreactors), preparation of solutions and cleaning or sterilization of work tools and instruments.

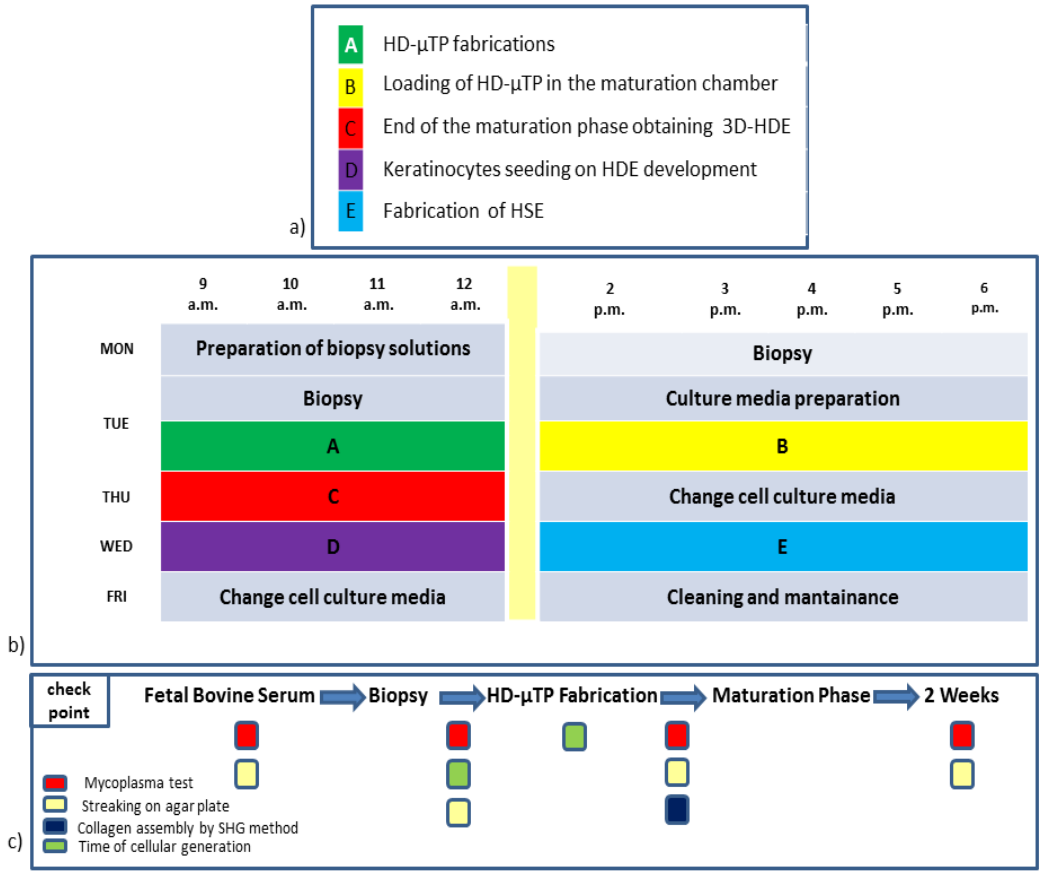

Figure 7. Schematization of weekly working plan of tissue process. a) Tissue process division in 5 different critical steps; b) organization of laboratory activities during the working day of one operator who can started a whole bioprocess each week compatibly with the duration of each activities; c) selective check points and quality controls of each preparative procedure and critical step of the bioprocess.

The distribution of each laboratory activity was defined on the basis of duration and complexity of single operation, compatibly with the working day of an individual operator, in order to produce skin tissues in series, starting with a tissue process every week ensuring a constant tissue yield for month. In fact, as schematized in the Figure 7b, a tissue process, from step A to step E, was started and completed over the week, thanks to production in series, and bioreactors operating in parallel. The accurate organization of each working day activities

represented a powerful strategy in a view of an industrial scale-up of tissue production. The last schematization, in the Figure 7c, represents the check points and quality controls introduced in each single step of the whole bioprocess in order to ensure the good manufacture of our tissue products. The crucial quality controls were applied not only in tissue process steps but also to check reagents, FBS, and cell source. The main check points were: mycoplasma detection assay, streaking on BHI agar plate, collagen assembly evaluation by SHG imaging and calculation of cellular generation. These controls were made on serum aliquots, culture media of cells and of HD-µTP at the end of 9 days in spinner flask, and during the maturation phase.

Mycoplasma and bacterial contaminations, could result from FBS [23], [26], from bioptical samples or acquired during the routine operation of change media. Collagen assembly evaluation was assessed by SHG imaging on HD-µTP before the loading in a maturation chamber and finally, cellular time generation was calculated on cell culture and on HD-µTP, during the 9 days of assembling in dynamic culture in order to evaluate cellular proliferation. This accurate plan had the purpose to intensify and improve the production of 3D endogenous skin models by a scale-up strategy in order to make available our products on the market as a competitive tissue system in the industry of equivalents skin models.

4.3.5 Quality control of HD-µTP

With the aim of guarantee the best quality of final tissue products, we introduced several check points in each critical step of our bioprocess. The first critical step of the bioprocess is the evaluation of HD-µTP after 9 days of dynamic culture in spinner flasks. During this period, primary dermal fibroblasts inoculated in gelatin microcarriers, began to proliferate, produce and assembly a collagenous matrix

that embedded cells and beads as a dense structural network. To verify this conditions, before molding of HD-µTP, an immunofluorescence for α-SMA and SHG imaging were performed on fixed 3D samples. As shown in Figure 8, we compared poor quality α-SMA-positive HD-µTP with optimal HD-µTP, negative for α-SMA expression. α-SMA is marker of transition from dermal fibroblasts to contractile fibroblasts. Poor quality HD-µTP were characterized also for the absence of collagen deposition evaluated by SHG signal (Figure 8a and c). On the contrary, optimal HD-µTP showed the absence of α-SMA signal, and an high deposition of collagen (Figure 8b and d, respectively) at the end of 9 day of dynamic culture in spinner flasks.

The best quality HD-µTP in fact, showed a compact structure composed of cells and porous microbeads, totally embedded in a dense collagenous matrix. It was interested to observe that collagen bundles (Figure 8d in grey) were assembled not only around the HD-µTP, but also inner each microbeads, indicating that cells penetrated inside gelatin scaffolds thanks to their interconnected porosity. With this check point on the first phase of tissue process, it was possible to evaluated the best proprieties of building blocks, discarding all poor quality HD-µTP that did not respond to our needs. In fact, in order to obtain optimal endogenous human skin models in terms of morphological, structural and functional characteristics, it was necessary to select only the best HD-µTP, enriched in cells and collagen.

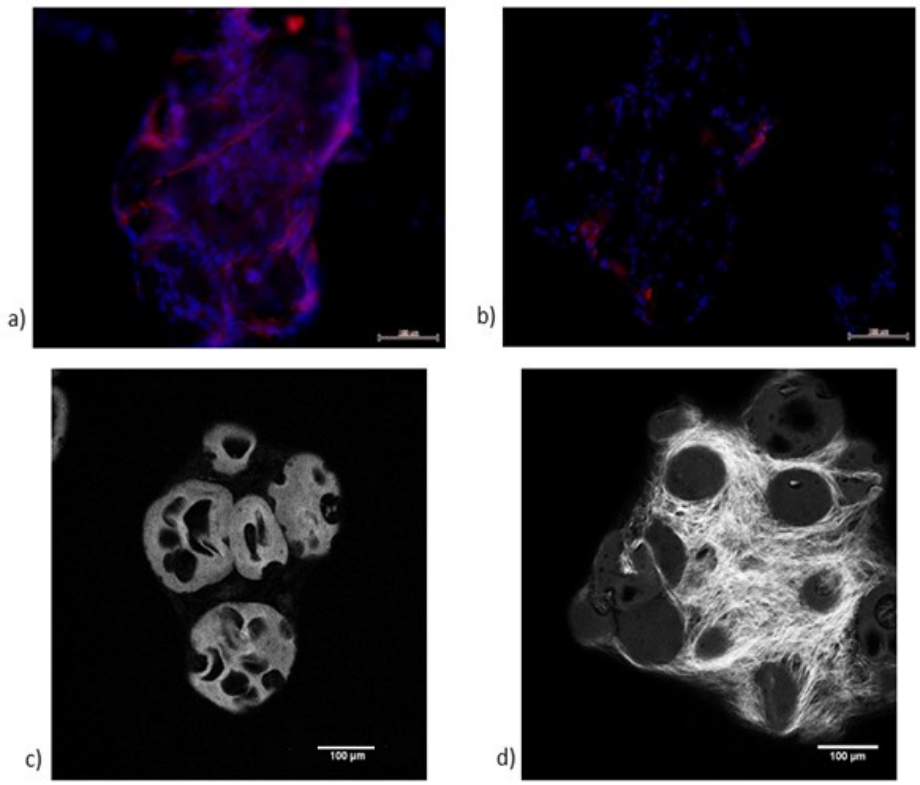

Figure 8. Quality control check point of HD-µTP at the end of 9 days in spinner flasks. a) poor quality HD-µTP showed positivity for α-SMA expression (in red) with a low collagen deposition (c); b) optimal HD-µTP showed the absence of α-SMA expression by fibroblasts and a significant collagen production visualized by SHG signal in grey (d). Nuclei were stained with DAPI. Bars are 100 µm.

With these results, we demonstrated the effectiveness of our quality control, in order to identify the bad products and discard them. The expression of α-SMA is related to the activation of dermal fibroblasts in modified contractile fibroblasts [19] that, for some reasons not yet fully clarified, reduced their duplication time and stop producing ECM during the dynamic culture. These abortifacient products compromise the development of final 3D human skin equivalent models because

of cells could not support a significant collagen deposition during the maturation phase, basic requirements for a good development of dermal compartment.

4.3.6 Quality control of endogenous 3D human dermis equivalent models

The second check point of our tissue process was the quality control of 3D human dermis equivalent during the maturation phase. We assessed that by using poor quality HD-µTP, we obtain abortifacient dermal compartment that could not support keratinocytes differentiation and stratification to form a good *epithelium* comparable to native counterpart. During the maturation, HD-µTP molded in the maturation chamber interacts each other: cells migrate from one to another HD-µTP producing and assembling ECM enriched of collagen, elastic fibers and glycosaminoglycans that confer firmness and resistance to dermal compartment. To verify this optimal conditions of dermis, before the development of a full thickness skin system, a morphological analysis on tissue sections was performed. As shown in Figure 9, H&E stained sections revealed several differences between two types of human dermis equivalent models. In the Figure 9a it was evident the poor quality of dermal compartment of samples examined: ECM, stained in pink, was disrupted, not compact and inhomogeneous. It was possible still to see traces of microbeads partially degraded inside dermis that did not show any continuity along the sample. On the contrary, the Figure 9b showed a perfect dermal compartment, which cells, stained in purple, were completely embedded in a compact, homogenous and structured matrix (in pink), with the disappearance of microscaffolds, that were degraded during the cellular remodeling of the ECM.

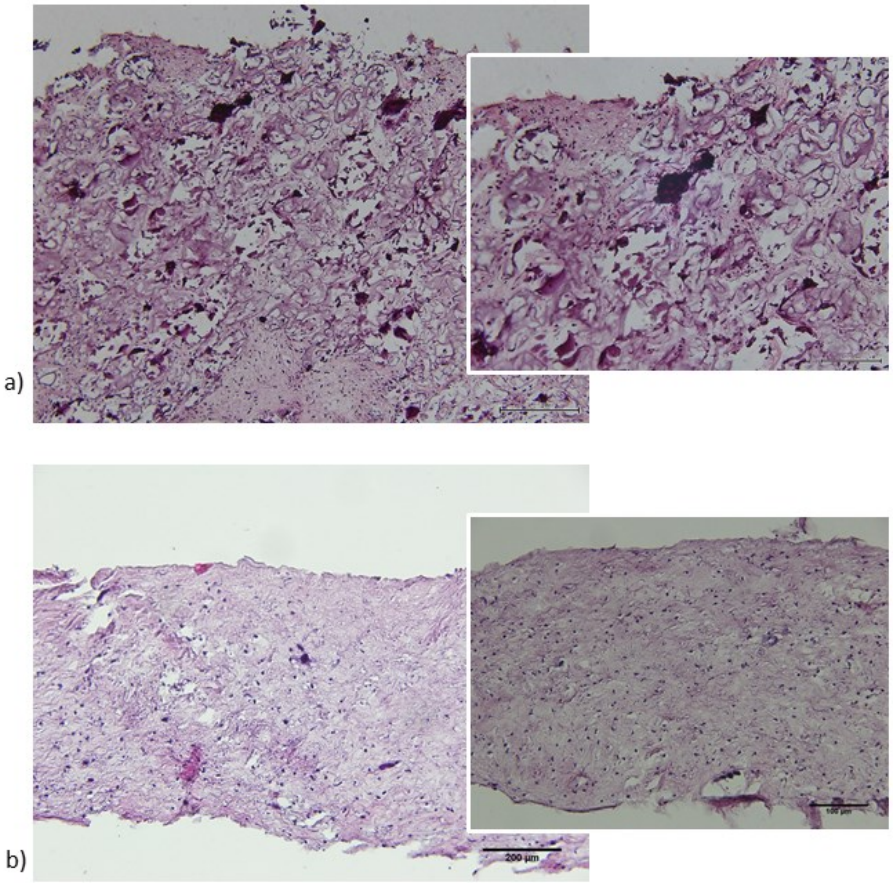

Figure 9. Morphological analysis of 3D human dermis equivalent models. a) H&E staining on tissue sections of 3D-HDE which showed poor quality dermal compartment with microscaffolds not completely disappeared and an ECM scarcely homogenous; b) an optimal dermal compartment which cells were well distributed and closely embedded in a compact and dense ECM with no trace of microscaffolds, completely degraded by cells remodeling process. Bars in a-b) are 200 µm; bars in magnified images are 100 µm.

These data suggest that this second tissue process check point was crucial to verify the best quality of dermal compartment before keratinocytes seeding. As known from literature, dermal fibroblasts support and sustain keratinocytes differentiation [30], and for these reasons a good dermis is required for the fabrication of a functional full thickness skin systems.

4.3.7 Quality control of endogenous 3D human skin equivalent models

With the aim of evaluating the manufacture of endogenous 3D human skin equivalent models, a last quality control was carried out on samples at the end of tissue process. H&E staining images showed two type of samples with different morphological features.

The Figure 10a showed a poor quality 3D-HSE sample, which highlighted an inhomogeneous ECM with empty spaces leaved by microbeads just disappeared, and an inadequate *epithelium*, characterized of a single layer of keratinocytes not stratified attached on dermis surface. Conversely, in the Figure 10b, it was possible to observe an optimal quality of 3D-HSE, which showed a compact and continuous ECM enriched in cells and collagen, with a continuous dermal-epidermal junction composed of keratinocytes belonged to the germinative layer that reproduced a differentiated and completely stratified *epithelium* at the end of air-liquid interface. These data highlighted the powerful of check points at each step of our bioprocess.

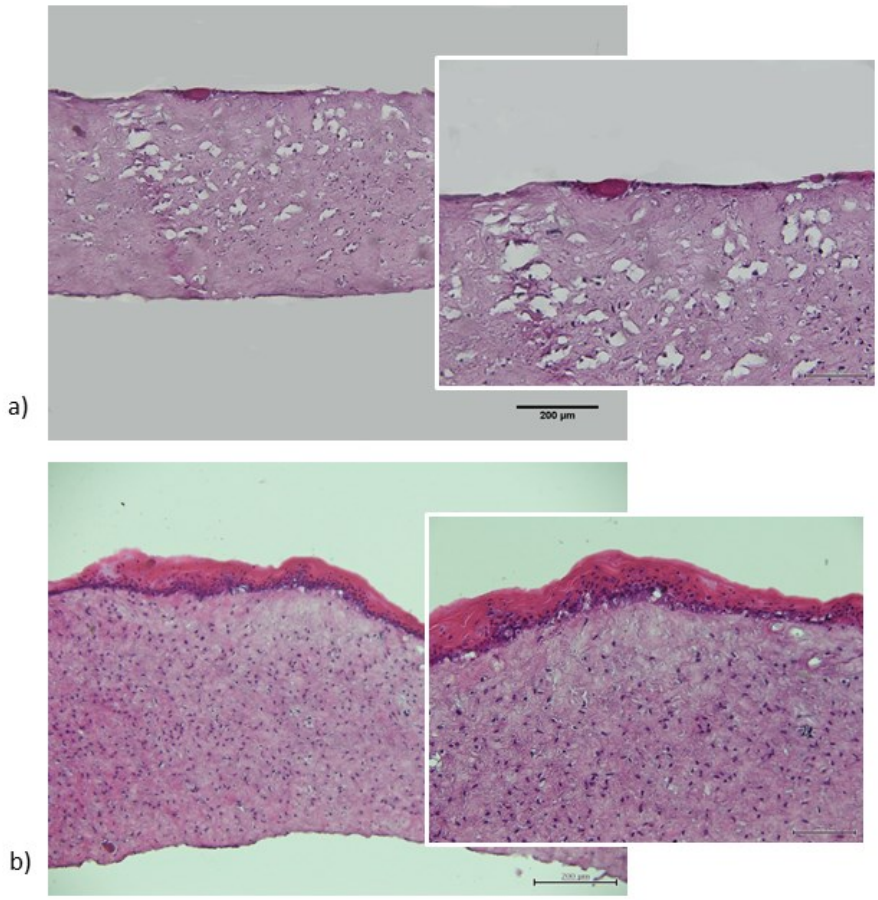

Figure 10. Morphological analysis of 3D human skin equivalent models. H&E staining on tissue sections of 3D-HSE after 14 days of air-liquid interface culture conditions; a) poor quality dermal compartment with an inhomogeneous ECM (in pink) and an undifferentiated *epithelium* on the top of dermis; b) compact dermal compartment and continuous ECM with a stratified *epithelium*, completely differentiated on dermis surface. Bars in a-b) are 200 µm; bars in magnified images are 100 µm.

Finally, in the light of these results, we obtained a functional and responsive 3D human skin equivalent models widely characterized in previous chapters, composed of an endogenous ECM secreted by primary dermal fibroblasts themselves and a completely and well differentiated *epithelium*. As we have

already discussed in the chapter 2 and 3, the effectiveness of our models was related to the endogenous dermal compartment and to the interaction between dermal and epidermal compartment, thanks to a complex cross-talk between fibroblasts and keratinocytes that communicate and interact each other during the assembly of dermis and *epithelium* [30], [33]–[35]. In particular, dermal fibroblasts population support human skin development [36] and, in skin substitutes, ensure a superior keratinocytes differentiation, and the formation of a functional dermal-epidermal junction, compared to acellular matrices that do not support an efficient epidermal stratification [37].

This tissue configuration made our models functional and responsive to external stimuli and to active compounds treatment that could be administered also in a topical formulation.

With these constant check points and quality controls, we could ensure a good quality products, developed by standardized procedures improved during the scale-up of our bioprocess. Our 3D skin models represented a complex tissue system as a powerful testing platform for cosmetic testing which could compare with other existing skin models commercially available both in terms of efficacy, main features and yield in an industrial point of view.

4.3.8 Scale-up of 3D human skin equivalents models

Thanks to an accurate working plan defined to increase the large-scale production of our tissue models, we obtained the maximal yields during last 2 years of my PhD period by the application of a scale-up strategy. We ensured about 200 3D-endogenous skin equivalent models per month. In the Table 4 we schematized all the operations of tissue process done step by step as final inner check control. By examining an ideal month and identifying each new tissue process with an identification number, we traced each tissue bench over the time, and the

percentage of successes. As shown in the Table 4, tissue processes were numbered and every critical step done was checked. Likewise, each failure during the bioprocess was identified in order to control the percentage of unsuccessful. An accurate costs analysis, over the ideal month of maximal production was estimated, with the aim of controlling not only the critical points of bioprocess but also the total spending for a single finished product. Table 5 was obtained by a costs evaluation for all reagents, components, chemicals or additives used for culture maintenance and finally we estimated an approximate monthly spending of about 10959 euro and 47,8 euro for each HSE produced. The final cost of the final product is related to the most expensive reagents used for the tissue process, as FBS and culture medium for maintenance of human keratinocytes.

These data allowed us to better control the single step of our bioprocess, the yield of production, costs for a month of production and for one final tissue model. Furthermore, this planning allowed to estimate not only percentage of failures, over a month, but also to identify the most critical step more prone to failure. The main cause of failure was: i) the risks of fibroblasts transition from a dermal phenotype to an activated contractile phenotype probably due to the heterogeneity of cellular population extracted from biopsy; ii) bacterial and mycoplasma contaminations, that could affect human biopsy or acquired during the culture time and during the air-liquid interface culture condition, that seemed to be the most critical step of the entire bioprocess.

The introduction of bioptical samples quality control allowed us to avoid the contaminations of extracted cells that might compromise all tissue processes upstream. The quality control of reagent and culture media before use contributed to reduce the percentage of failure during the air-liquid interface conditions, that remained the most delicate step of bioprocess.

feb-16	HD-μ TP fab.	DONE	3D-HDE mold.	DONE	3D-HDE completed	DONE	ker seeding	DONE	3D-HSE production	DONE
1										
2			n°22	✓		✓		✓	56	✓
3					n°1					
4	n° 24	✓					biopsy			
5										
6										
7										
8			n°23	✓						
9									50	✓
10										
11										
12	n°25	✓	n°24	✓						
13										
14					n°2	✓			50	✓
15										
16							biopsy	✓		
17										
18										
19										
20	n°26	✓	n°25	✓						
21							biopsy	✓		
22					n°3	✓			44	✓
23										
24										
25										
26	n°27	✘								
27										
28							biopsy	✓		
29			n°26	✓		✓				

Table 4. HSE production plan in an ideal month. In order to control each critical operation, every new tissue process was numbered and traced over the time; every critical step done was checked. For each failure, we identified the reason.

HSE yields	200/month
Contaminations during HDE maturation	0 %
Contaminated biopsy	25%
Contamination during ALI	20%
Events of cellular transition	20%
Monthly spending	10959 eu
HDE costs	47,8 eu

Table 5. Costs analysis for each month. ALI is referred to air-liquid interface culture condition.

4.4 DISCUSSIONS AND FUTURE PROSPECTIVE

In this chapter, we examined our process divided in individual steps that make it up. The whole bioprocess is composed of 5 main steps and every step represents a critical phase that required a check control. In an industrial point of view, we set up a standardized method to increase tissue process productivity, following an accurate scale-up strategy. Our purpose was the improvement of human skin models fabrication and the realization of a start-up for sealing of 3D skin tissue, named "SmarTissue" as an effective platform commercially available for cosmetic testing that could compete with current skin model already known. To better control the quality of our final tissue products, several meticulous quality controls were introduced on the critical step of tissue process. The introduction of quality controls allowed not only to verify the good quality of tissues, but also to discard all abortifacient samples avoiding to affect subsequent steps of the bioprocess. The industrialization of tissue production and the working plan provided useful methods to optimize every activity and laboratory operations, allowing to estimate a percentage of failures and a costs analysis.

The market idea is the realization of a start-up named SmarTissue s.r.l. which the strengths are:

- **Technological supremacy**: the presence of a dermal layer provides the ability to study critical *phenomena* (as skin aging, damage from ionizing radiations, photo-damage), ensuring a highly predictive screening on the native tissue effects;
- **Expanding market:** ability to make innovative new tests and create new highly profitable market niches (i.e. studies for the evaluation of structural changes that occur in the dermis);
- **Know-How:** mix of knowledges and expertise in tissue engineering of tissues medical biotechnology of the SmarTissue team;
- **Personalized therapies:** ability to test/develop drugs and personalized therapies from cells extracted from the patient.

In the same time, we identified initiative weaknesses:

- **Fundraising**: the transition the current prototype to the final product requires a necessary and decisive fundraiser;
- **Competition:** big international companies and industries which fabricated the principal gold standard tissue models commercially available represent a crucial hurdle.

With the development of our complex skin equivalent system that we intend to implement it will be possible:

- To assess the skin irritation, and the cytotoxicity of a compound simultaneously in fibroblasts (dermis) that in keratinocytes (epidermis);
- To evaluate the ability to protect the genomic DNA, the antioxidant capacity, the induction of new collagen, the protection from degradation of new collagen, moisturizing ability, stability of the extracellular matrix –cell system, and skin elasticity;
- The ability to spread through the skin of certain substances, and then determine the optimal doses of administration;
- To test the properties bleaching or tanning, anti-inflammatory properties;
- To study the influence of the vehicle (formulation) on improving the absorption/efficacy of the compound being analyzed.

APPLICATIONS	ENDPOINTS
• Photodamage / UV protection • Wound Healing • Antiaging • Skin Hydration • Irritation / Toxicity	Gene expression; Protein analyses; Histological / Immunohistological analyses; Mechanical properties; Collagen texture; ECM composition; Drug permeability.

Table 6. Possible applications of 3D human skin equivalent models designed by us.

As already described in the chapter 1, there were several industries and companies which have developed various skin models as effective platform for chemical and applications in order to substitutes animal models [11]. Several companies such as L'Oréal, SkinEthic, Henkel and MatTek Corporation realize and employ skin models for pharmaceutical, cosmetic and chemical compound testing in order to study barrier function, drug permeability, cutaneous irritancy and corrosion of topically applied products and active compounds [12] (Table 7).

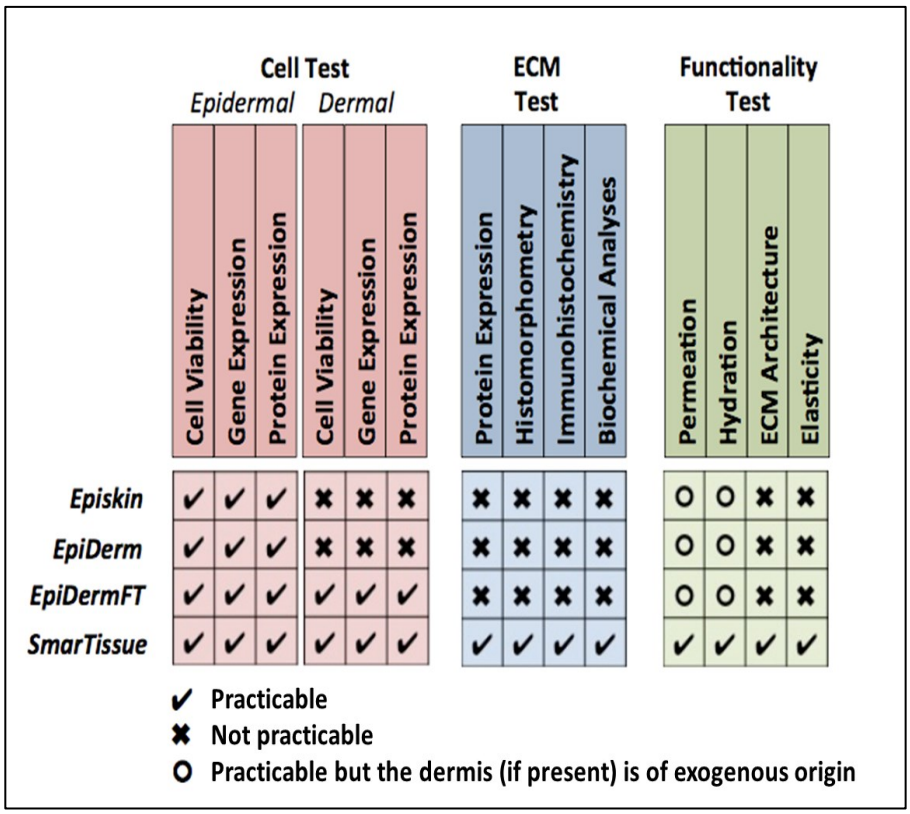

Table 7. Comparison of the main practicable assay carried with SmarTissue and those of best competitors (MatTek, L'Oréal)

Therefore, the competitors of SmarTissue are able to realize the skin equivalent models that only partially duplicate the human skin, lacking a complex stromal tissue and its relative cellular component. When present, the dermal compartment is composed of an exogenous matrix and inert proteins in which the cells are immersed. It follows that the limits of the models of the competitors also limit the quality of competitor products.

Briefly, as shown in the Table 8 the idea of strategy was realization of a provider of products and services, articulating the start-up activities in two divisions:

a) **Screening Platform** divided in 3 sections:

- products/services early phase drug screening and discovery (customers pharma, biotech and cosmetic treatment for pre-phase of clinical tests). activated within 6 months from the founding of the start-up;
- •products/services chemical and / or post-introduction tests statement EU REACH (customers interested in the evaluation of toxicity and / or risk the health of workers who handle their own products). activated from 6 months to 1 year after the founding of the start - up to adapt to EU standards in this respect and properly certify the platform;
- products/services for the Pharma industry (customers interested in phase 1-2 clinical trials). Since it will be necessary authorizations AIFA (ITA), EMA (in EU), FDA (USA), the area will be activated by 2 to 3 years from the Foundation of the start -up.

b) **Therapeutics**:

- products for the pharmaceutical industry, area activated from the third year on the foundation of the start -up, after the necessary regulatory approvals for the marketing of medical-surgical Category 3 (invasive).

SmarTissue is planning to implement product / service lines organizing the main activities in units:

- **Tissue Factory Unit (TFU):** the production line that will be fully operative after 6 months from the start-up foundation. It will be capable of

producing a defined number of final products to the sale for external screening;

- **Tissue Testing Unit (TTU):** it represents the testing service, in order to study of the effect of active ingredients, chemical compounds, environmental factors or radiation on human skin.

Tissue Testing Unit will be divided into a series of platform services:

•Cell-Test Unit. Assays on the cellular component, toxicity testing, cell viability and irritation and molecular profiling to be performed on the complete model or on the simplified model (only epidermis) activated after 6-8 months after the start-up foundation;

•ECM-Test Unit. Assays on extracellular component, morphological tests using histological, Immunohistochemical and biochemical analysis activated after 6-8 months after the start-up foundation;

•Functionality-Test Unit. Assays on the products functionality in order to obtain information about the state of hydration, mechanical properties, permeability, architecture of the extracellular matrix; activated after 12-18 months from the start-up foundation;

•Tissue Specific Test Unit. Assays designed specifically for customized tissues

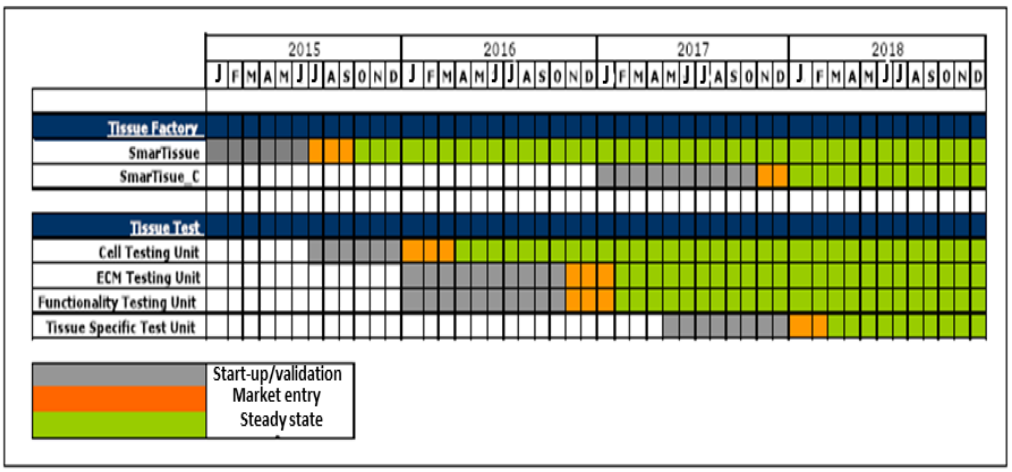

Table 8. Strategy for the realization of SmarTissue start-up and division of all functional units.

4.5 CONCLUSIONS

In this first part of the 4th chapter, we conducted a comparison between our 3D human skin equivalent models and gold standard skin models commercially available as Phenion Full-Thickness skin model and EpiDerm 312X FT skin model fabricated by Henkel and by MatTek Corporation, respectively.

The morphological and histological analysis highlighted that best skin models had significant limitations related to the lack of complexity of dermal compartment, composed, in both exogenous tissue systems, of an inert matrix (a mixture of collagen and GAGs or reconstituted collagen type I), which not mimic all characteristics and functions of native skin. In particular, in the Phenion Full-Thickness skin model, we observed an epidermal compartment not completely stratified and differentiated; while, on the contrary, EpiDerm 312X FT showed a well stratified *epithelium* on an exogenous rudimentary dermal matrix. The main goal of best gold standard skin models is related to faster production times of endogenous skin systems: international companies, in fact, developed simpler protocols to fabricate tissue models using a mixture of exogenous matrices and fibroblasts as dermal compartment, obtained in about 7 days of culture. After 7 days, dermal fibroblasts proliferate inside the exogenous matrix to form a simple dermis ready to be enriched in human keratinocytes, seeded on its surface, in order to obtain a differentiated and stratified *epithelium*, after 14 days of air-liquid culture conditions. On the contrary, our 3D tissue models were obtained with a more complex procedure, according to a bottom-up approach, with the employment of cell and porous gelatin micro-carries, as support for cellular attachment and proliferation. After 9 days of dynamic culture, cells and microcarriers formed the building blocks of tissue, HD-µTP, composed of cells, microbeads and collagen partially assembled. HD-µTP were loaded in the maturation chamber in order to develop 3D human dermis equivalent models,

after 6 weeks in bioreactor. During this time, HDF secreted and assembled collagen and all proteins of ECM, forming an endogenous matrix. 3D-HDE extracted from maturation chamber were enriched in keratinocytes, to produce a fully differentiated *epithelium* on dermis surface. The production times of our endogenous skin systems are about 10 weeks, necessary to fabricate complex and endogenous 3D HSE that mimic all features of *in vivo* counterpart.

In the second part of this chapter we tried to set up an innovative scale-up strategy with the aim to improve the production of 3D human skin equivalent model as a competitive testing platform commercially available. To better ensure the quality of our final products and to intensify the yield of the production, we introduced big bioreactors operating in parallel at their maximal capacity; a working plan to organize each laboratory activities and several check points in each critical phase of our tissue process. Finally, we obtained a safety and standardized protocols to ensure about 200 tissue products per month available for several tests and applications as useful alternative to animal testing.

These scale-up strategy paves the way to the realization of a stat-up, (SmarTissue), that will be a benchmark in the European market for HSEs, focusing the attention on scientific excellence-technology, innovation, production and organizational flexibility. The start-up will take care to engineer, manufacture and market products and services directly related to their HSE models.

4.6 REFERENCES

[1] S. Schuerlein *et al.*, "A versatile modular bioreactor platform for Tissue Engineering," *Biotechnol. J.*, Aug. 2016.

[2] Y. Wang, J. Chu, Y. Zhuang, Y. Wang, J. Xia, and S. Zhang, "Industrial bioprocess control and optimization in the context of systems biotechnology," *Biotechnol. Adv.*, vol. 27, no. 6, pp. 989–995, Dec. 2009.

[3] J. S. Alford, "Bioprocess control: Advances and challenges," *Comput. Chem. Eng.*, vol. 30, no. 10–12, pp. 1464–1475, Sep. 2006.

[4] M. Micheletti and G. J. Lye, "Microscale bioprocess optimisation," *Curr. Opin. Biotechnol.*, vol. 17, no. 6, pp. 611–618, Dec. 2006.

[5] B. Mayr, A. Moser, E. Nagy, and P. Horvat, "Scale-up on basis of structured mixing models: A new concept," *Biotechnol. Bioeng.*, vol. 43, no. 3, pp. 195–206, Feb. 1994.

[6] F. Bylund, A. Castan, R. Mikkola, A. Veide, and G. Larsson, "Influence of scale-up on the quality of recombinant human growth hormone," *Biotechnol. Bioeng.*, vol. 69, no. 2, pp. 119–128, Jul. 2000.

[7] L.-K. Ju and G. G. Chase, "Improved scale-up strategies of bioreactors," *Bioprocess Eng.*, vol. 8, no. 1–2, pp. 49–53, Oct. 1992.

[8] J. Y. Oldshue, "Fermentation mixing scale-up techniques," *Biotechnol. Bioeng.*, vol. 8, no. 1, pp. 3–24, Feb. 1966.

[9] C. M. Cooper, G. A. Fernstrom, and S. A. Miller, "Performance of Agitated Gas-Liquid Contactors," *Ind. Eng. Chem.*, vol. 36, no. 6, pp. 504–509, Jun. 1944.

[10] P. Neubauer, N. Cruz, F. Glauche, S. Junne, A. Knepper, and M. Raven, "Consistent development of bioprocesses from microliter cultures to the industrial scale," *Eng. Life Sci.*, vol. 13, no. 3, pp. 224–238, May 2013.

[11] B. DE WEVER, D. PETERSOHN, and K. R. MEWES, “Overview of human three-dimensional (3D) skin models used for dermal toxicity assessment,” *HPC Today*, vol. 8, no. 1, pp. 18–22, 2013.

[12] S. Pappinen, E. Pryazhnikov, L. Khiroug, M. B. Ericson, M. Yliperttula, and A. Urtti, “Organotypic cell cultures and two-photon imaging: tools for *in vitro* and *in vivo* assessment of percutaneous drug delivery and skin toxicity,” *J. Control. Release Off. J. Control. Release Soc.*, vol. 161, no. 2, pp. 656–667, Jul. 2012.

[13] S. K. Nadkarni *et al.*, “Measurement of Collagen and Smooth Muscle Cell Content in Atherosclerotic Plaques Using Polarization-Sensitive Optical Coherence Tomography,” *J. Am. Coll. Cardiol.*, vol. 49, no. 13, pp. 1474–1481, Apr. 2007.

[14] L. Rich and P. Whittaker, “Collagen and picrosirius red staining: a polarized light assessment of fibrillar hue and spatial distribution,” *Braz J Morphol Sci*, vol. 22, no. 2, pp. 97–104, 2005.

[15] A. Mavon, H. Zahouani, D. Redoules, P. Agache, Y. Gall, and P. Humbert, “Sebum and *stratum corneum* lipids increase human skin surface free energy as determined from contact angle measurements: A study on two anatomical sites,” *Colloids Surf. B Biointerfaces*, vol. 8, no. 3, pp. 147–155, Mar. 1997.

[16] J. Krawczyk, “Surface free energy of the human skin and its critical surface tension of wetting in the skin/surfactant aqueous solution/air system,” *Skin Res. Technol.*, vol. 21, no. 2, pp. 214–223, May 2015.

[17] S. T. Boyce and R. G. Ham, “Calcium-regulated differentiation of normal human epidermal keratinocytes in chemically defined clonal culture and serum-free serial culture,” *J. Invest. Dermatol.*, vol. 81, no. 1 Suppl, p. 33s–40s, Jul. 1983.

[18] L. I. Bernstam, F. L. Vaughan, and I. A. Bernstein, “Keratinocytes grown at the air-liquid interface,” *Vitro Cell. Dev. Biol. J. Tissue Cult. Assoc.*, vol. 22, no. 12, pp. 695–705, Dec. 1986.

[19] B. Hinz, G. Celetta, J. J. Tomasek, G. Gabbiani, and C. Chaponnier, “Alpha-smooth muscle actin expression upregulates fibroblast contractile activity,” *Mol. Biol. Cell*, vol. 12, no. 9, pp. 2730–2741, Sep. 2001.

[20] G. Gabbiani, G. B. Ryan, and G. Majne, “Presence of modified fibroblasts in granulation tissue and their possible role in wound contraction,” *Experientia*, vol. 27, no. 5, pp. 549–550, May 1971.

[21] G. Gabbiani, “The myofibroblast in wound healing and fibrocontractive diseases: The myofibroblast,” *J. Pathol.*, vol. 200, no. 4, pp. 500–503, Jul. 2003.

[22] B. Hinz, “Formation and Function of the Myofibroblast during Tissue Repair,” *J. Invest. Dermatol.*, vol. 127, no. 3, pp. 526–537, Mar. 2007.

[23] S. M. Shiigi and R. I. Mishell, “Sera and the *in vitro* Induction of Immune Responses,” *J. Immunol.*, vol. 115, no. 3, p. 741, Sep. 1975.

[24] F. C. Chu, J. B. Johnson, H. C. Orr, P. G. Probst, and J. C. Petricciani, “Bacterial virus contamination of fetal bovine sera,” *In vitro*, vol. 9, no. 1, pp. 31–34, Jul. 1973.

[25] U. B. Göbel and E. J. Stanbridge, “Cloned mycoplasma ribosomal RNA genes for the detection of mycoplasma contamination in tissue cultures,” *Science*, vol. 226, no. 4679, pp. 1211–1213, Dec. 1984.

[26] H. G. Drexler and C. C. Uphoff, “Mycoplasma contamination of cell cultures: Incidence, sources, effects, detection, elimination, prevention,” *Cytotechnology*, vol. 39, no. 2, pp. 75–90, Jul. 2002.

[27] H. Carsin *et al.*, “Cultured epithelial autografts in extensive burn coverage of severely traumatized patients: a five year single-center experience with 30 patients,” *Burns*, vol. 26, no. 4, pp. 379–387, Jun. 2000.

[28] G. Imparato *et al.*, “A novel engineered dermis for *in vitro* photodamage research: A dermis equivalent for investigating UVA damage *in vitro*,” *J. Tissue Eng. Regen. Med.*, p. n/a-n/a, 2016.

[29] R. Hagens *et al.*, “Contact angle measurement - a reliable supportive method for screening water-resistance of ultraviolet-protecting products *in vivo*,” *Int. J. Cosmet. Sci.*, vol. 29, no. 4, pp. 283–291, Aug. 2007.

[30] K. Boehnke, N. Mirancea, A. Pavesio, N. E. Fusenig, P. Boukamp, and H.-J. Stark, “Effects of fibroblasts and microenvironment on epidermal regeneration and tissue function in long-term skin equivalents,” *Eur. J. Cell Biol.*, vol. 86, no. 11–12, pp. 731–746, Dec. 2007.

[31] A. El Ghalbzouri, P. Hensbergen, S. Gibbs, J. Kempenaar, R. van der Schors, and M. Ponec, “Fibroblasts facilitate re-epithelialization in wounded human skin equivalents,” *Lab. Investig. J. Tech. Methods Pathol.*, vol. 84, no. 1, pp. 102–112, Jan. 2004.

[32] T. Schweder *et al.*, “Monitoring of genes that respond to process-related stress in large-scale bioprocesses,” *Biotechnol. Bioeng.*, vol. 65, no. 2, pp. 151–159, Oct. 1999.

[33] D.-Y. Lee and K.-H. Cho, “The effects of epidermal keratinocytes and dermal fibroblasts on the formation of cutaneous basement membrane in three-dimensional culture systems,” *Arch. Dermatol. Res.*, vol. 296, no. 7, pp. 296–302, Jan. 2005.

[34] F. Duplan-Perrat *et al.*, “Keratinocytes influence the maturation and organization of the elastin network in a skin equivalent,” *J. Invest. Dermatol.*, vol. 114, no. 2, pp. 365–370, 2000.

[35] A. El Ghalbzouri, M. F. Jonkman, R. Dijkman, and M. Ponec, “Basement membrane reconstruction in human skin equivalents is regulated by fibroblasts and/or exogenously activated keratinocytes,” *J. Invest. Dermatol.*, vol. 124, no. 1, pp. 79–86, Jan. 2005.

[36] G. Sriram, P. L. Bigliardi, and M. Bigliardi-Qi, “Fibroblast heterogeneity and its implications for engineering organotypic skin models *in vitro*,” *Eur. J. Cell Biol.*, vol. 94, no. 11, pp. 483–512, Nov. 2015.

[37] N. C. Krejci, C. B. Cuono, R. C. Langdon, and J. McGuire, “*In vitro* Reconstitution of Skin: Fibroblasts Facilitate Keratinocyte Growth and Differentiation on Acellular Reticular Dermis,” *J. Invest. Dermatol.*, vol. 97, no. 5, pp. 843–848, Nov. 1991.